AERODYNAMICS OF SEEING ON LARGE TRANSPORT AIRCRAFT

PROGRESS REPORT

DECEMBER 1, 1985 THROUGH MAY 31, 1986

Prepared for:

NASA-AMES RESEARCH CENTER

MOFFETT FIELD, CA 94035

UNDER NASA GRANT

NCC 2-382

by:

WILLIAM C. ROSE

ENGINEERING RESEARCH AND DEVELOPMENT CENTER

UNIVERSITY OF NEVADA, RENO

RENO, NV 89557

PROGRESS REPORT

DECEMBER 1, 1985 THROUGH MAY 31, 1986

I. BACKGROUND

The operation of large transport aircraft containing optical surveillance or radiation projection systems is currently of interest to a broad spectrum of users of such systems. The quality of either received or transmitted images of coherent radiation of wavelengths from the short visible to the far infrared is of interest. Two major issues influence the overall performance of optical systems. The first is the mechanical environment in which the optical system must perform in flight. This environment includes the vibration input to the optical system through aircraft motions as well as unsteady pressure variations imposed on the structure that may exist as a result of the aerodynamic flow over and within the open cavity. Such unsteady pressure loads may conceivably produce deflections or unsteady misalignments of optical elements placed within the cavity and, hence, degrade the quality of the received or transmitted signals. Once a strategy is chosen to minimize the so-called aero-mechanical effects discussed above, the resulting aerodynamic flowfields may have an adverse impact on the optical systems through the production of unwanted index-of-refraction fluctuations that produce distortions of the optical wavefronts. This latter subject of aero-optics is of primary interest in the current Grant.

Three Government agencies have combined resources to undertake several years of research on the investigation of aero-optical effects of full-scale flight installations. The agencies are the NASA-Ames Research Center, sponsor of

this Grant; the U.S. Army Space Defense Command, Huntsville, Alabama; and the U.S. Air Force Weapons Laboratory, Kirtland Air Force Base, New Mexico. These three agencies are participating in a joint programmatic effort to investigate aero-optics of large open cavity installations.

A major wind tunnel test (related to the Airborne Optical Adjunct [AOA]) at the NASA-Ames Research Center's 14' transonic wind tunnel was completed last year and has produced a body of experimental data taken on turbulent aerodynamic flow over open cavities. These data were obtained over a Mach number range that is applicable to large transports of interest in the present effort. In the wind tunnel test, both aero-mechanical and aero-optical data were obtained for a wide range of flow control devices, including the Boeing Aerospace Company's active flow control system as well as the more classical porous fence configurations. Aero-optical investigations included the open cavity's thermal environment and the turbulent shear layer over the open cavity. Data obtained with a porous fence are directly related to those obtained under the present grant in January of 1986 on the NASA-Ames Kuiper Airborne Observatory (KAO).

In addition to the aerodynamic data obtained on the turbulence levels and appropriate scale sizes in the shear layers existing over the fence quieted cavities, direct optical focal plane data were also obtained by the MIT team from the Department of Earth, Atmospheric and Planetary Science. Data referred to from the AOA wind tunnel test are taken from References 1 and 2, and it is assumed that the reader has access to, and is familiar with, these references.

Data obtained during the present study on the KAO are presented in this report and are discussed in light of their impact on "seeing" through the

shear layer. In addition, scaling relationships can be validated by comparing the wind tunnel to full scale KAO data. Validated scaling relationships will prove useful in extending the KAO data to other proposed large aircraft.

II. INTRODUCTION

Errors in optical wavefronts produced by aerodynamic flowfields are the source of the inability to focus that wavefront to either the optical diffraction limit of the system. Wavefront errors induced by aerodynamically induced index-of-refraction variations arise because of fluid density fluctuations. A proven interrelationship between the wavefront error and three important aerodynamic parameters is given in Equation 1.

$$\sigma^2 = 2\beta^2 \int_0^L \overline{\rho'^2}\ \ell_z dz \qquad (1)$$

The fluid density fluctuations, the scale lengths over which they occur, and the total path length through the turbulence are the important aerodynamic parameters that must be known in order to calculate the expected wavefront error produced along any ray through the turbulence. Since only the statistics of the density fluctuations are known, it is only the statistics of the wavefront error given by Equation 1. Techniques for determining these aerodynamic parameters are discussed in detail elsewhere (e.g. Reference 3), and will not be repeated here other than to say that the density fluctuations are derivable from knowledge of mean flowfield and parameters that may be deduced from high response instrumentation positioned at several locations throughout a given shear layer. The result is that a wavefront error, σ, can be produced that is applicable along a ray from aerodynamic data alone taken along that same ray.

What effect that given σ, or a distribution of wavefront errors over the aperture will have on focal plane quality depends on many parameters. The

first parameter is the decision as to what focal plane characterization is of interest. In general, there are three characteristics. The first is the focal plane spot size (also known sometimes as the "blur" circle), which limits the resolution of point objects in the focal plane or equivalently limits the resolution between two closely spaced point objects in the focal plane. The second parameter is the focal plane jitter (also sometimes known as "beam wander") and represents the temporal behavior of the focal plane spot as it is affected by the temporal characteristics of the wavefront error. The temporal characteristics of the wavefront error, of course, are deriven by the characteristics of the fluctuating density field and associated scale lengths. The third focal plane parameter is the combination of the previous two. As the ratio of "exposure" time to the characteristic time of the wavefront error increases, jitter contributes more to the spot size. For example, for very long exposure times, the focal plane image results from the spot, coupled with the motion of that spot over an area on the focal plane, producing significantly larger spot sizes than those observed over very short exposure times. The minimum spot size is obtained at very short exposure times and represents degradations due to index-of-refraction fluctuations that are contained within the field of view at the instant of the exposure. Further discussion of this distinction between observed focal plane behavior and time characteristics of the turbulent density fluctuations is discussed in Reference 1.

When one decides what focal plane characteristic is of interest, then the effect that a given wavefront error has on that quality is, in general, a function of the amplitude of the phase variations, the scales over which they occur, and the wavelength of the radiation considered. Furthermore, in general, one must consider both the optical limits and diffraction limits of the

particular optical system operated within the aerodynamic flowfield. Precisely how all of these parameters combine is not clearly understood. Insights into the nature of observed focal plane quality and the aerodynamic flows producing the degraded images are investigated here.

Scaling the observed focal plane image quality to other full-scale flight situations is of interest. In general, optical performance is scaleable only through aerodynamic scaling and knowledge of how aerodynamic flows affect the optical performance. Scaling relationships for aerodynamic flowfields have been proposed (e.g. Reference 1); however, remain largely unvalidated due to the lack of a reliable body of data obtained over large open ports on full scale aircraft. Such a body of data was obtained during the present study and is the basis for the remainder of this report.

III. THE EXPERIMENT

The Kuiper Airborne Observatory operates routinely with a large open cavity in the fuselage of a modified C141 aircraft. The open cavity is prevented from resonating and producing large pressure fluctuations through the use of a porous fence located all along and just ahead of the upstream opening of the cavity. The fence has a length of approximately 8 inches and is made from 40 percent porosity material. The fence may be positioned continuously at any angle between 30 deg up from the fuselage line to 90 deg (or perpendicular) to the fuselage. During normal astronomy flights the fence angle is set at 30 deg. For reference later in this report, in the terminology developed in the AOA wind tunnel test, the 30 deg KAO fence is described as an 8/40/30 fence. The boundary layer upstream of the fence was deduced in the present study to be approximately 4.2 inches. The length of the opening of the cavity is approximately 54 inches in the streamwise direction. The location of the rectangular aperture can be varied in elevation through positioning of the telescope which is interlocked to a sliding door. Measurement of the aerodynamic parameters in the AOA wind tunnel test was done along a line of sight located near the center of the aperture. In the KAO, measurement of the shear layer properties at the center of the aperture with aerodynamic instrumentation would have made normal astronomy impossible, so a scheme was devised that would allow measurement of the shear layer properties on a non-interferring basis with ongoing astronomy flights. This non-interferring arrangement allowed the successful and early completion of the aerodynamic shear layer experiment discussed here. A 37 sensor position rake was attached to the fuselage just downstream of the open cavity. The rake was fixed; i.e., that it was not positionable in flight, and was instrumented with both high

response aerodynamic film sensors and interchangeable pitot pressure probes. The measurement station was just at the aft edge of the cavity and resulted in a distance between the top of the porous fence to the measurement station of approximately 64 inches. The rake was designed by Northrop Services Company, Sunnyvale, California, based on expected unsteady and steady loads consistent with experience gained during the US Air Force Airborne Laser Laboratory Program. The rake was designed to be airworthy in the dynamic pressure environment on any of today's operational aircraft. The rake was fabricated by MicroCraft and delivered to NASA-Ames in the fall of 1985. Figure 1 shows closeup photographs of the rake installed on the KAO in both the pitot pressure and hot-film anemometer configurations. Figure 2 is a rake installation photograph showing its position relative to the telescope door and the remaining forward portion of the KAO fuselage.

The airborne experiment was conducted in December 1985 and January 1986. Three flights in December were used to obtain the mean flow pressure data; i.e., the pitot pressure coupled with the static cavity pressure. These data allow one to determine the variation of mean Mach number and density throughout the shear layers. Tests were conducted at primary Mach numbers of 0.7 and 0.8. In addition, a Mach number of 0.73 which is representative of the typical astronomy flight Mach number was also studied. During January, in conjunction with the Kuiper Infrared Technology Experiment (KITE) flights, selected pitot pressure tubes were replaced with hot-film sensors for the determination of the unsteady density field. Two flights using the latter instrumentation were flown. During all of the flights the boundary layer control fence angle was varied between 30 deg and 90 deg and altitudes between 37,000 and 41,000 feet MSL were flown.

Unsteady voltages related to the unsteady density at each sensor location were recorded on a 28 track, wideband group I, analog tape recorder at 60 ips. Data were also converted in real time to the rms value of the fluctuating voltage at each sensor site and were recorded along with the appropriate mean value of the sensor voltage on the ADAMS airborne data system operational on the KAO. These data were combined with pressure data giving Mach number and mean density to produce values of the unsteady density fluctuation for each sensor site. These data are presented in the Appendix for use by others.

Plots of the rms density fluctuation as a function of distance away from the fuselage are also shown for each test condition in the Appendix. In order to obtain the optical wavefront error, as noted in conjunction with the discussion of Equation 1, values of the integral scale length must also be known. These values were determined by cross-correlating adjacent fluctuating signals throughout the shear layer. Scale length data obtained this way are also summarized in the Appendix. The remaining aerodynamic parameter required to produce the optical wavefront error term is the total path through the turbulence which can easily be derived as the full width of the fluctuating density curves discussed above. All of these data are summarized graphically for optical considerations in the plot of the integrand of Equation 1 as a function of distance from the fuselage given in the Appendix. Integrals of the integrand plots; i.e., the rms wavefront error, σ, and σ/λ for $\lambda = 0.5$ μm are also shown in tabular form in the Appendix.

These data have been reviewed from the viewpoint of optical degradation and scaling considerations and serve as the basis for the following discussion.

IV. RESULTS AND DISCUSSION

IV.1 KAO Shear Layer Data

The wavefront error deduced from the aerodynamic data shown in the Appendix is summarized in Figure 3 for Mach numbers of 0.7 and 0.8, for the range of altitudes tested in the present study. In examining this figure, several features are noteworthy. Initially the solid symbols taken at M=0.8 for all altitudes and all fence angles produce a wavefront error of approximately .21 to .23 μm. Within this data set, there is a tendency toward slightly lower wavefront errors to occur with higher altitude, as would be expected. In contrast to the general behavior noted in the AOA Wind Tunnel Test, the wavefront error data from the KAO at M=0.7, generally lie above the bulk of the data for M=0.8, they exhibit more scatter, but do generally indicate a trend of decreasing wavefront error with increasing altitude. Reasons for the increased wavefront error and attendant scatter in the data set are believed to be related to a low frequency component in the spectrum of the M=0.7 data that is indicative of an instability in the shear layer. This increase in the low frequency component of the shear layer can be seen in the spectra shown in Figure 4, which compare the spectra for M=0.7 and 0.8 at the same altitude for a 30 deg fence setting. Both spectra are taken from sensors located at the maximum rms density fluctuation in the layers. The reason for this apparent instability is unknown, although it might be related to the low Mach number operation of the aircraft at high altitude and the potential influence of the wing root pressure field. This pressure field might affect the behavior of the shear layer near the aft edge of the cavity where

these data are obtained. It is felt that this behavior with decreasing Mach number, whatever its actual cause, is a specific aircraft related problem and does not give the trend that one can expect with Mach number for full scale flight flush installations. It may also be noted that the data shown in the Appendix for M=0.73, the typical astronomy operating Mach number, lie within the general grouping of the data shown in Figure 3. These values of σ and the attendant aerodynamic values of L and ℓ_z are shown in tabular form in Figure 5 for the KAO data at 0.8 and 0.7 Mach number.

IV.2 Scaling Aerodynamic Data

In general, optical performance is scaleable only through aerodynamic scaling relationships and knowledge of how the resulting aerodynamic flows affect optical performance. Thus, in order to scale optical information obtained for example, in a wind tunnel experiment or on another aircraft to any other full sized aircraft, one must be able to first scale the aerodynamic flows. Relationships between the aerodynamic flow and optical performance can be established in sub scale tests, as was done in the test discussed in References 1 and 2. Then these aero-optical relationships can be used to determine what the resulting optical effects will be for a coherent wavefront passing through the aerodynamic flow at any arbitrary wavelength.

Data obtained in the present study on the KAO are very nearly geometrically scaled to the forward cavity of the AOA wind tunnel test. Aerodynamic scaling laws were proposed in Reference 1 as a result of that wind tunnel test. However, these scaling relationships remained experimentally unvalidated prior to the data obtained in the present study. This full scale data set, in conjunction with previously obtained data in another full scale experiment conducted on the United States Air Force ALL Diagnostic Aircraft (Tail Number 60-0371), can be used to shed light on scaling relationships for turbulent shear layers. Together, these three experiments form the basis for establishing a valid scaling of the aerodynamic flow. In particular, two quantities of interest (see Equation 1) for any given configuration, Mach number and altitude, are the width for the shear layer at any position downstream of its origin, L, and the turbulence integral scale length, ℓ_z. Details of the wind tunnel and A/C

371 data are given elsewhere. However, as pointed out previously, the notation developed in Reference 1 for describing fence length, porosity and angle denote the KAO fence as an 8/40/30 (at the 30 deg position). In contrast, the 371 fence is a 6/40/90, while wind tunnel configurations best scaled to the KAO are the 2/40/30 and 2/40/60 configurations.

Data from the three above discussed experiments are available for a Mach number near 0.8, whereas for Mach number 0.7, only the wind tunnel and KAO data are available. The data for total shear layer thickness, L, are shown in Figure 6. A linear fit to the bulk of the data appears useful as an engineering representation of the behavior of the width of the shear layer as a function of distance downstream of the origin of the shear layer. The proportionality constant appears to be 20-23 percent of the distance downstream. Similar behavior of the data is shown for turbulence integral scale length, ℓ_z, in Figure 7, where the proportionality constant is approximately 4-4.4 percent of the distance downstream of the origin of the shear layer. Taking both of these data sets into consideration, one can see that the ratio of integral scale length to shear width for all of the data shown is about .20 ± .02; that is, the integral scale length appears to be approximately 20 percent total shear layer width for both the M=0.8 and 0.7 conditions. This linear behavior occurs over a wide range of unit Reynolds number and, thus, does not appear to depend strongly on that number. This linear behavior of the data with distance downstream is the simple scaling discussed in Reference 1. The behavior of the data shown here with both wind tunnel and full scale flight conditions validate the simple geometric scaling of two of the important parameters useful for determining optical performance. The

remaining parameter is that of the amplitude of the density fluctuations, $\overline{\rho'^2}$ (see Equation 1). The density fluctuations are driven by the difference in density between the inside and outside of the shear layer and the integral scale length through the layer as discussed in detail in Reference 1. This difference is a function of the external flow Mach number and the outside fluid density.

Since the outside density drops with increasing altitude, one can expect a variation of about 15 percent in σ over the range of operating altitudes of the KAO. This behavior is observed in the discussion in Section IV.1.

As a further verification of the correct aerodynamic simulation occurring between the AOA wind tunnel forward cavity and the full scale KAO, comparisons between spectra obtained in the wind tunnel at Mach numbers of 0.8 and 0.7 for the 2/40/30 fence configuration are shown in Figure 8. The upper frequency shown here for the wind tunnel data is 40 kHz while the data obtained for the KAO is 5 Khz. The ratio of a factor of 8 in frequency corresponds to the geometric scaling of the distance between the origin of the shear layer and the aerodynamic instrumentation station. This is shown schematically in Figure 9 where the geometric ratio is seen to be 7.5. The increased low frequency content in the KAO spectra at M=0.7 is not seen in the wind tunnel data, and further supports the argument that the M=0.7 KAO data behavior is specific to that aircraft. The excellent agreement in the nature of the spectra shown further supports the linear scaling relationship.

To summarize scaling, the three aerodynamic parameters required to infer the optical wavefront error, σ, are given by the established

simple geometric scaling relationships, the aircraft Mach number and external fluid density; i.e., the wind tunnel freestream density, or, in the flight environment, the atmospheric density. With knowledge of these scaling relationships in hand, one may proceed to discuss the dependence of focal plane optical performance on these aerodynamic parameters and how the focal plane optical performance may then scale with the optical wavelength.

IV.3 Aero-Optical Considerations for the KAO

In Reference 1, wavefront error values were converted to expected focal plane performance for three significant parameters. The first is the long-time focal plane spot size, or blur circle diameter. All diameters discussed here are the full width at half maximum intensity (FWHM). The second is the short exposure time focal plane spot size. The third is focal plane image motion, or jitter. Relationships for determining each of these three parameters from the aerodynamic data similar to those discussed above were proposed in Reference 1. The long term spot size is discussed here because of its importance in demonstrating the unique interrelationship between aerodynamic data and observed focal plane images and is important to the astronomy on the KAO. Reference 1 hypothesizes the interrelationship between long term spot size, $\langle P_{LT} \rangle$ and the aerodynamic parameter as follows. P_{LT} is assumed to be related to the structure function as shown in Equation 2.

$$P_{LT}^2 = \frac{2^2 D_\phi(D)}{k^2 \ell_z^2} \tag{2}$$

Equation 2 can be written in terms of the optical phase variance, σ_ϕ^2, shown in Equation 3 where R_ϕ is the phase auto-correlation function.

$$P_{LT}^2 = \frac{2^2 \, 2\sigma_\phi^2 \, [1 - R_\phi(D)]}{k^2 \ell_z^2} \tag{3}$$

When R_ϕ becomes negligible over distances small compared to the diameter of the aperture, its consideration may be eliminated from Equation 3 resulting in the simplified equation for the long-time spot size shown in Equation 4.

$$P_{LT}^2 = \frac{8\sigma_\phi^2}{k^2 \ell_z^2} = \frac{8\sigma^2}{\ell_z^2} \qquad (4)$$

This long term spot size is assumed to be representative of the diameter that would occur at the 1/e point of the intensity distribution. In Reference 1 this value was divided by 1.2 to be representative of the FWHM point in the intensity distribution. This leaves a final simplified equation for spot size as shown in Equation 5.

$$\langle P_{LT} \rangle = \frac{\sqrt{8}\,\sigma}{1.2\,\ell_z} = 2.36\,\frac{\sigma}{\ell_z} \qquad (5)$$

Equation 5 is independent of wavelength and, thus, if it can be representative of the true focal plane aero-optical relationship, it must somehow apply to a limited range of wavefront error values. Since the publication of Reference 1 and considerations involved in the present study, it is now believed that Equation 5 can only represent the diameter of the long term spot size when the wavefront errors are large compared to the wavelength. Further, this spot size represents the maximum diameter spot that can be produced by the aerodynamic flow, but, depending on wavelength, it might be smaller.

The exact behavior of spot size with wavelength can be envisioned with the aid of the following discussion. The focal plane spot size produced from a focused coherent wavefront in the absence of turbulence is limited by the well known diffration formula given in Equation 6.

$$\text{Diffraction Limit Diameter} = \frac{2.4\lambda}{D} \qquad (6)$$

For comparison purposes here, half of this value is representative of the FWHM values discussed throughout the rest of this report. Nearly all of the energy is contained in the central spot of undiffracted light. As weak turbulence begins to modify this focal plane intensity, some of the energy from the central spot is taken away and scattered into a much larger diameter. The peak intensity decreases; however, there is still a central spot clearly observable. This weak turbulence range is treated by the theory given in Reference 4 by Hogge, et al. When the peak intensity of the central spot has decreased to approximately 5 percent of its original value; i.e. the Strehl ratio about 0.05, most of the energy is found in the diffraction wings of the focal plane pattern and a blur circle is produced. The diameter of this blur circle is many times that of the diffraction limited central spot. This enlarged diameter is determined from the magnitudes of the wavefront error; i.e., the amplitude of the wavefront variations, and the scale lengths over which they occur. The relationship is very much analagous to Equation 5. When the wavefront amplitude variations become so large that nearly geometric bending of the incoming waves occurs, then a domain of wavelength independence is established and the diameter of the spot no longer increases as wavelengh decreases. In the weak turbulence (Hogge) region, the decrease in intensity of the central spot is extremely wavelength dependent, whereas in the strong turbulence region (as discussed by Goodman, Reference 5) wavelength dependence vanishes. The exact trajectory that the long-time spot size takes with wavelength between these two limiting conditions is currently under investigation (Reference 6). However, it is now believed that the strong aberration region must start when the wavefront error exceeds

approximately $\lambda/3$, whereas the Hogge region is assumed to apply to wavefront errors less than approximately $\lambda/8$. The Strehl ratio of the very strongly aberrated spot can not be obtained from the Hogge analysis. Although the exact distribution of intensity in the focal plane is unknown at this time, estimates of peak intensity relative to that of the diffraction limited peak may be made by assuming a Gaussian distribution with the strongly aberrated FWHM containing all the initial energy. The spot size behavior with wavelength is given for the KAO in the following section on scaling to larger installations.

The above discussion addresses only the long time spot size. The smallest spot can be obtained when the exposure time is reduced to a value for which only density variations occurring with scales less than the aperture are present. This short-time spot size must be calculated from the appropriately filtered σ as discussed in Reference 1. Image motion, or jitter, is produced by wavefront errors larger than the aperture and can be calculated from Equation 7.

$$\langle\theta\rangle = \sqrt{2}\,\frac{\sigma}{D} \tag{7}$$

For the KAO, values of the jitter induced by the shear layer are less than 0.5 μrad.

IV.4 Scaling the Data to SOFIA Class Installations

NASA-Ames Research Center is considering a new airborne observatory for infrared astronomy (SOFIA). Discussions about the aero-mechanical and aero-optical implications of aerodynamic flowfields on such an observatory are underway. In light of the procurement of the new airborne observatory, it is useful to use the data described in earlier sections of this report and the relevant scaling of those data to a situation which is similar to that expected on a SOFIA-class aircraft. For purposes of consideration here, it is assumed that the telescope aperture is approximately 3 to 3½ times the size of the one currently employed on the KAO. Figure 10 presents a bulk of relevant information concerning the observed behavior of the focal plane long-time spot size as a function of wavelength. We will examine the behavior of the KAO optical performance in light of the shear layer data obtained in this study as well as other previously obtained data. Figure 10 shows the FWHM diffraction limit lines for both the KAO and the SOFIA. These lines have a slope which is half of that given in Equation 6, since it is desirable to translate all information to the FWHM basis.

In addition to these diffraction limit lines, the FWHM optical limit, which is currently operative on the KAO and is expected to be obtainable on the SOFIA, is also shown. This value is approximately 5 μrad, or one arc sec. Ideally, operating in the absence of any aerodynamically induced distortions, the expected spot size is the larger of either of the optical or diffraction limits. For example, in the KAO, the optical limit would apply up to approximately $\lambda = 3.5$ μm, whereas for the SOFIA the optical limit applies to nearly $\lambda = 11$ μm. Also noted in the lefthand side

of Figure 10 are two different pieces of information. Near the top of the figure, there is an indication of the "Erickson data" obtained between approximately 1.65 and 3.1 μm. These data were obtained on the basis of 85 percent encircled energy in the focal plane. However, even when translated to the FWHM equivalent by dividing by 1.5, the data remain off the scale of Figure 10. Also indicated near the $\lambda = 0.5$ μm area is a range of previous data obtained in the visible wavelengths and a data point at approximately 3.5 arc sec which is the smallest image obtained by Dunham and Elliott in the first Seeing study. These data lie well above either the optical or diffraction limits discussed earlier.

The previous visible data and the Erickson data were obtained prior to July of 1985 when large cabin-to-cavity interface leaks were discovered and these data are quite possibly tainted by the addition of warm, moist cabin air leaking into the telescope cavity. Suspicions for implicating the cavity thermal environment in producing the large spot sizes are supported by the following discussion that shows only a small shear layer contribution to those large images. Figure 10 indicates a spot size curve labeled KAO that starts at approximately 14 μrad and drops from that value near $\lambda = 0.4$ μm to the optical limit at approximately $\lambda =$ 1 μm. The basis of this curve is the data discussed previously in this study for the shear layer.

The 14 μrad value is obtained by adding the expected contribution due to the aerodynamics of the shear layer to the value of the optical limit. Values for the long-time spot size were given in tabular form for the shear layer data obtained in this study in Figure 5. Since the long-time spot size is calculated from aerodynamics by the value of σ/ℓ_z and it

is known that both these parameters scale linearly with distance from the origin, then the value of P_{LT} (as calculated in Equation 5) will remain in effect over the entire aperture. However, the magnitude of σ itself does not remain constant over the aperture so that the average σ (for example taken at the midpoint of the aperture) will be approximately 60 percent of the σ obtained at the aft edge of the cavity where the current aerodynamic data were taken. Thus, the σ data shown in Figure 5 must be multiplied by 0.6 and instead of a σ of approximately .22 μm, we would expect a value of approximately 0.13 μm to be representative of that occurring at the midpoint of the KAO aperture. As was discussed in the previous section, the strong turbulence aberration region would be expected then to occur up to a value of the wavelength of approximately three times this value of σ; i.e., approximately $\lambda = 0.4\ \mu$m. Continuing to follow the arguments presented in the previous section, the shear layer aberration will be expected to drop to near zero at $\sigma \cong \lambda/10$ or $\lambda = 1.3\ \mu$m. In the present case, the optical aberrations drop only to the optical limit of the telescope since that limit is larger than the diffraction limit near 1 μm. As noted previously, the exact path for connecting these two asymptotes is not known; however, the range of physically plausible paths is not large. Thus, Figure 10 represents a schematic interpretation of the behavior with wavelength of the spot size between the aerodynamic limit of 14 μrad to the optical limit of 5 μrad for the KAO.

For the moment consider the SOFIA to be a porous-fence quieted open cavity geometrically enlarged from the KAO. When considering scaling the KAO data to the SOFIA, because of the linear growth arguments demonstrated previously, the value of σ/ℓ_z near the midpoint of the

SOFIA aperture will not differ from those of the KAO and, thus, the same spot size for strongly aberrated case as found in the KAO will prevail. However, the values of the wavefront error will be increased by the increase in scale size of the SOFIA over the KAO. This has the net effect of increasing the wavelength range over which the strong aberrations can be expected to occur and commensurately will increase the wavelength range over which there can be expected some aerodynamic aberrations. Numerically, with respect to Figure 10, we can expect to see the SOFIA (as a scaled KAO) to exhibit a 14 μrad spot size up to λ = 1.0 μm and then decrease continuously until the optical limit is obtained at a value of λ near 3 μm. Thus, Figure 10 summarizes the behavior of the KAO shear layer as interpreted from the experimental data, as well as demonstrating the scaling of those data to a larger airborne installation.

It is assumed that previous data indicating very large spot sizes must have been influenced by the thermal behavior of the cavity, since they lie far above what could be expected from the shear layer alone. It is assumed that, with proper engineering design and attention to detail, that one may optimistically be able to operate the SOFIA as indicated in the scaled KAO line of Figure 10. It is interesting to note that for wavelengths on the KAO which may be optically limited, on the SOFIA may now become influenced by the aerodynamic flows. This would occur in the range of wavelengths between 1 and 3 μm.

Since the simply scaled KAO porous fence concept to the SOFIA might not represent the current state-of-the-art in shear layer flow control, it is interesting to scale the wind tunnel data obtained on a combination active and passive flow control system developed by the Boeing

Aerospace Company (BAC). This technique involved the use of contoured aerodynamic rear lips and an active flow injection system at the forward lip of the cavity. No porous fence was used in this concept. Figure 11 shows the scaling of the relatively small scale wind tunnel experiment to the SOFIA class aperture size. In the wind tunnel, approximately a 30 percent improvement in spot size was obtained through a 30 percent reduction in wavefront error. Both of these items combine to produce an improved optical performance in the visible and near infrared regions as shown in Figure 11. The scaled data from the wind tunnel do not necessarily represent an optimum shear layer control technique and other methods should be examined to determine what the minimum optical impact of the aerodynamic flowfields could be on the SOFIA. Tradeoff studies between the improvement in optical performance and the additional cost to the modification of the aircraft and/or decrease in aircraft performance should be carried out as soon as possible to guide the selection in an appropriate aero-mechanical suppression technique for use on the SOFIA.

V. CONCLUDING REMARKS

Data have been obtained in the full scale flight environment of the Kuiper Airborne Observatory (KAO) on the nature of the turbulent shear layer over the open cavity. These data have been used to verify proposed aerodynamic scaling relationships to describe the behavior of the turbulent layers and to estimate the optical performance of systems of various wavelengths operating within the KAO environment. These data and wind tunnel data are used to scale the expected optical effects for a potential stratospheric observatory for infrared astronomy (SOFIA) in which a telescope approximately $3\frac{1}{2}$ times larger than that on the KAO is envisioned. It appears that the use of combinations of active and passive aero-mechanical flow control techniques can improve the optical behavior of systems in the SOFIA environment. Experiments to verify these potential improvements can be performed on the KAO with sufficient modifications to the cavity and aero-mechanical technique installations.

VI. REFERENCES

1. Rose, W.C. and Cooley, J.M.: "Analysis of the Aerodynamic Data from the AOA Wind Tunnel Test and Implications for the AOA Platform." Final Report Contract DAAH01-85-C-0312, 29 October 1985.

2. Dunham, E.W. and Watts, A.W.: "AOA Wind Tunnel Test Interim Report." Unpublished, May 1985.

3. Rose, W.C.; Craig, J.E. and Raman, K.R.: "Nearfield Aerodynamics and Optical Propagation Characteristics of a Large-Scale Turret Model." AFWL TR-81-28, February 1982.

4. Hogge, C.B.; Butts, R.R. and Burlakoff, M.: "Charcteristics of Phase Aberrated Nondiffraction-Limited Laser Beams," Applied Optics, Vol. 13, p. 1065, May 1974.

5. Goodman, J.W.: "Statistical Optics," pp. 374-384, John Wiley and Sons, New York, 1985.

6. Young, E. and Dunham, E.W.: Private Communications, Mar-May 1986.

VII. FIGURES

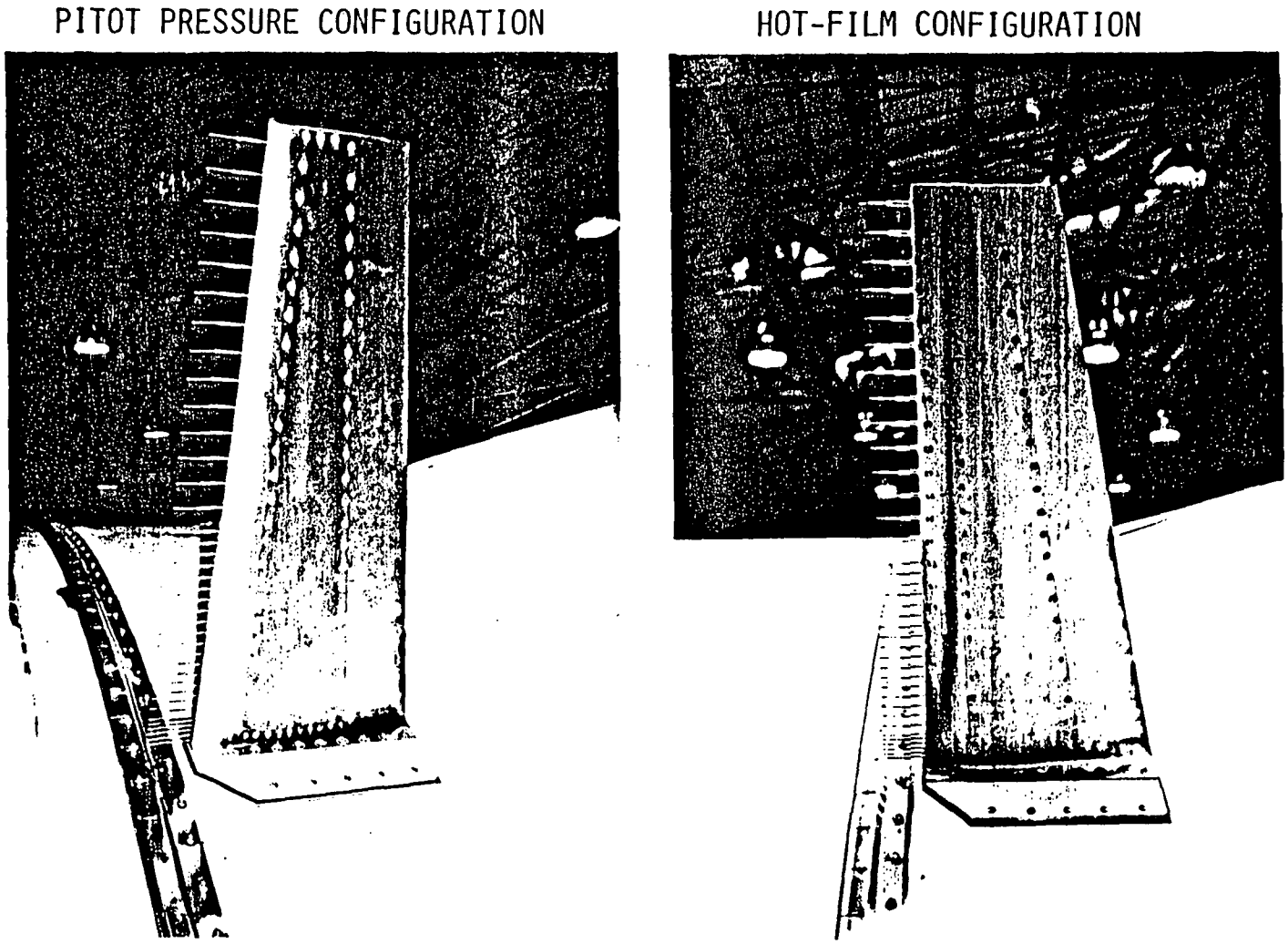

Figure 1. Aerodynamic rake mounted on KAO in pressure and hot-film configurations.

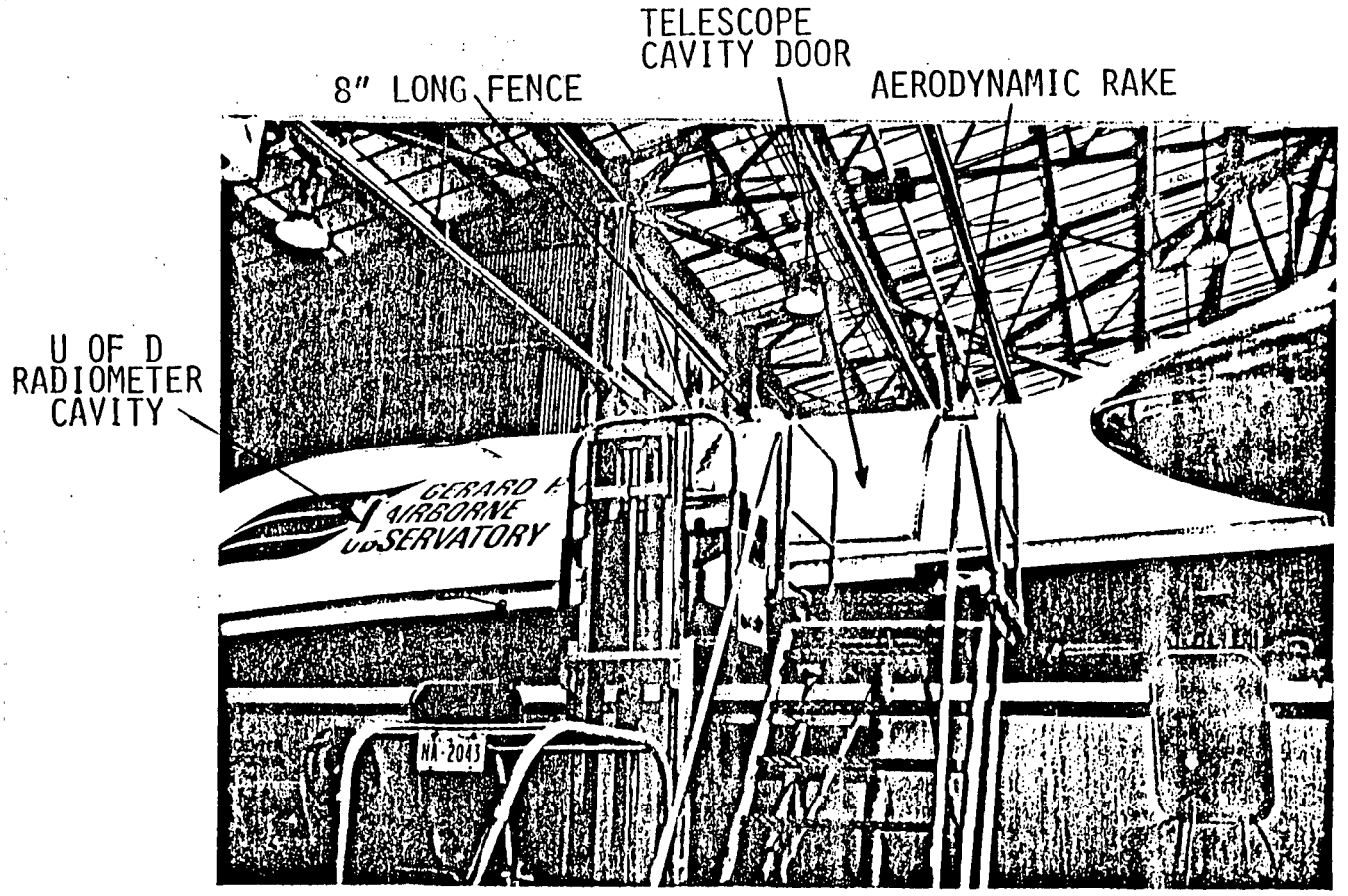

Figure 2. Aerodynamic rake installation on KAO.

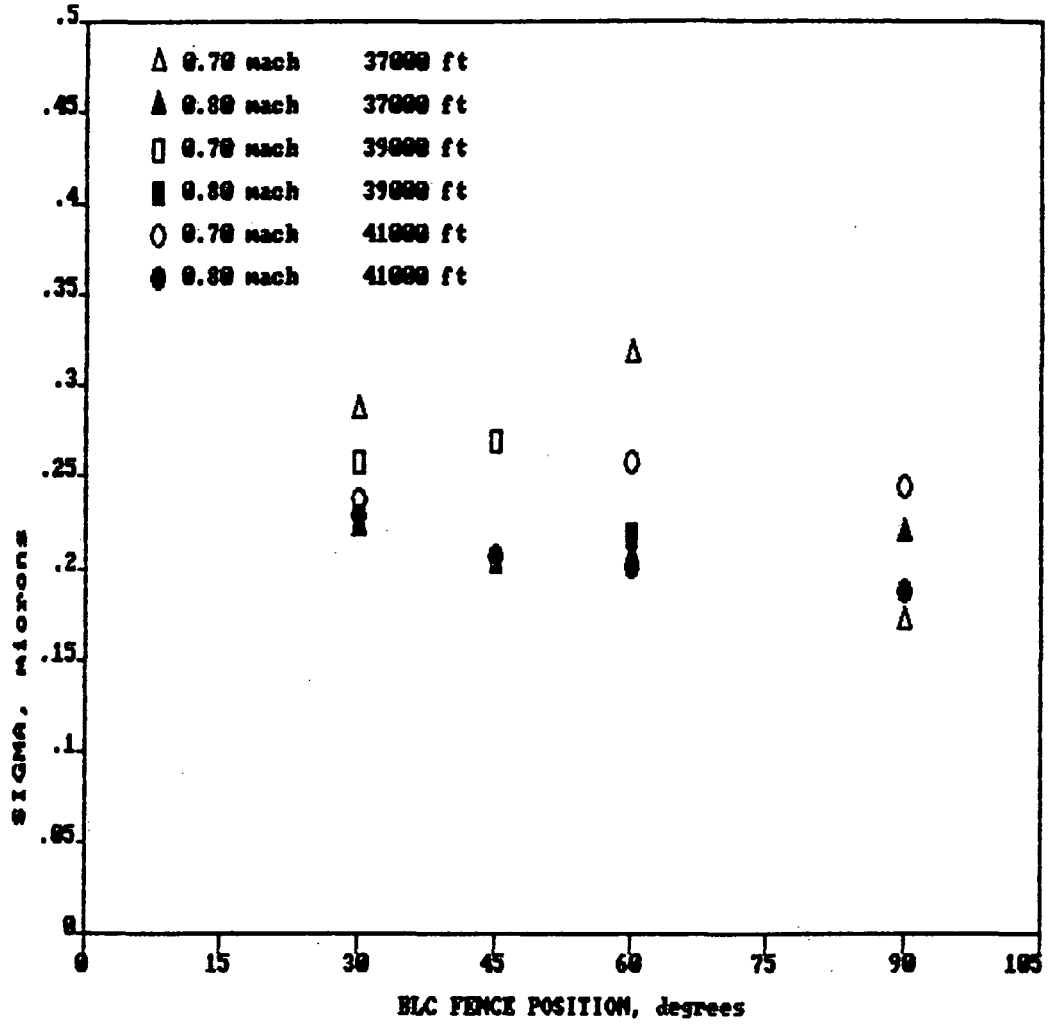

Figure 3. Summary of wavefront error data from the KAO at M=0.8 and 0.7

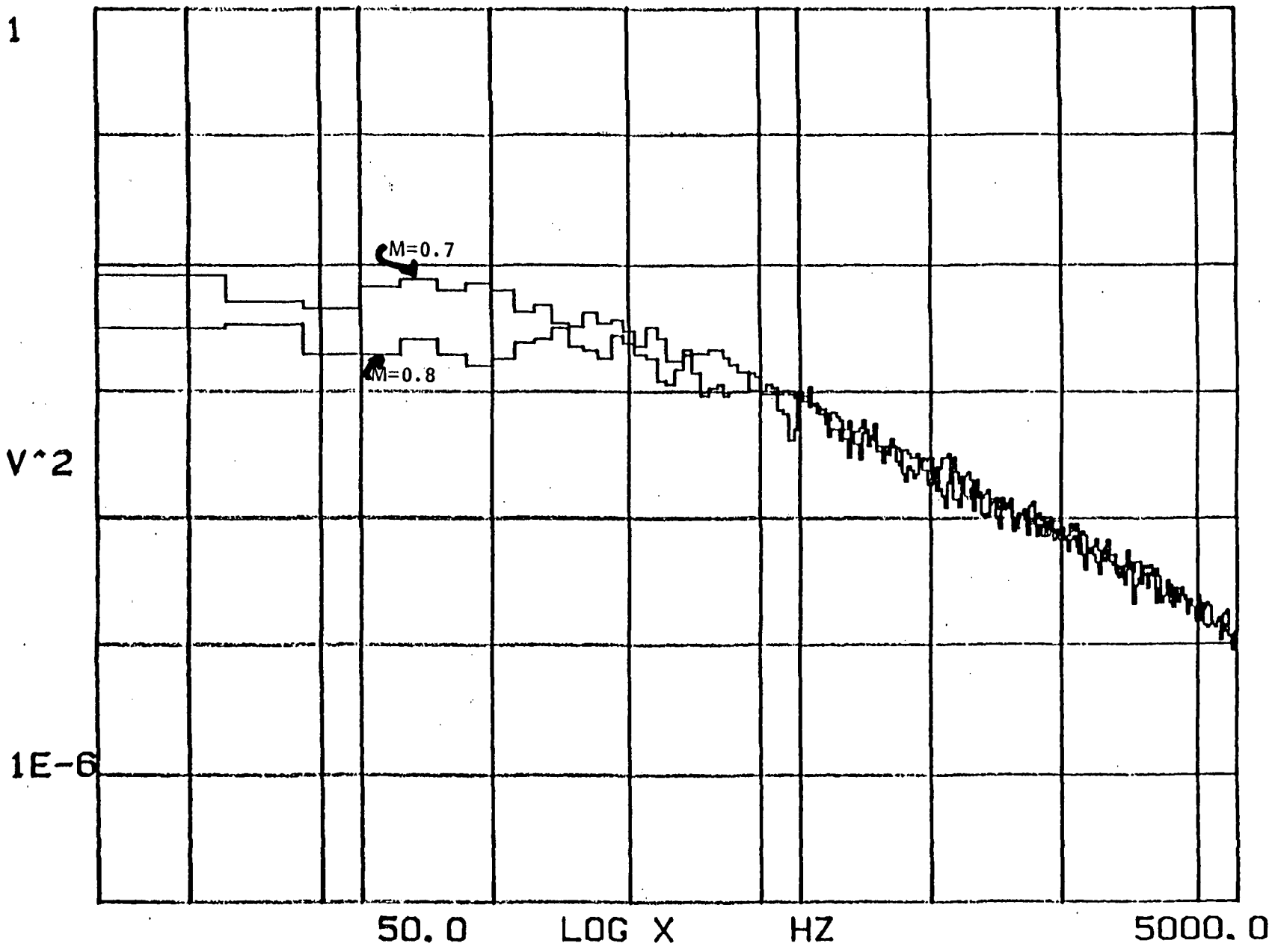

Figure 4. Comparison of shear layer spectra on KAO at M = 0.8 and 0.7, 8/40/30 fence.

Fence Angle	Alt, Ft	L, in	$\bar{\ell}_z$, in	σ, μm	$\langle P_{LT} \rangle$, μrad
30°	37,000	11.0	2.35	.222	8.68
↓	39,000	12.0	2.30	.226	9.03
↓	41,000	12.5	2.45	.231	8.66
45°	39,000	10.0	2.20	.205	8.56
↓	41,000	10.0	2.20	.207	8.64
60°	37,000	12.5	2.35	.206	8.05
↓	39,000	12.5	2.40	.219	8.38
↓	41,000	12.0	2.50	.235	8.63
90°	37,000	14.0	2.10	.219	9.58
↓	41,000	14.5	2.10	.188	8.22

Figure 5. Summary of aerodynamic properties from the KAO
a) M = 0.8

Fence Angle	Alt, Ft	L, in	ℓ_z, in	σ, μm	$\langle P_{LT} \rangle$, μrad
30°	37,000	12.5	2.65	.286	9.91
↓	39,000	12.5	2.50	.257	9.44
	41,000	11.0	2.70	.237	8.06
45°	39,000	12.0	3.10	.269	7.97
60°	37,000	13.0	3.05	.316	9.52
↓	39,000	12.5	2.80	.218	7.15
	41,000	12.0	2.85	.258	8.32
90°	37,000	12.0	3.00	.170	5.21
↓	41,000	13.0	3.00	.244	7.47

Figure 5. Concluded

b) M = 0.7

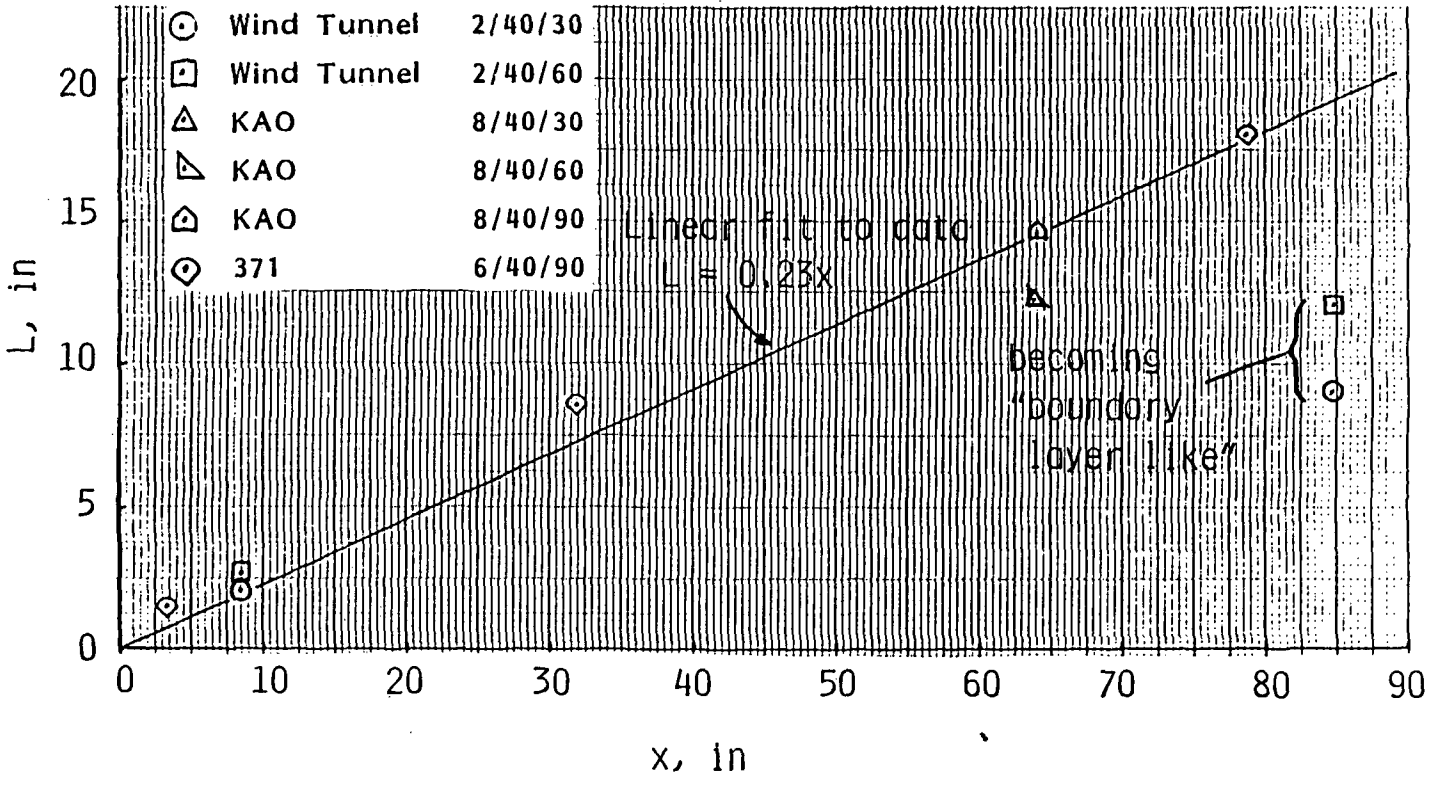

Figure 6. Growth of shear layer width with distance downstream of origin.

a) M = 0.8

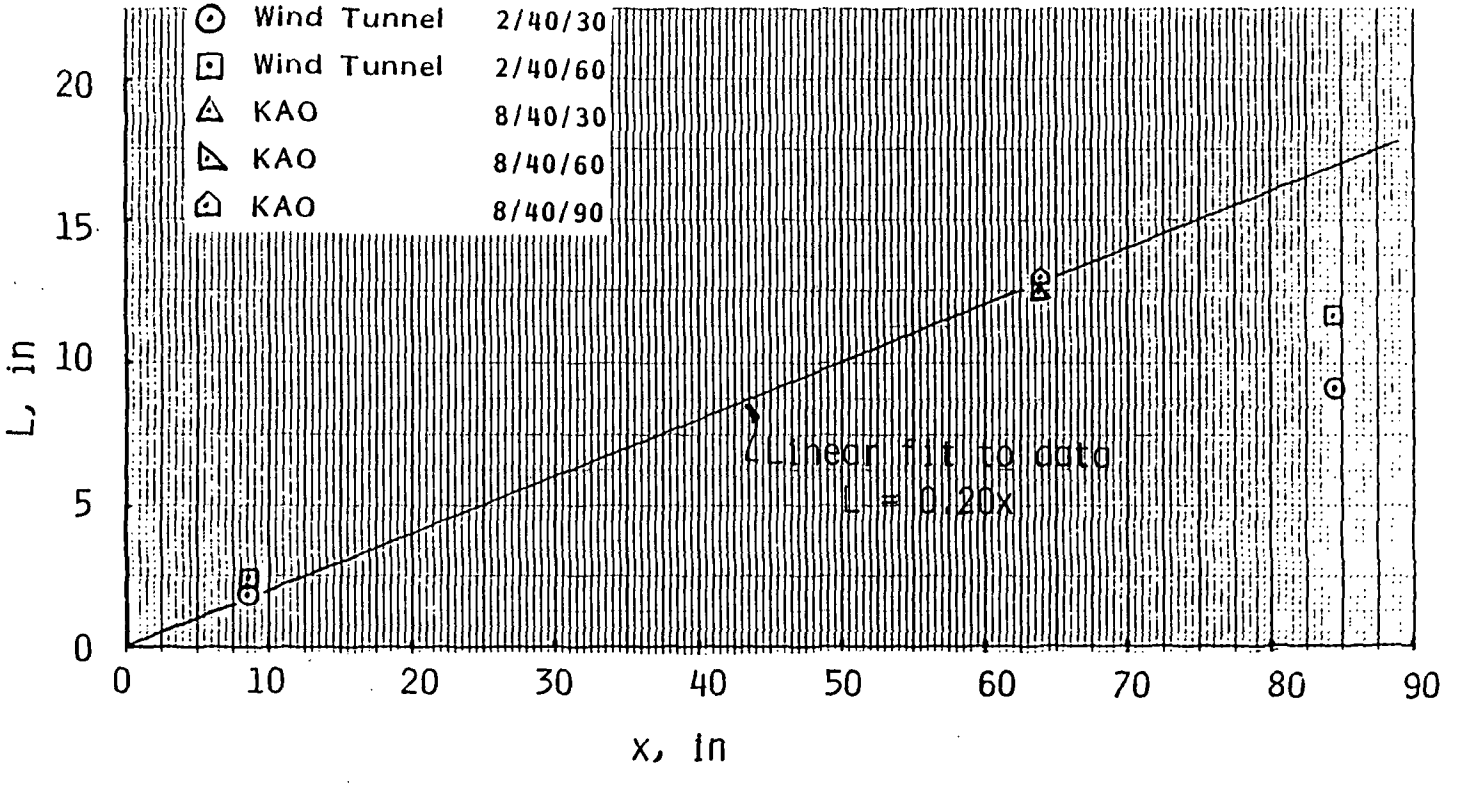

Figure 6. Concluded

b) M = 0.7

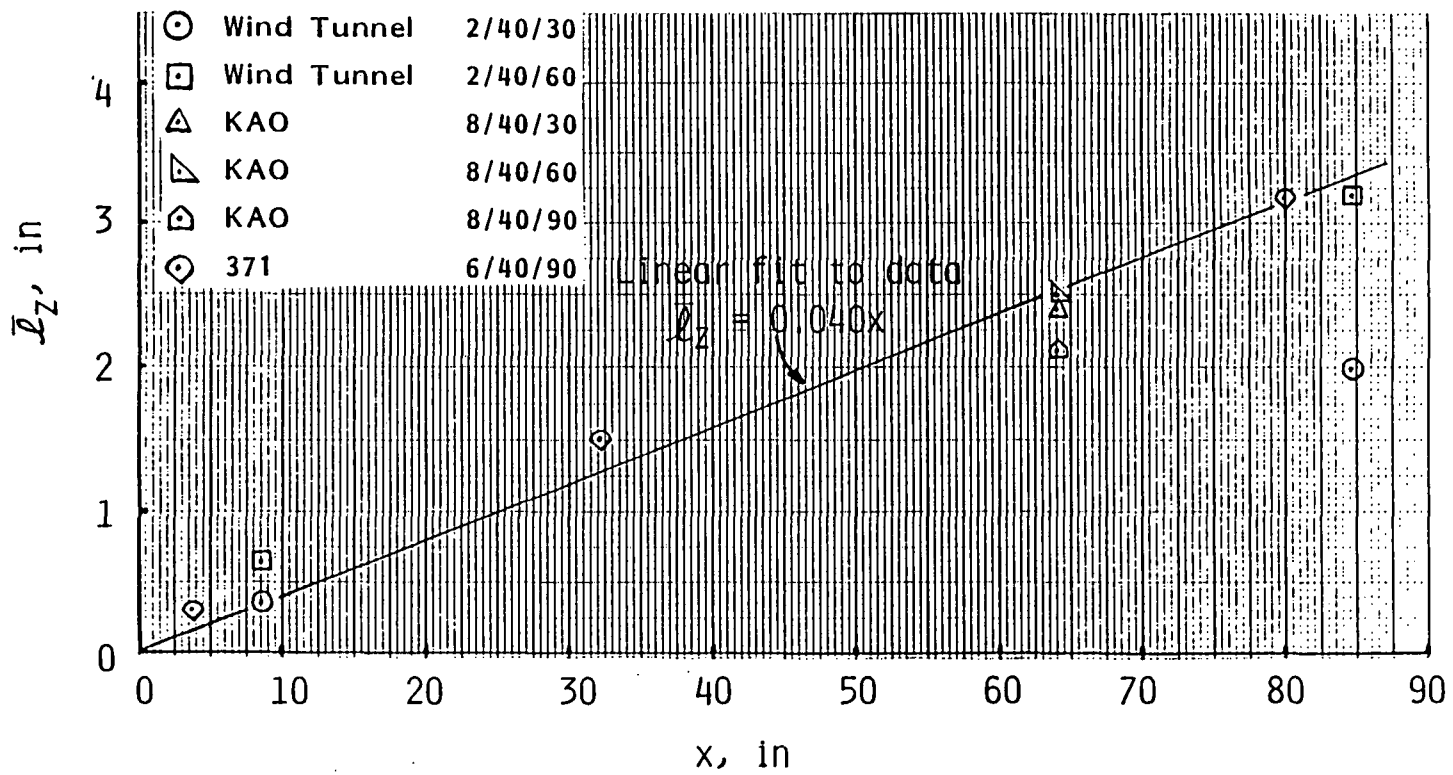

Figure 7. Growth of integral scale length with distance downstream of origin.
a) M = 0.8

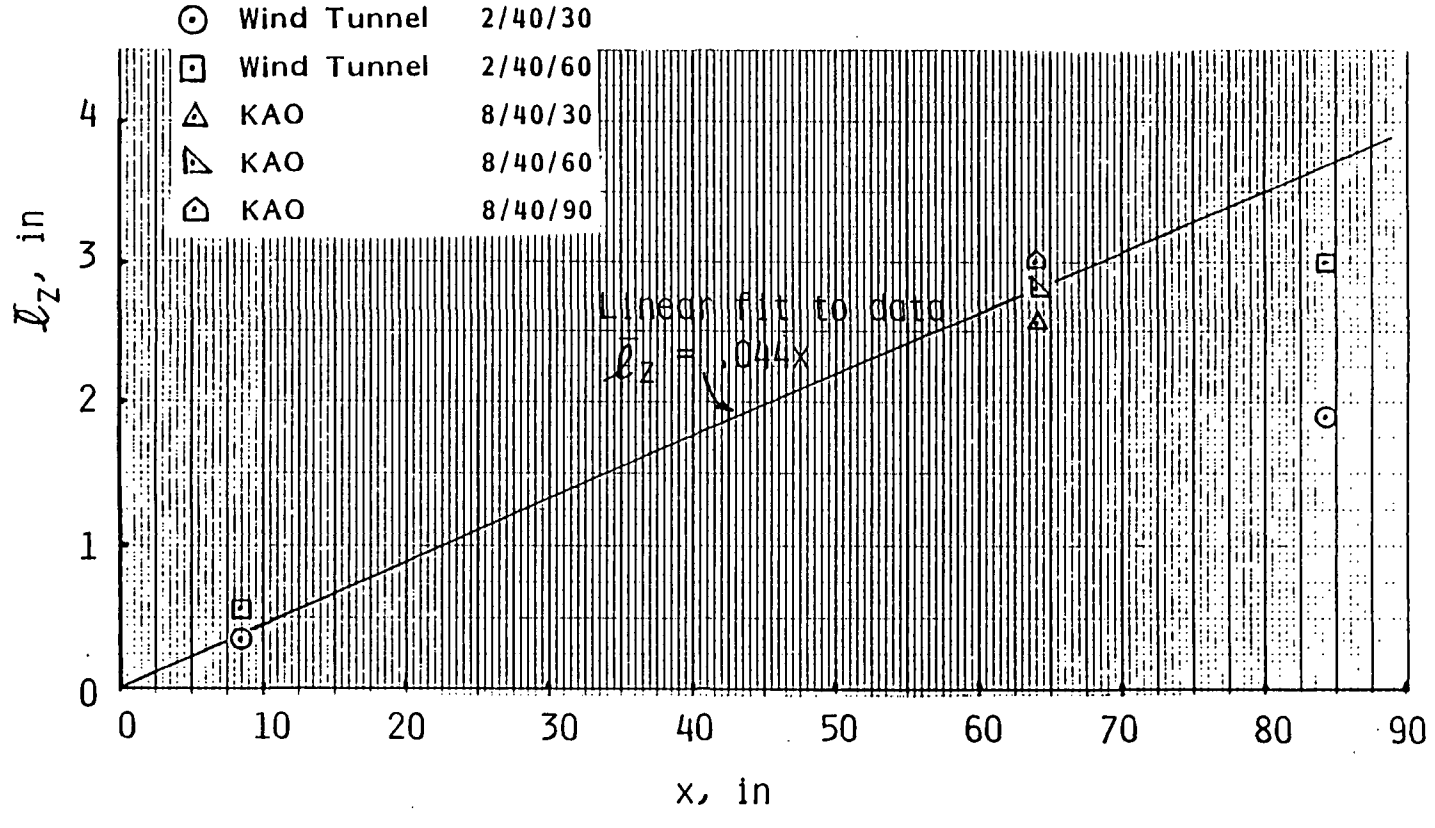

Figure 7. Concluded

b) M = 0.7

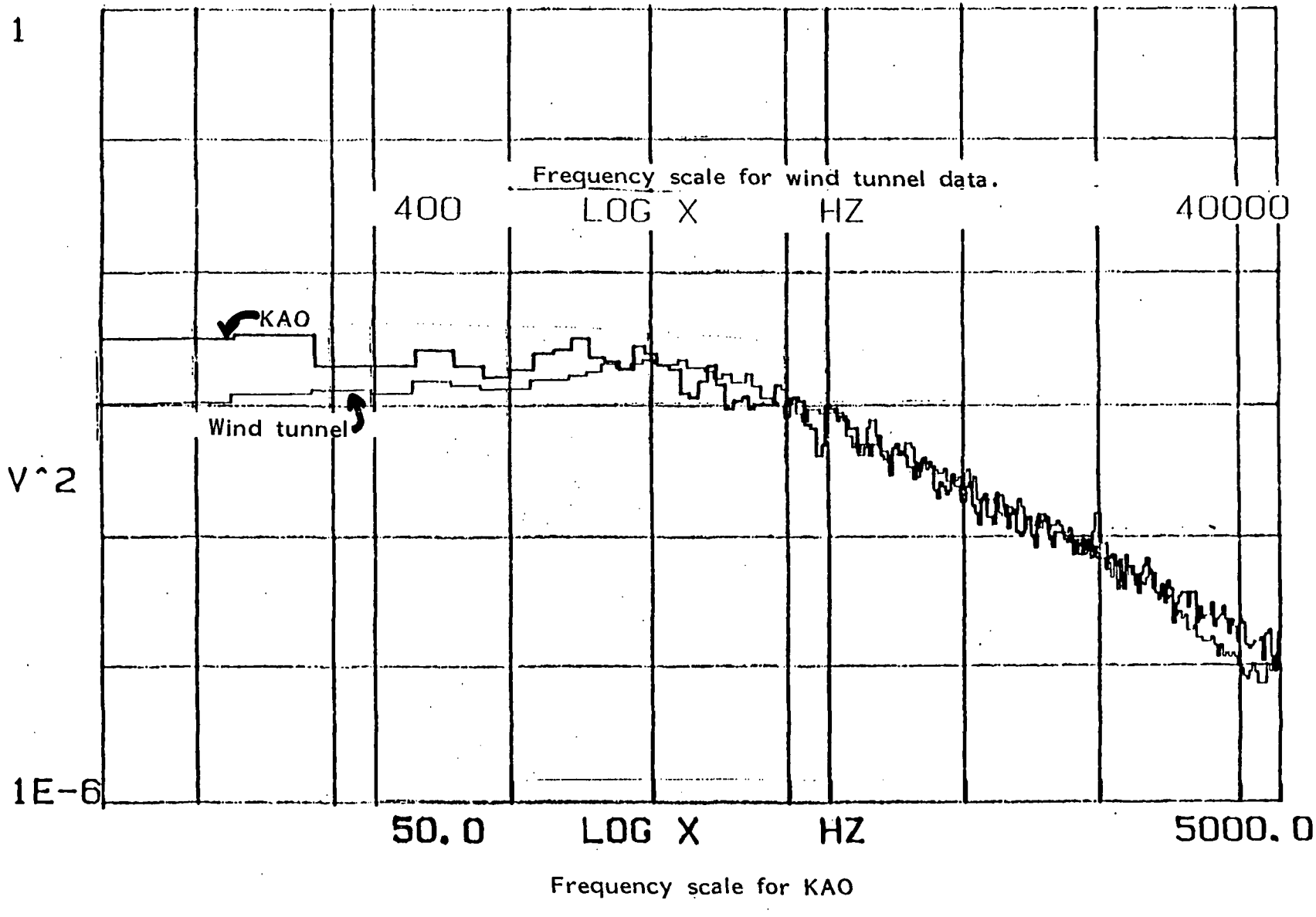

Figure 8. Comparison of KAO and wind tunnel spectra for 8/40/30 & 2/40/30 fences.

a) M = 0.8

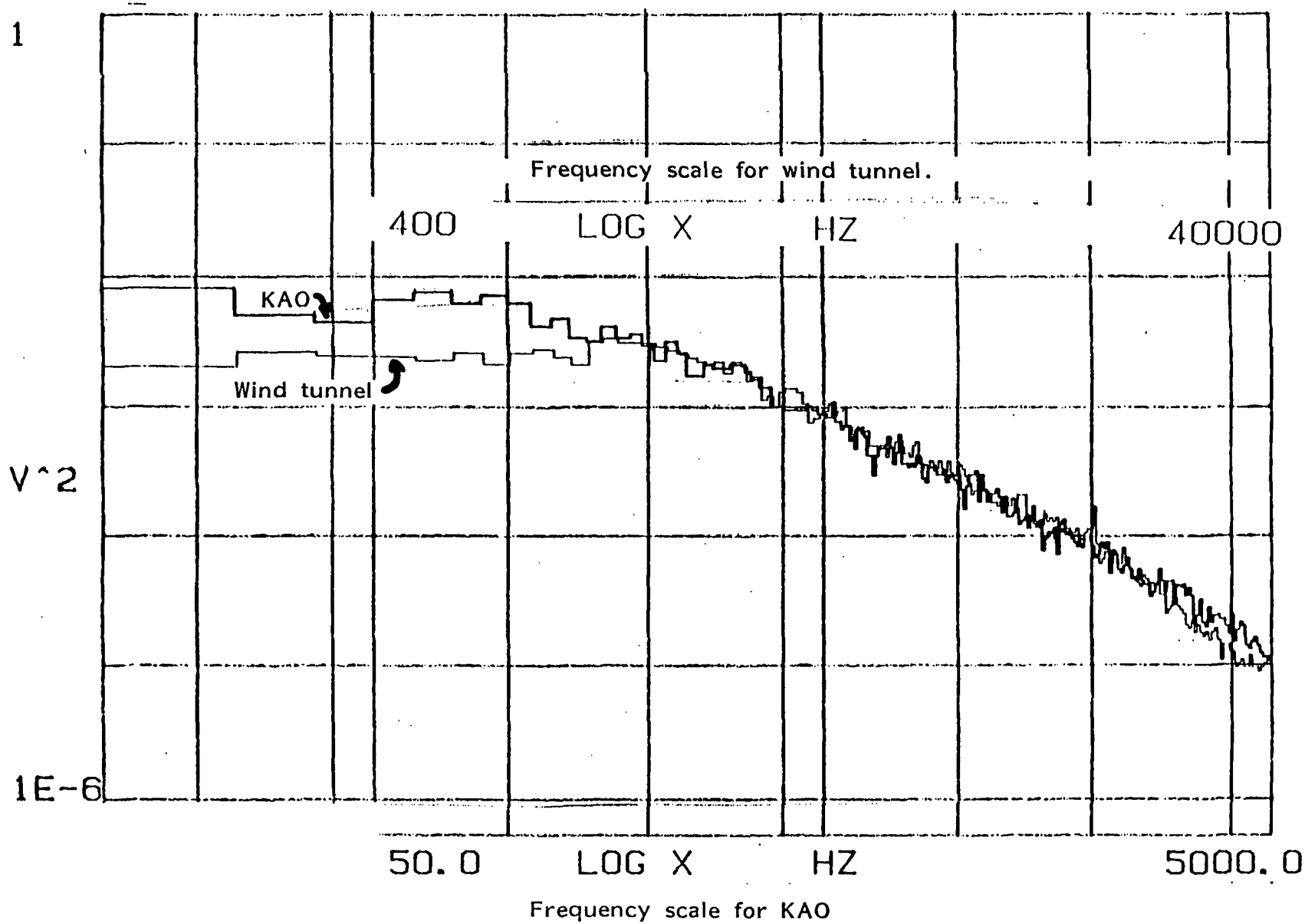

Figure 8. Concluded

b) M = 0.7

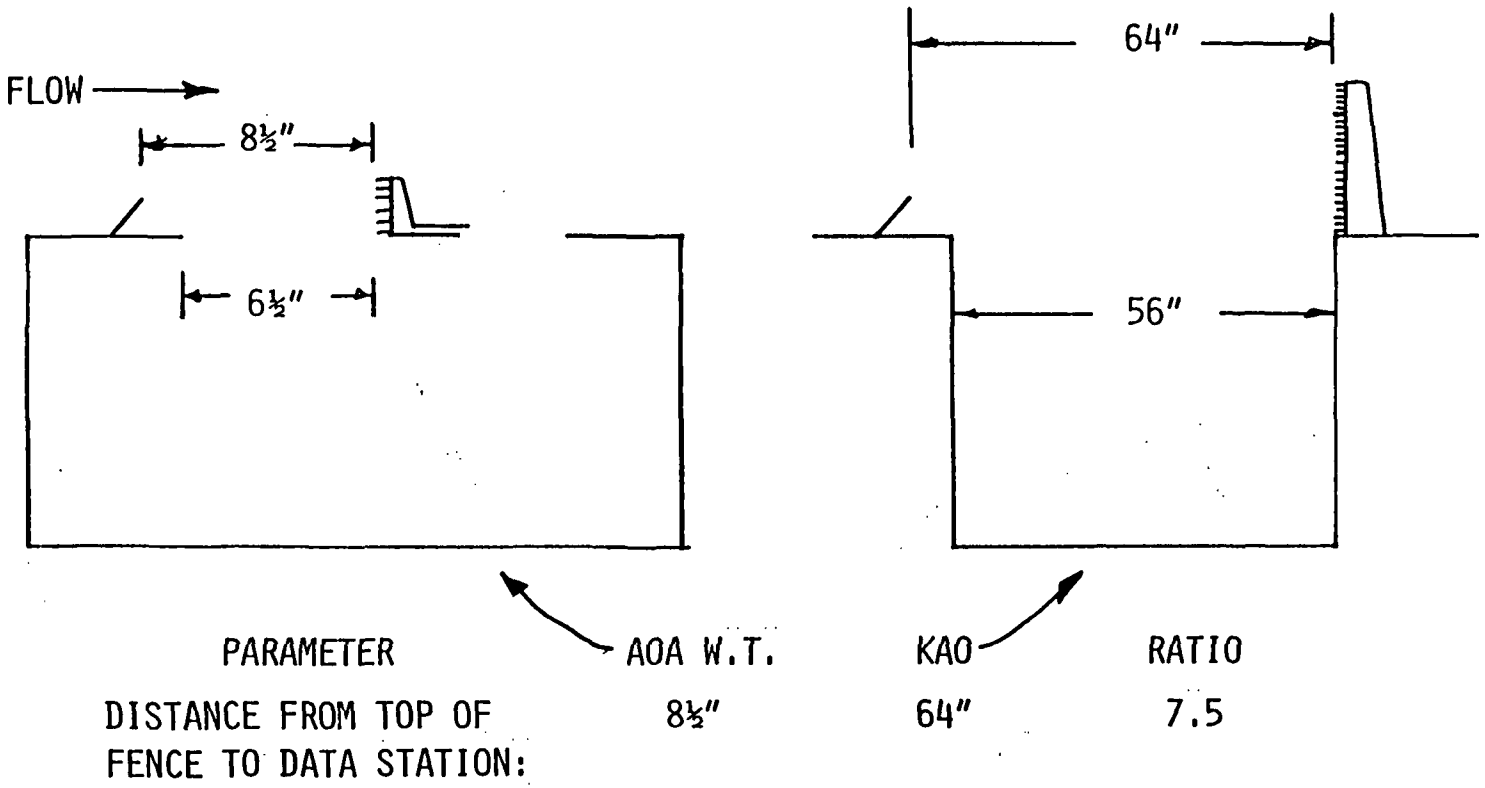

Figure 9. Schematic of wind tunnel and KAO cavity and instrumentation.

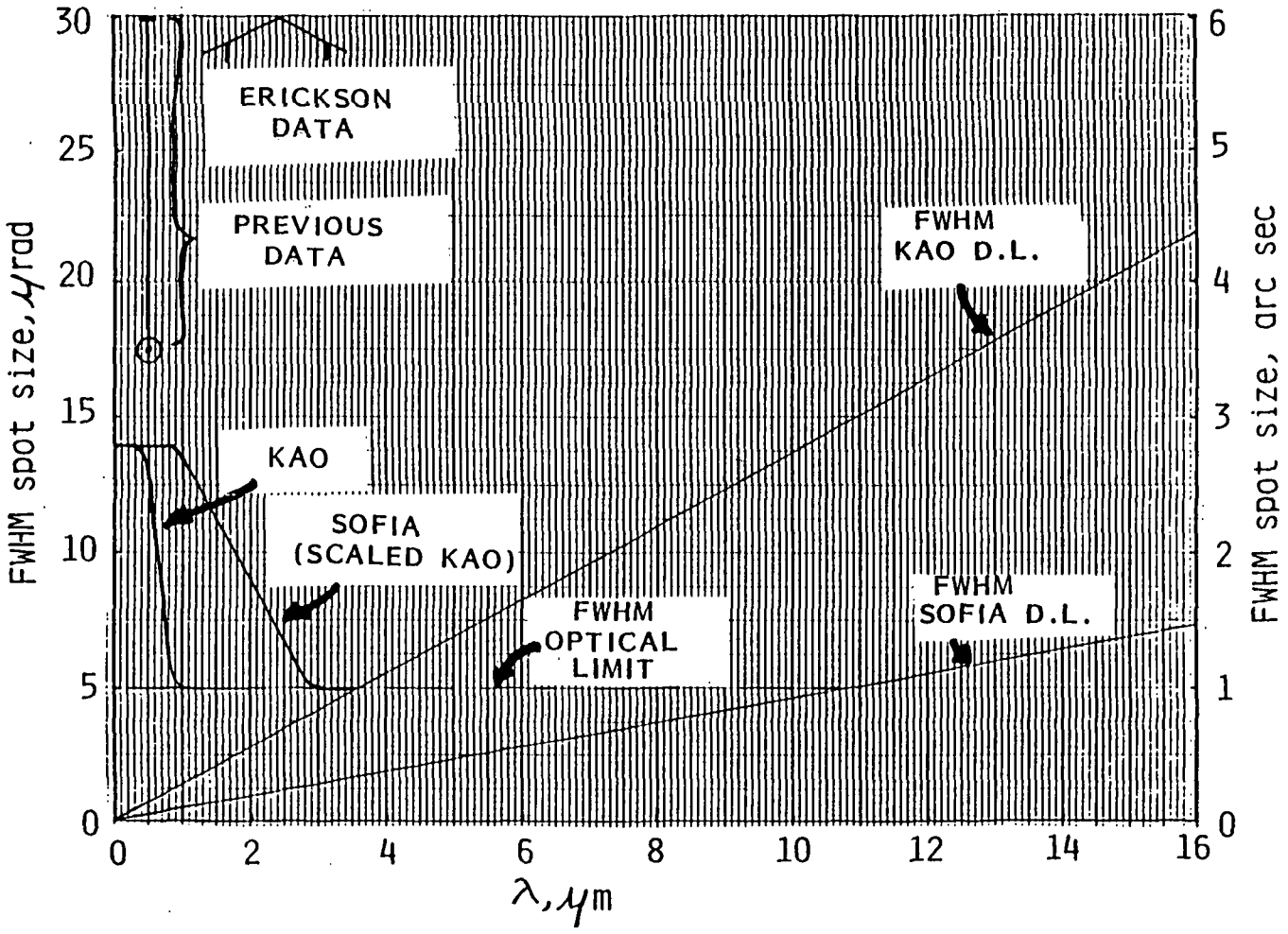

Figure 10. Behavior of focal plane long-time spot size with wavelength.

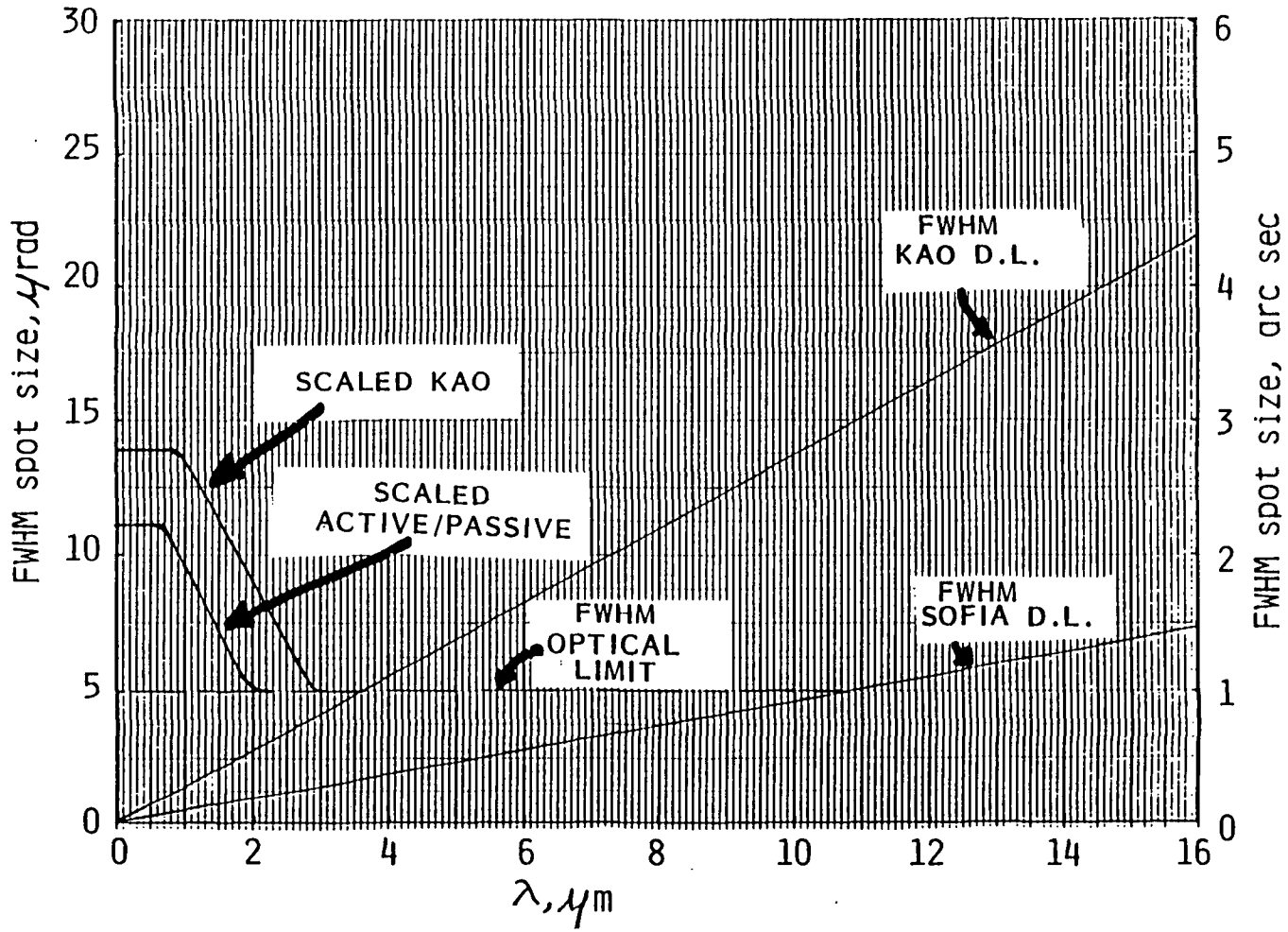

Figure 11. Potential improvement in visible and near IR regions due to active control.

VIII. APPENDIX

APPENDIX A

DATA OBTAINED AT M = 0.70

APPENDIX A.1

FLIGHT ALTITUDE 37,000 ft

BLC ANGLES 30°, 60°, 90°

ANEMOMETER DATA SET

ALTITUDE: 36500 FT
MACH NO: 0.70
BLC POS: 30 DEG
SEQ NO: 2

FLIGHT NO: KITE 5
DATE: 28 JANUARY 1986

AIR TEMP: -38.3

SEN NO	DIST	DC VOL	RMS VOL	MACH NO	FLU DEN	RHO'*1.0E6	Lz
21	9	4.0346	0.4060	0.225	0.0006324	6.315472	2.28
24	11	4.4580	0.3729	0.355	0.0006422	12.889927	2.70
26	13	5.1891	0.3494	0.500	0.0006550	20.047004	2.77
28	15	5.4551	0.1931	0.628	0.0006727	16.223111	2.37
30	17	5.5821	0.0659	0.690	0.0006829	6.448602	1.02
32	19	5.1921	0.0262	0.693	0.0006834	2.778543	
34	21	4.7301	0.0003	0.695	0.0006842	0.035133	
36	23	6.3387		0.693	0.0006848		

AERODYNAMIC WAVEFRONT ERROR

DIST	RHO'SQ*Lz	SIGMA SQ
9	6.138E-07	
11	3.028E-06	9.7870E-15
13	7.514E-06	3.8117E-14
15	4.210E-06	6.9625E-14
17	2.863E-07	8.1709E-14

SIGMA = 2.8585E-07 , meters

SIGMA = 0.286 , microns

SIGMA/LAMDA = 0.539 , wave

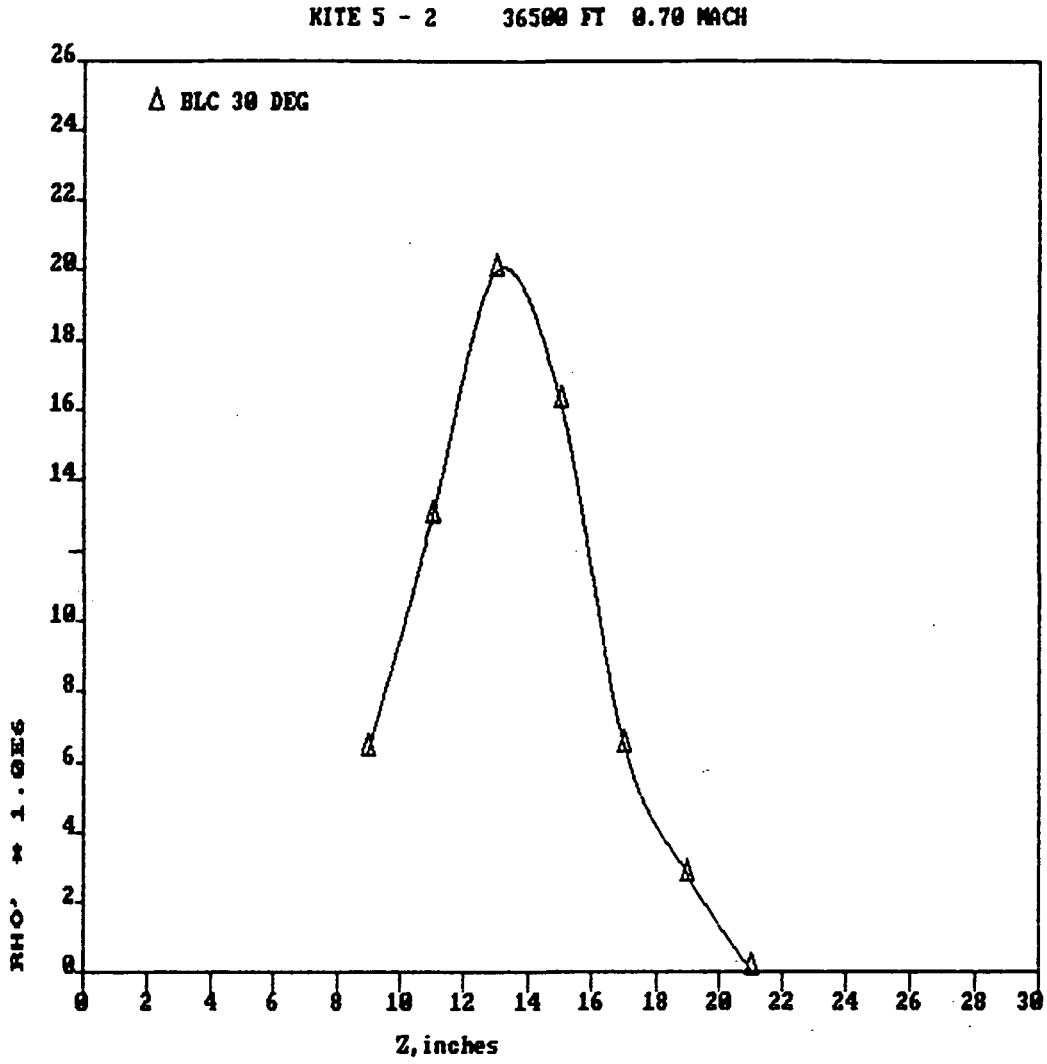
KITE 5 - 2 36500 FT 0.70 MACH
Δ BLC 30 DEG
RHO' * 1.0E6
Z, inches
0
2
4
6
8
10
12
14
16
18
20
22
24
26
28
30

ANEMOMETER DATA SET

ALTITUDE: 36600 FT
MACH NO: 0.70
BLC POS: 60 DEG
SEQ NO: 3

FLIGHT NO: KITE 5
DATE: 28 JANUARY 1986

AIR TEMP: -39.5

SEN NO	DIST	DC VOL	RMS VOL	MACH NO	FLU DEN	RHO'*1.0E6	Lz
21	9	3.7970	0.3647	0.130	0.0006406	2.065727	2.41
24	11	3.7298	0.3364	0.140	0.0006398	2.244446	2.07
26	13	4.0784	0.4143	0.192	0.0006420	4.738440	2.35
28	15	4.3936	0.4207	0.260	0.0006466	8.150364	3.01
30	17	4.6926	0.3924	0.380	0.0006580	15.022818	3.07
32	19	4.6840	0.2637	0.522	0.0006761	18.704502	3.14
34	21	4.5046	0.1486	0.628	0.0006919	15.550310	2.89
36	23	6.2826	0.0579	0.695	0.0007023	5.240160	

AERODYNAMIC WAVEFRONT ERROR

DIST	RHO'SQ*Lz	SIGMA SQ
9	6.942E-08	
11	7.039E-08	3.7570E-16
13	3.562E-07	1.5220E-15
15	1.350E-06	6.1060E-15
17	4.677E-06	2.2301E-14
19	7.415E-06	5.4796E-14
21	4.717E-06	8.7400E-14
23	0	1.0008E-13

SIGMA = 3.1635E-07 ,meters

SIGMA = 0.316 ,microns

SGMA/LAMDA = 0.597 ,wave

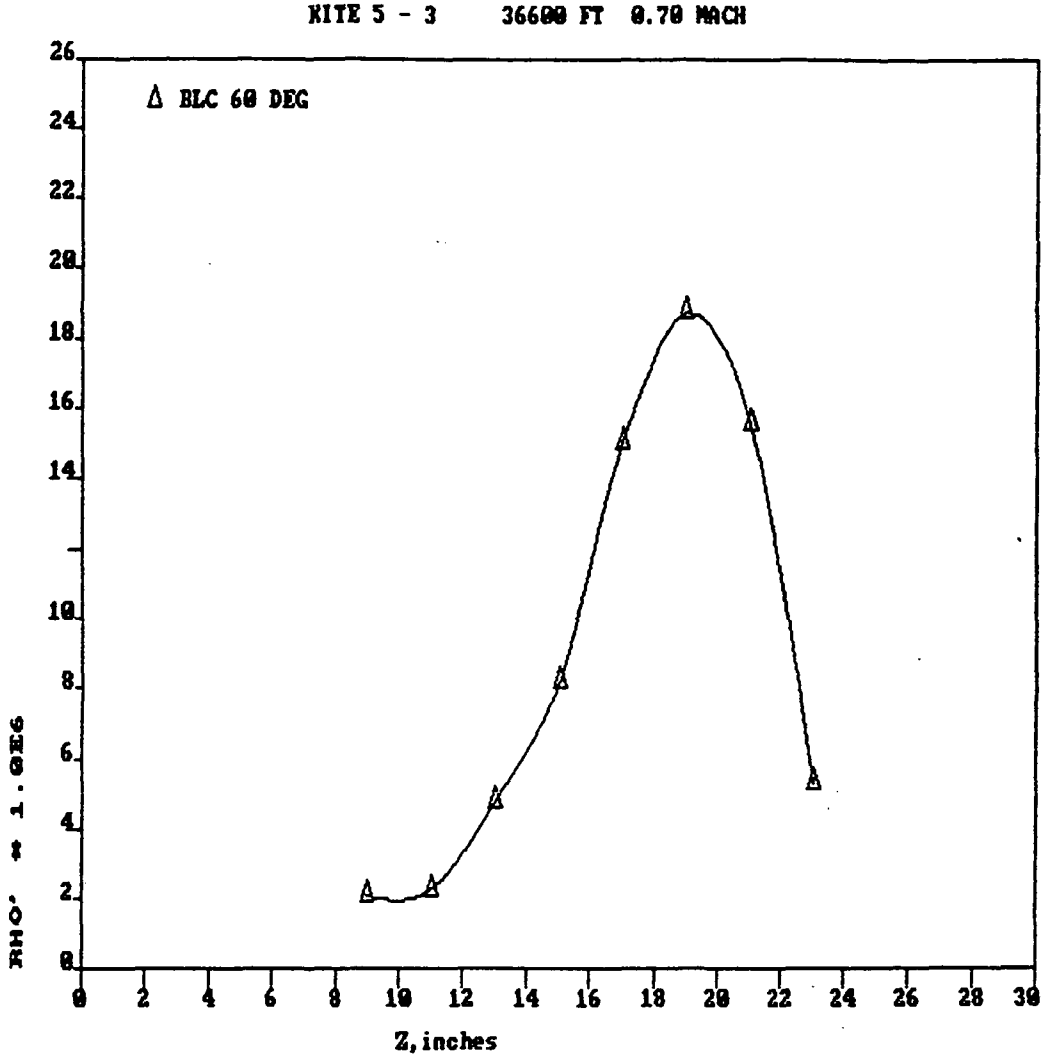
KITE 5 - 3 36600 FT 0.70 MACH
Δ BLC 60 DEG
RHO' * 1.0E6
Z, inches
0
2
4
6
8
10
12
14
16
18
20
22
24
26
28
30

ANEMOMETER DATA SET

ALTITUDE: 36800 FT
MACH NO: 0.70
BLC POS: 90 DEG
SEQ NO: 4

FLIGHT NO: KITE 5
DATE: 28 JANUARY 1986

AIR TEMP: -38.6

SEN NO	DIST	DC VOL	RMS VOL	MACH NO	FLU DEN	RHO'*1.0E6	Lz
21	9	3.7197	0.3490	0.025	0.0006065	0.071113	3.04
24	11	3.6849	0.3386	0.025	0.0006046	0.069427	2.28
26	13	3.8547	0.4006	0.025	0.0006046	0.078522	1.67
28	15	4.0476	0.3869	0.100	0.0006129	1.167044	2.45
30	17	4.5218	0.3531	0.215	0.0006157	4.364210	2.94
32	19	4.4876	0.3320	0.355	0.0006216	11.034758	2.69
34	21	4.4299	0.1483	0.485	0.0006349	9.139301	3.25
36	23	6.1473	0.1212	0.610	0.0006560	8.378228	

AERODYNAMIC WAVEFRONT ERROR

DIST	RHO'SQ*Lz	SIGMA SQ
9	1.038E-10	
11	7.418E-11	4.7822E-19
13	6.950E-11	8.6434E-19
15	2.252E-08	6.1580E-17
17	3.780E-07	1.1378E-15
19	2.211E-06	8.0952E-15
21	1.832E-06	1.8961E-14
25	0	2.8809E-14

SIGMA = 1.6973E-07 , meters

SIGMA = 0.170 , microns

SIGMA/LAMDA = 0.320 , wave

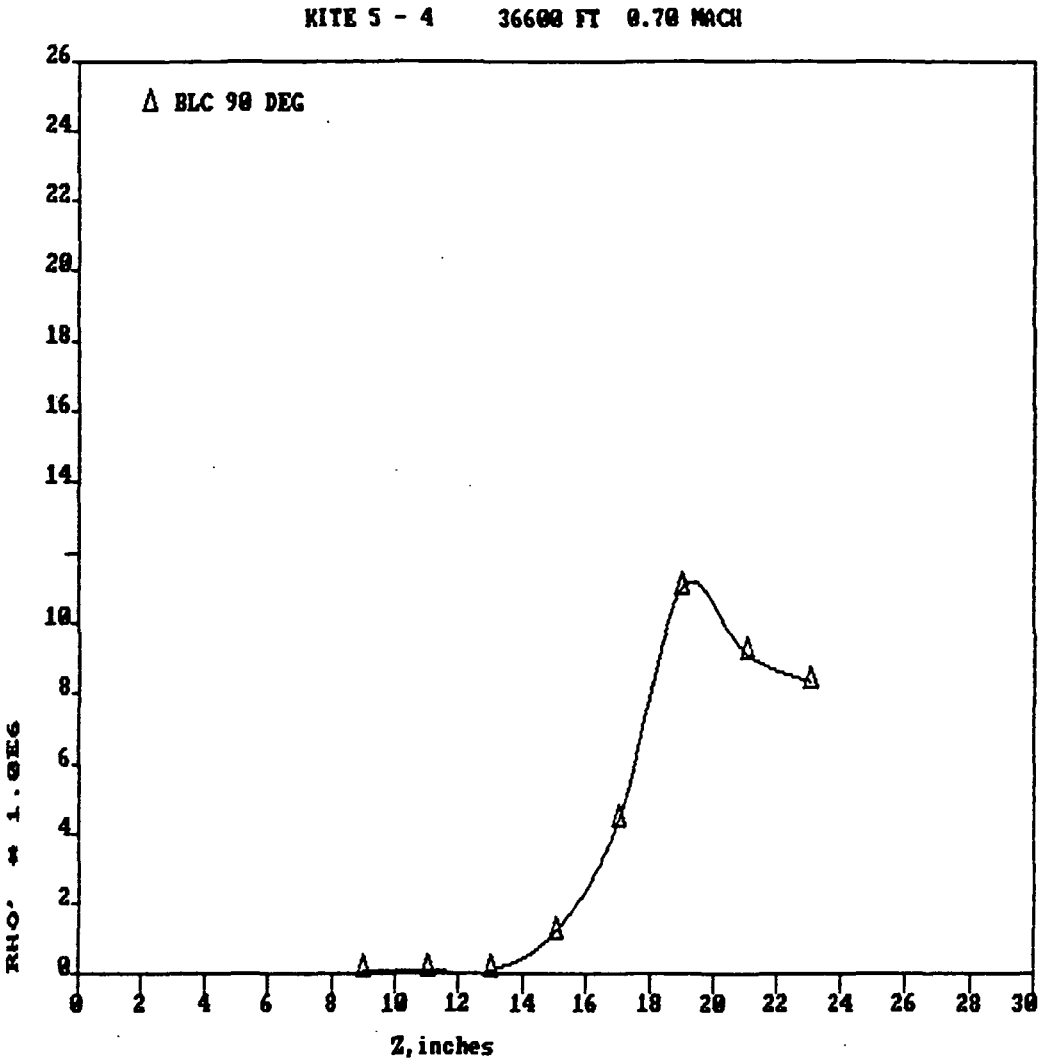

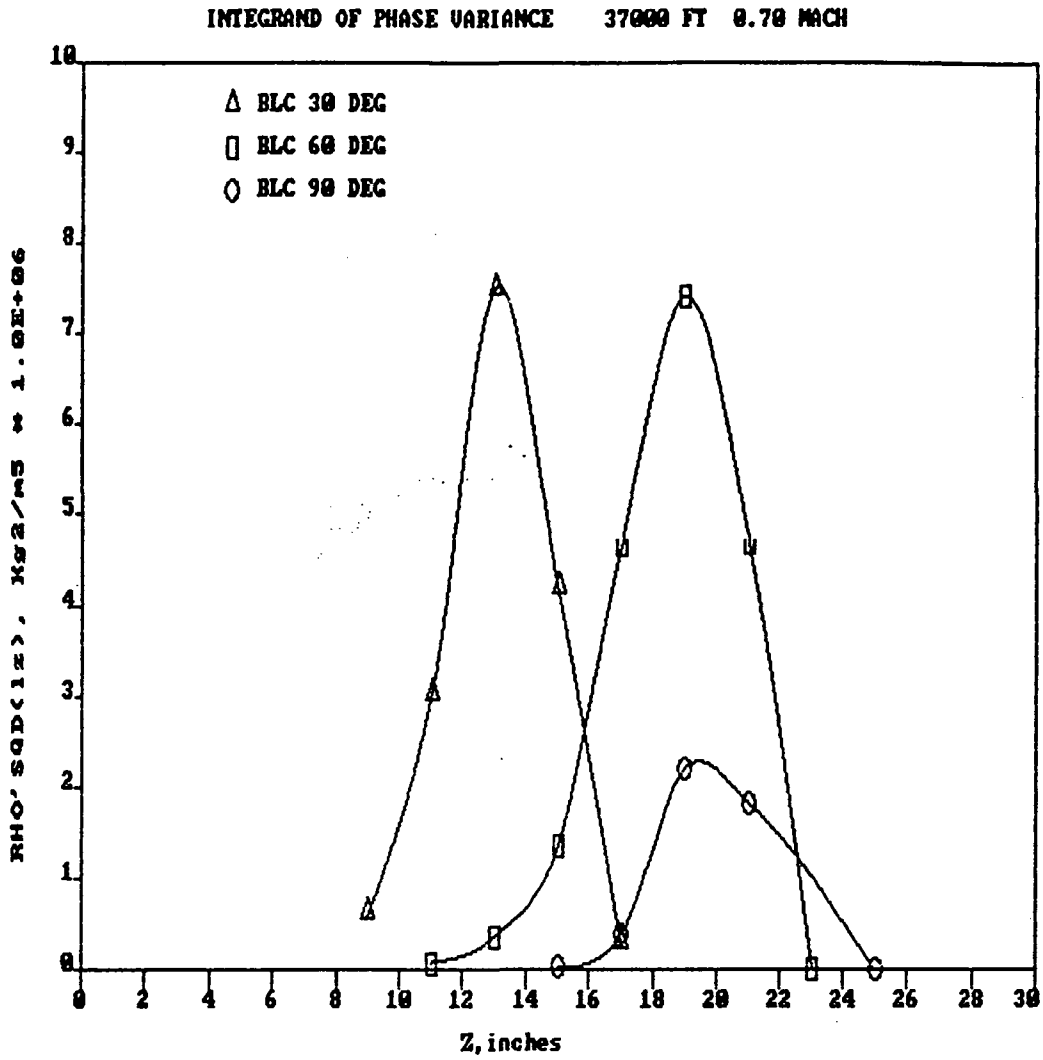
INTEGRAND OF PHASE VARIANCE 37000 FT 0.70 MACH
Δ BLC 30 DEG
□ BLC 60 DEG
○ BLC 90 DEG
RHO*SQD(1z), Kg2/m5 * 1.0E+06
Z, inches
0
1
2
3
4
5
6
7
8
9
10
0
2
4
6
8
10
12
14
16
18
20
22
24
26
28
30

APPENDIX A.2

FLIGHT ALTITUDE 39,000 ft

BLC ANGLES 30°, 45°, 60°

ANEMOMETER DATA SET

ALTITUDE: 38700 FT
MACH NO: 0.70
BLC POS: 30 DEG
SEQ NOS: 1A, 1B

FLIGHT NO: KITE 4
DATE: 25 JANUARY 1986

AIR TEMP: -45.1

SEN NO	DIST	DC VOL	RMS VOL	MACH NO	FLU DEN	RHO'*1.0E6	Lz
19	8	3.9097	0.3980	0.192	0.0005902	4.365300	1.83
21	9	3.8836	0.3848	0.209	0.0005911	5.028766	2.17
23	10	4.3934	0.4533	0.259	0.0005945	8.014322	2.38
24	11	4.1646	0.3781	0.324	0.0005980	10.939334	2.37
25	12	4.4933	0.3477	0.397	0.0006010	13.790299	2.59
26	13	5.0282	0.3677	0.469	0.0006174	18.255794	2.64
27	14	5.1718	0.2938	0.538	0.0006162	18.161373	2.45
28	15	5.3164	0.1796	0.602	0.0006261	13.389503	2.23
29	16	5.9707	0.1680	0.653	0.0006355	13.027495	2.13
30	17	5.5101	0.0833	0.684	0.0006419	7.648782	2.51
31	18	5.1847	0.0633	0.691	0.0006455	6.319074	1.90
32	19	5.1497	0.0231	0.693	0.0006467	2.337313	
33	20	4.9215	0.0016	0.695	0.0006470	0.170298	

AERODYNAMIC WAVEFRONT ERROR

DIST	RHO'SQ*Lz	SIGMA SQ
8	2.354E-07	
9	3.704E-07	8.1399E-16
10	1.032E-06	2.6981E-15
11	1.914E-06	6.6569E-15
12	3.325E-06	1.3696E-14
13	5.939E-06	2.6144E-14
14	5.455E-06	4.1453E-14
15	2.699E-06	5.2408E-14
16	2.440E-06	5.9313E-14
17	9.912E-07	6.3923E-14
18	5.121E-07	6.5943E-14

SIGMA = 2.5679E-07 , meters

SIGMA = 0.257 , microns

SIGMA/LAMDA = 0.485 , wave

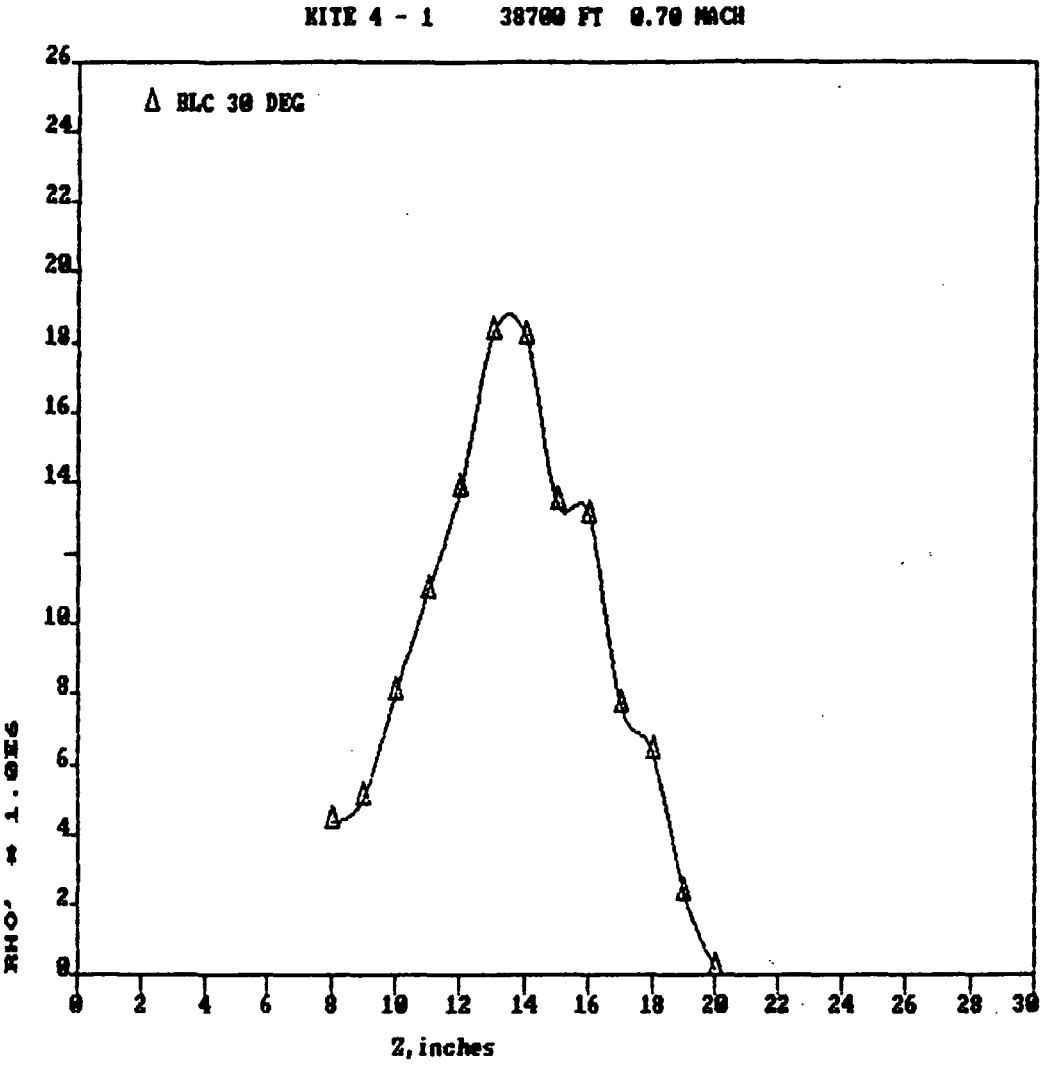
KITE 4 - 1 38700 FT 0.70 MACH
Δ BLC 30 DEG
RHO' * 1.0E6
Z, inches
0
2
4
6
8
10
12
14
16
18
20
22
24
26
28
30

ANEMOMETER DATA SET

ALTITUDE: 38800 FT
MACH NO: 0.70
BLC POS: 45 DEG
SEQ NOS: 2A, 2B, 2C

FLIGHT NO: KITE 4
DATE: 25 JANUARY 1986

AIR TEMP: -46.2

SEN NO	DIST	DC VOL	RMS VOL	MACH NO	FLU DEN	RHO'*1.0E6	Lz
19	8	3.1699	0.3009	0.155	0.0005935	2.681249	1.98
21	9	3.2066	0.2977	0.155	0.0005935	2.622373	1.36
23	10	3.5674	0.3464	0.164	0.0005939	3.069091	1.45
24	11	3.6687	0.3374	0.185	0.0005945	3.691926	1.71
25	12	3.7383	0.3551	0.208	0.0005956	4.812120	2.13
26	13	4.2144	0.4738	0.248	0.0005980	8.071213	2.78
27	14	4.5121	0.4528	0.304	0.0006018	10.764463	3.03
28	15	5.2804	0.4159	0.365	0.0006069	12.092247	3.26
29	16	5.4058	0.3751	0.421	0.0006126	14.070541	3.29
30	17	5.1096	0.2654	0.485	0.0006196	13.838399	3.21
31	18	4.8839	0.2268	0.562	0.0006285	16.368754	2.67
32	19	5.0232	0.1567	0.632	0.0006284	13.502592	2.65
33	20	4.8343	0.1185	0.682	0.0006459	12.417836	2.24
34	21	4.6908	0.0650	0.700	0.0006495	7.374634	1.32
35	22	5.6100	0.0174	0.708	0.0006513	1.686941	0.56
36	23	6.2416		0.711	0.0006519		
37	24	5.7143		0.712	0.0006519		

AERODYNAMIC WAVEFRONT ERROR

DIST	RHO'SQ*Lz	SIGMA SQ
8	9.608E-08	
9	6.313E-08	2.1393E-16
10	9.219E-08	4.2262E-16
11	1.573E-07	7.5789E-16
12	3.329E-07	1.4166E-15
13	1.222E-06	3.5065E-15
14	2.370E-06	8.3334E-15
15	3.218E-06	1.5841E-14
16	4.397E-06	2.6072E-14
17	4.149E-06	3.7555E-14
18	4.829E-06	4.9619E-14
19	3.261E-06	6.0489E-14
20	2.332E-06	6.8004E-14
21	4.846E-07	7.1788E-14
22	1.076E-08	7.2453E-14

SIGMA = 2.6917E-07 , meters

SIGMA = 0.269 , microns

SIGMA/LAMDA = 0.508 , wave

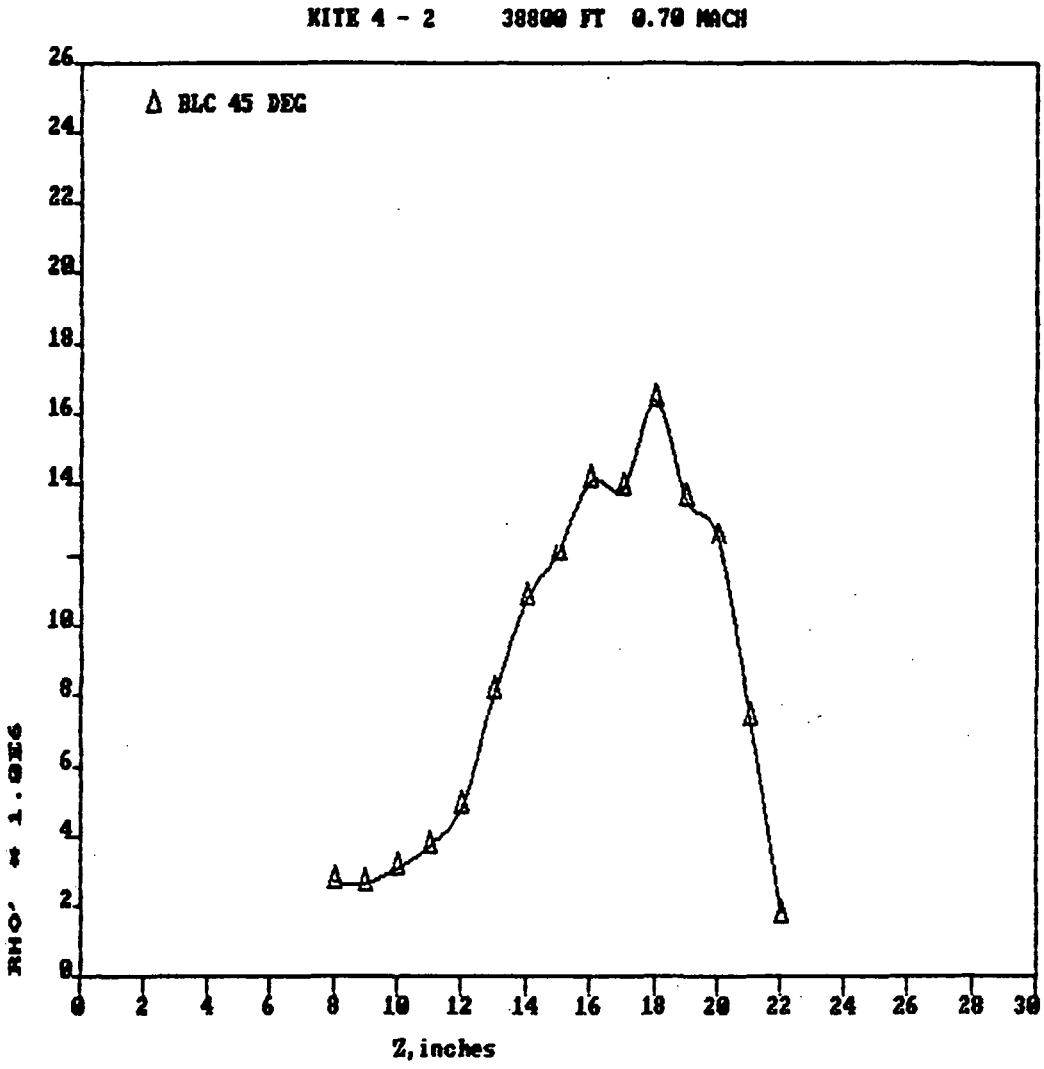
KITE 4 - 2 38800 FT 0.70 MACH
Δ BLC 45 DEG
RHO' * 1.0E6
Z, inches
0
2
4
6
8
10
12
14
16
18
20
22
24
26
28
30

ANEMOMETER DATA SET

ALTITUDE: 38900 FT
MACH NO: 0.70
BLC POS: 60 DEG
SEQ NOS: 3A, 3B, 3C

FLIGHT NO: KITE 4
DATE: 25 JANUARY 1986

AIR TEMP: -46.8

SEN NO	DIST	DC VOL	RMS VOL	MACH NO	FLU DEN	RHO'*1.0E6	Lz
19	8	3.5689	0.3564	0.120	0.0005931	1.696014	2.67
21	9	3.0837	0.2983	0.120	0.0005938	1.644824	2.41
23	10	3.3411	0.3703	0.130	0.0005945	2.212111	1.97
24	11	3.6751	0.3272	0.138	0.0005896	1.984239	1.95
25	12	3.6400	0.3203	0.140	0.0005945	2.034707	1.77
26	13	3.4849	0.3577	0.160	0.0005952	3.096257	1.76
27	14	3.4904	0.3419	0.192	0.0005963	4.243889	2.42
28	15	4.2730	0.3673	0.232	0.0005985	5.421347	2.75
29	16	5.1097	0.4141	0.260	0.0006001	6.402105	2.87
30	17	4.6768	0.3826	0.310	0.0006033	9.134851	3.15
31	18	4.6480	0.3341	0.380	0.0006093	11.957808	2.76
32	19	4.6426	0.2493	0.450	0.0006142	12.356633	2.85
33	20	4.6741	0.2115	0.522	0.0006240	13.875190	2.85
34	21	4.4637	0.1616	0.572	0.0006307	13.212262	2.68
35	22	5.4714	0.1137	0.628	0.0006392	9.049653	2.38
36	23	6.1854	0.0554	0.670	0.0006455	4.400457	2.80
37	24	5.7111	0.0502	0.682	0.0006465	4.457059	

AERODYNAMIC WAVEFRONT ERROR

DIST	RHO'SQ*Lz	SIGMA SQ
8	5.184E-08	
9	4.401E-08	1.2879E-16
10	6.507E-08	2.7536E-16
11	5.182E-08	4.3243E-16
12	4.946E-08	5.6852E-16
13	1.139E-07	7.8801E-16
14	2.942E-07	1.3364E-15
15	5.456E-07	2.4647E-15
16	7.940E-07	4.2647E-15
17	1.774E-06	7.7156E-15
18	2.664E-06	1.3679E-14
19	2.937E-06	2.1205E-14
20	3.704E-06	3.0128E-14
21	3.158E-06	3.9348E-14
22	1.316E-06	4.5359E-14
23	3.660E-07	4.7618E-14

SIGMA = 2.1822E-07 , meters

SIGMA = 0.218 , microns

SIGMA/LAMDA = 0.412 , wave

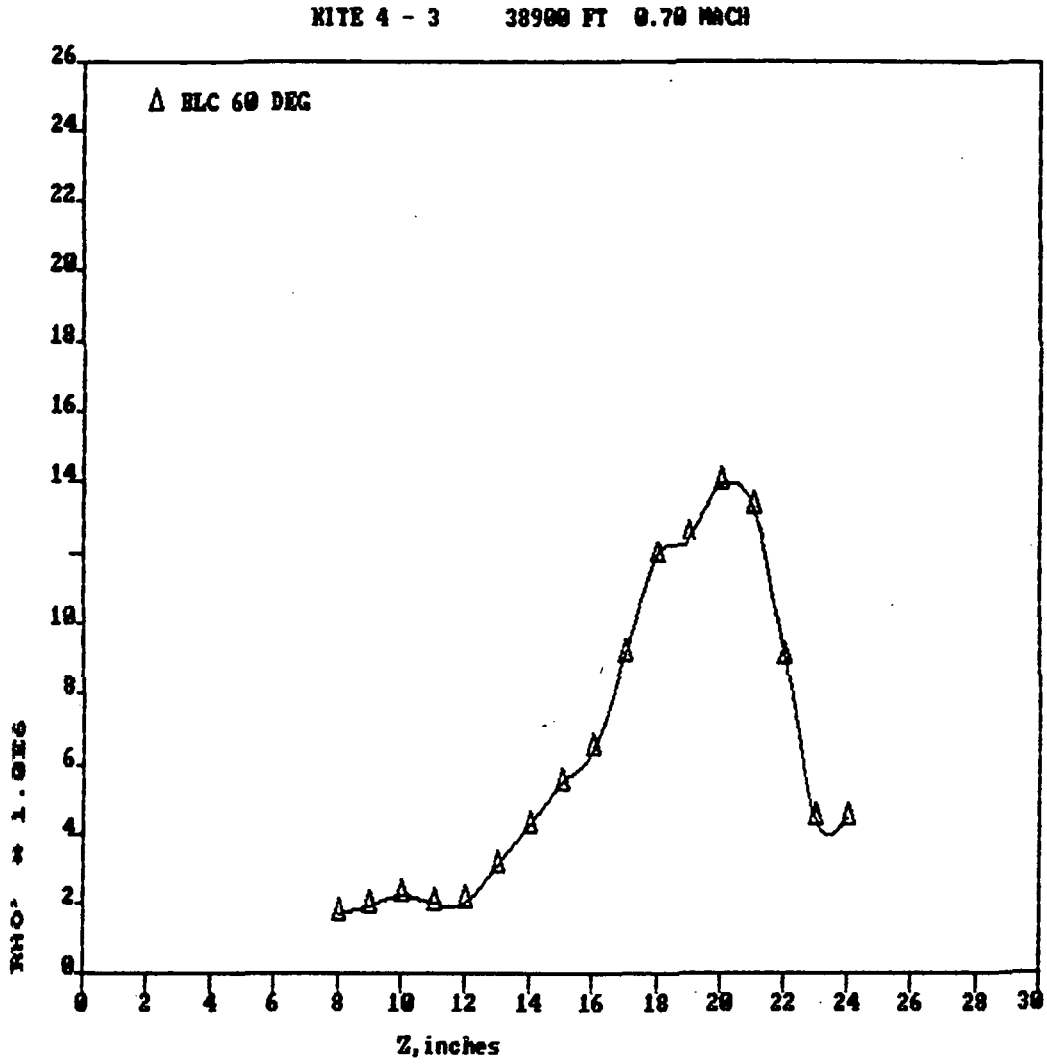
KITE 4 - 3 38900 FT 0.70 MACH
Δ HLC 60 DEG
RHO' * 1.0E6
Z, inches
0
2
4
6
8
10
12
14
16
18
20
22
24
26
28
30

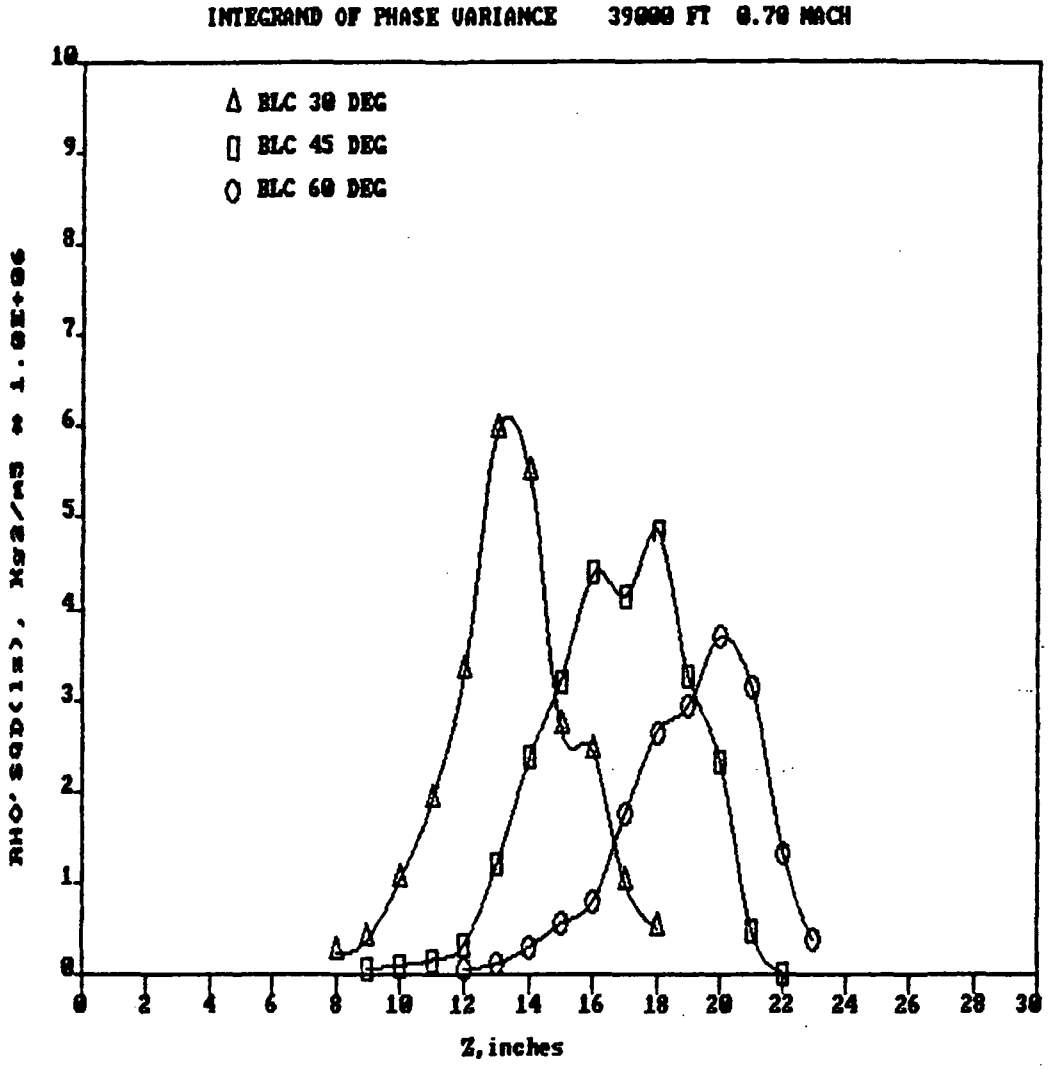
INTEGRAND OF PHASE VARIANCE 39000 FT 0.70 MACH
Δ ELC 30 DEG
[] ELC 45 DEG
○ ELC 60 DEG
RHO*SQD(1=), Xs2/m3 * 1.0E+06
Z, inches
0
1
2
3
4
5
6
7
8
9
10
0
2
4
6
8
10
12
14
16
18
20
22
24
26
28
30

APPENDIX A.3

FLIGHT ALTITUDE 41,000 ft

BLC ANGLES 30°, 60°, 90°

ANEMOMETER DATA SET

ALTITUDE: 41000 FT
MACH NO: 0.70
BLC POS: 30 DEG
SEQ NO: 16

FLIGHT NO: KITE 5
DATE: 28 JANUARY 1986

AIR TEMP: -40.4

SEN NO	DIST	DC VOL	RMS VOL	MACH NO	FLU DEN	RHO'*1.0E6	Lz
21	9	3.7636	0.3618	0.225	0.0005376	5.128765	2.65
24	11	4.1515	0.3460	0.355	0.0005476	10.951216	2.69
26	13	4.9110	0.3491	0.500	0.0005569	17.994279	2.73
28	15	5.1471	0.1798	0.628	0.0005711	13.591656	2.23
30	17	5.2881	0.0452	0.690	0.0005733	3.919597	
32	19	4.9748	0.0247	0.693	0.0005738	2.295439	
34	21	4.5281		0.695	0.0005743		
36	23	6.0502		0.693	0.0005743		

AERODYNAMIC WAVEFRONT ERROR

DIST	RHO'SQ*Lz	SIGMA SQ
9	4.705E-07	
11	2.178E-06	7.1164E-15
13	5.967E-06	2.9003E-14
15	2.781E-06	5.2510E-14
16	0	5.6246E-14

SIGMA = 2.3716E-07 , meters

SIGMA = 0.237 , microns

SIGMA/LAMDA = 0.447 , wave

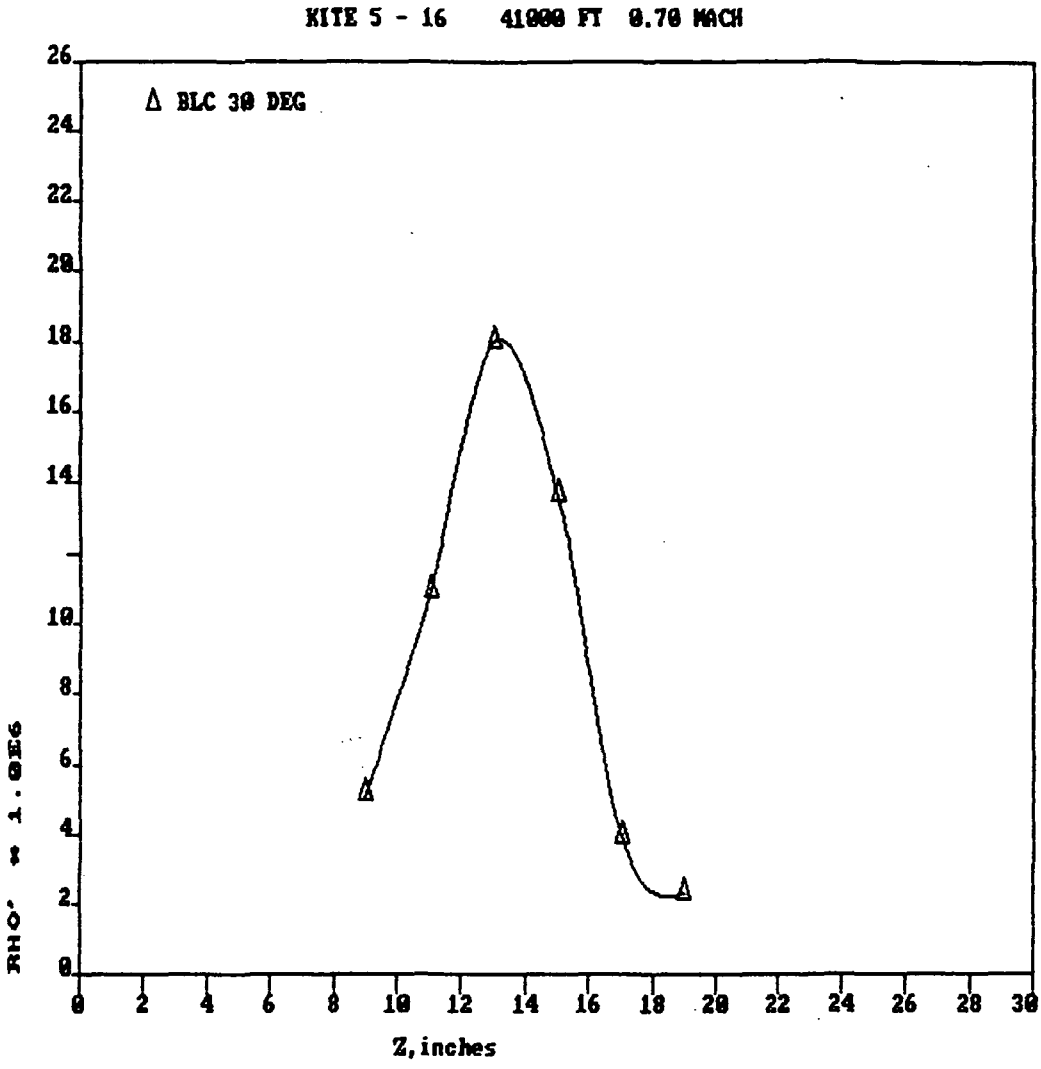
KITE 5 - 16 41000 FT 0.70 MACH
Δ BLC 30 DEG
RHO' * 1.0E6
Z, inches
0
2
4
6
8
10
12
14
16
18
20
22
24
26
28
30

ANEMOMETER DATA SET

ALTITUDE: 41000 FT
MACH NO: 0.70
BLC POS: 60 DEG
SEQ NO: 15

FLIGHT NO: KITE 5
DATE: 28 JANUARY 1986

AIR TEMP: -38.9

SEN NO	DIST	DC VOL	RMS VOL	MACH NO	FLU DEN	RHO'*1.0E6	Lz
21	9	3.6129	0.3247	0.130	0.0005232	1.578646	2.42
24	11	3.4914	0.3042	0.140	0.0005239	1.775426	1.53
26	13	3.8291	0.3849	0.192	0.0005254	3.837219	1.87
28	15	4.0334	0.3871	0.260	0.0005285	6.677074	2.61
30	17	4.4749	0.3393	0.380	0.0005359	11.094158	3.06
32	19	4.4610	0.2609	0.522	0.0005477	15.740791	2.75
34	21	4.2800	0.1422	0.628	0.0005624	12.730172	3.06
36	23	5.9634	0.0452	0.695	0.0005730	3.516267	

AERODYNAMIC WAVEFRONT ERROR

DIST	RHO'SQ*Lz	SIGMA SQ
9	4.071E-08	
11	3.255E-08	1.9688E-16
13	1.859E-07	7.8382E-16
15	7.854E-07	3.3940E-15
17	2.542E-06	1.2337E-14
19	4.599E-06	3.1528E-14
21	3.347E-06	5.2883E-14
24	0	6.6376E-14

SIGMA = 2.5764E-07 , meters

SIGMA = 0.258 , microns

SIGMA/LAMDA = 0.486 , wave

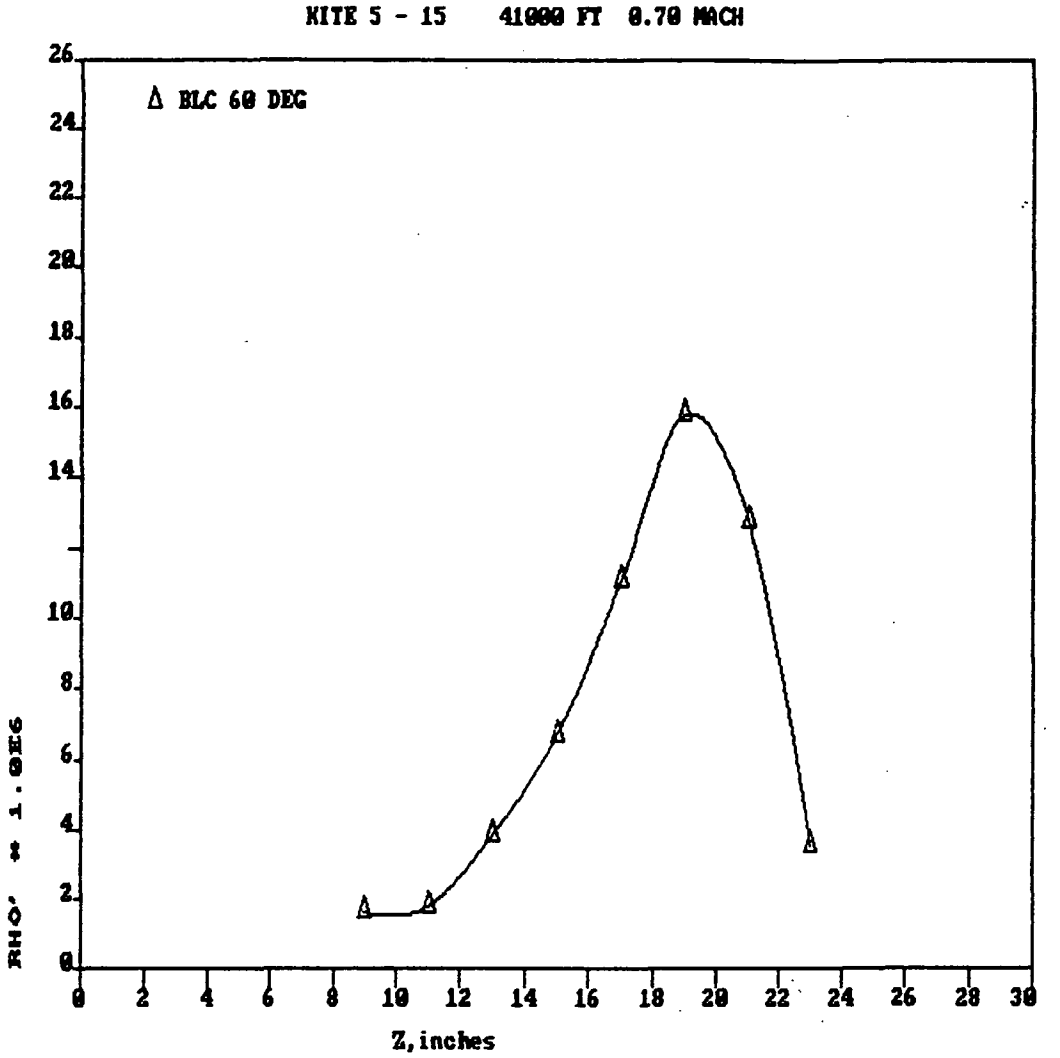
KITE 5 - 15 41000 FT 0.70 MACH
Δ ELC 60 DEG
RHO' * 1.0E6
Z, inches
0
2
4
6
8
10
12
14
16
18
20
22
24
26
28
30

ANEMOMETER DATA SET

ALTITUDE: 41200 FT
MACH NO: 0.70
BLC POS: 90 DEG
SEQ NO: 14

FLIGHT NO: KITE 5
DATE: 28 JANUARY 1986

AIR TEMP: -40.7

SEN NO	DIST	DC VOL	RMS VOL	MACH NO	FLU DEN	RHO'*1.0E6	Lz
21	9	3.5807	0.3277	0.025	0.0005221	0.059712	3.73
24	11	3.6831	0.3321	0.025	0.0005242	0.059068	2.35
26	13	3.8100	0.3778	0.025	0.0005255	0.065120	1.69
28	15	3.8342	0.3492	0.100	0.0005285	0.958828	1.93
30	17	4.0975	0.3778	0.215	0.0005373	4.496866	3.09
32	19	4.1319	0.3566	0.355	0.0005495	11.379602	3.58
34	21	4.1463	0.2180	0.485	0.0005620	12.705522	3.45
36	23	5.8072	0.1492	0.610	0.0005730	9.536451	

AERODYNAMIC WAVEFRONT ERROR

DIST	RHO'SQ*Lz	SIGMA SQ
9	8.977E-11	
11	5.535E-11	3.8998E-19
13	4.837E-11	6.6870E-19
15	1.198E-08	3.2984E-17
17	4.218E-07	1.1986E-15
19	3.129E-06	1.0741E-14
21	3.759E-06	2.9253E-14
27	0	5.9561E-14

SIGMA = 2.4405E-07 , meters

SIGMA = 0.244 , microns

SIGMA/LAMDA = 0.460 , wave

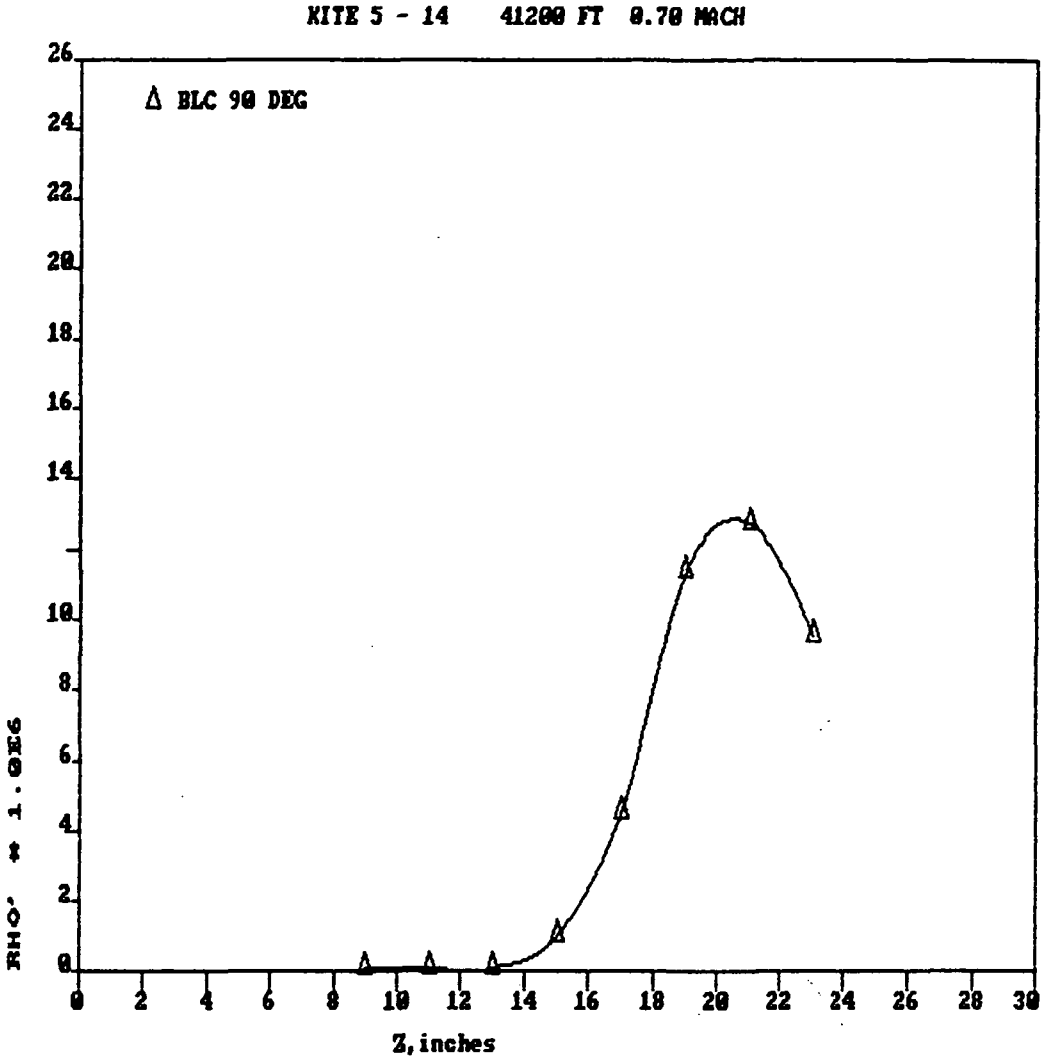
KITE 5 - 14 41200 FT 0.70 MACH
Δ BLC 90 DEG
RHO' * 1.0E6
Z, inches
0
2
4
6
8
10
12
14
16
18
20
22
24
26
28
30

ANEMOMETER DATA SET

ALTITUDE: 40900 FT
MACH NO: 0.73
BLC POS: 30 DEG
SEQ NOS: 11A, 11B, 11C

FLIGHT NO: KITE 4
DATE: 25 JANUARY 1986

AIR TEMP: -40.9

SEN NO	DIST	DC VOL	RMS VOL	MACH NO	FLU DEN	RHO'*1.0E6	Lz
19	8	3.6461	0.3514	0.201	0.0005533	4.240272	1.38
21	9	3.7774	0.3519	0.249	0.0005542	6.247154	1.60
23	10	4.3144	0.4257	0.317	0.0005572	10.622527	1.82
24	11	4.0721	0.3484	0.381	0.0005719	13.426031	2.09
25	12	4.8542	0.3339	0.464	0.0005834	15.909406	2.25
26	13	4.9137	0.3320	0.537	0.0005846	20.424742	2.41
27	14	5.1525	0.1879	0.613	0.0005918	14.100051	2.70
28	15	5.1340	0.1295	0.668	0.0005905	11.279529	2.07
29	16	6.5910	0.1283	0.710	0.0005927	9.680161	1.95
30	17	5.3753	0.0604	0.720	0.0005933	5.724885	1.34
31	18	5.6163	0.0400	0.721	0.0005933	3.636977	
32	19	4.9893	0.0117	0.721	0.0005933	1.197504	
33	20	5.4646	0.0023	0.721	0.0005933	0.214932	
34	21	4.5177	0.0193	0.721	0.0005933	2.181578	
35	22	6.1240		0.721	0.0005933		
36	23	6.0732		0.721	0.0005933		
37	24	6.2602		0.721	0.0005933		

AERODYNAMIC WAVEFRONT ERROR

DIST	RHO'SQ*Lz	SIGMA SQ
8	1.675E-07	
9	4.215E-07	7.9138E-16
10	1.386E-06	3.2203E-15
11	2.543E-06	8.4998E-15
12	3.844E-06	1.7082E-14
13	6.786E-06	3.1366E-14
14	3.623E-06	4.5353E-14
15	1.778E-06	5.2610E-14
16	1.233E-06	5.6656E-14
17	2.964E-07	5.8711E-14

SIGMA = 2.4230E-07 , meters

SIGMA = 0.242 , microns

SIGMA/LAMDA = 0.457 , wave

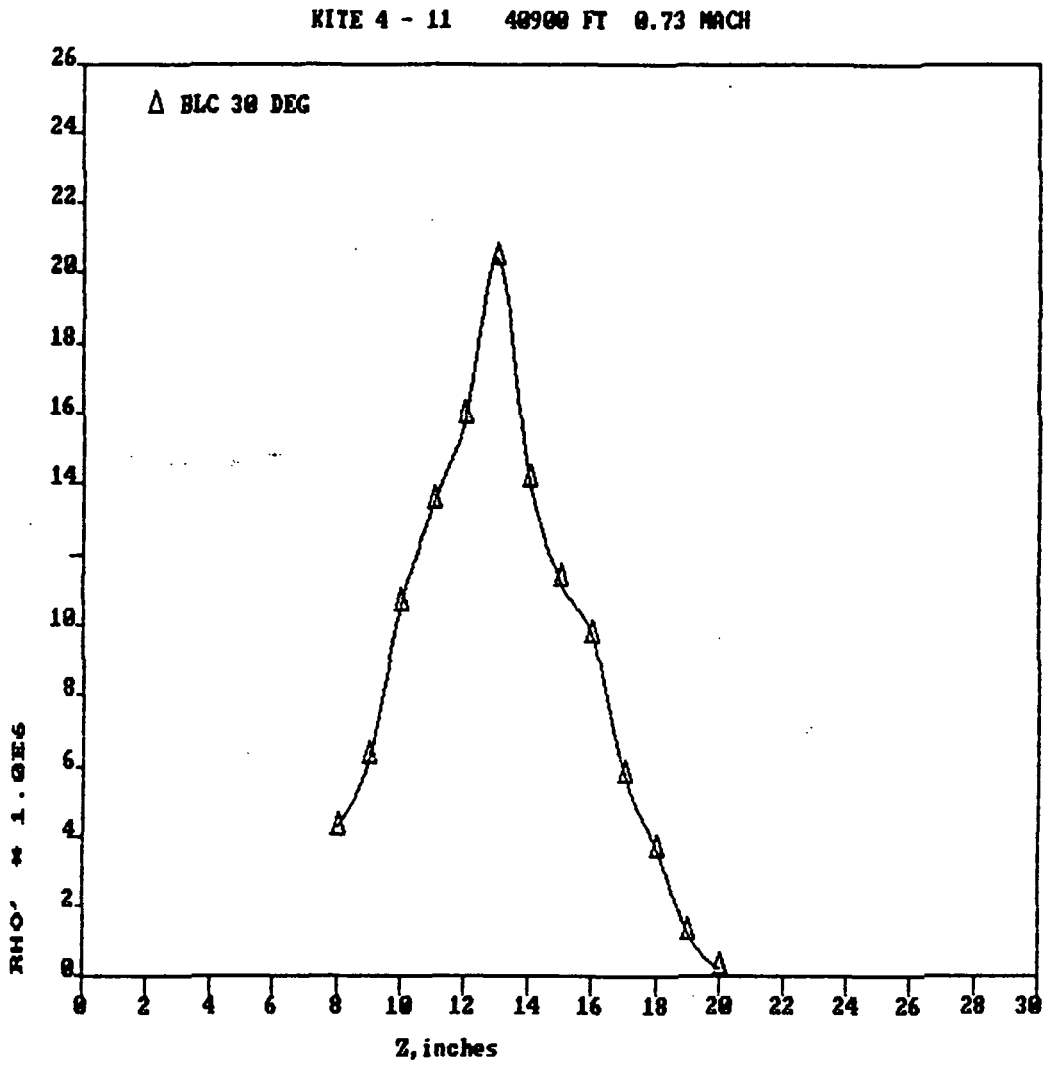
KITE 4 - 11 40900 FT 0.73 MACH
Δ BLC 30 DEG
RHO' * 1.0E6
Z, inches
0
2
4
6
8
10
12
14
16
18
20
22
24
26
28
30

ANEMOMETER DATA SET

ALTITUDE: 40900 FT
MACH NO: 0.73
BLC POS: 45 DEG
SEQ NOS: 10A,10B,10C

FLIGHT NO: KITE 4
DATE: 25 JANUARY 1986

AIR TEMP: -40.3

SEN NO	DIST	DC VOL	RMS VOL	MACH NO	FLU DEN	RHO'*1.0E6	Lz
19	8	3.5205	0.2938	0.155	0.0005487	2.179326	1.72
21	9	3.3529	0.2863	0.155	0.0005488	2.230255	1.49
23	10	3.6361	0.3507	0.173	0.0005492	3.133173	1.32
24	11	2.4860	0.3119	0.201	0.0005510	5.496999	1.69
25	12	4.1176	0.3874	0.240	0.0005550	5.879878	2.09
26	13	4.1271	0.4454	0.310	0.0005610	11.205727	2.46
27	14	4.4332	0.3622	0.372	0.0005685	12.180903	2.78
28	15	4.5974	0.3048	0.448	0.0005774	14.224221	2.65
29	16	6.0598	0.3579	0.500	0.0005872	15.764013	2.78
30	17	4.9987	0.2199	0.580	0.0005959	15.545334	2.65
31	18	5.3458	0.2081	0.641	0.0006022	16.544808	2.67
32	19	4.8124	0.1332	0.699	0.0006057	13.704289	2.37
33	20	5.3925	0.0847	0.721	0.0006074	8.211538	1.56
34	21	4.4778	0.0589	0.728	0.0006077	6.990887	
35	22	6.0802		0.731	0.0006077		
36	23	6.0342		0.733	0.0006077		
37	24	6.2313		0.733	0.0006077		

AERODYNAMIC WAVEFRONT ERROR

DIST	RHO'SQ*Lz	SIGMA SQ
8	5.514E-08	
9	5.003E-08	1.4131E-16
10	8.747E-08	3.2605E-16
11	3.447E-07	9.0674E-16
12	4.877E-07	2.0253E-15
13	2.085E-06	5.4822E-15
14	2.784E-06	1.2025E-14
15	3.619E-06	2.0629E-14
16	4.663E-06	3.1758E-14
17	4.323E-06	4.3831E-14
18	4.933E-06	5.6268E-14
19	3.004E-06	6.6934E-14
20	7.100E-07	7.1925E-14

SIGMA = 2.6819E-07 ,meters

SIGMA = 0.268 ,microns

SIGMA/LAMDA = 0.506 ,wave

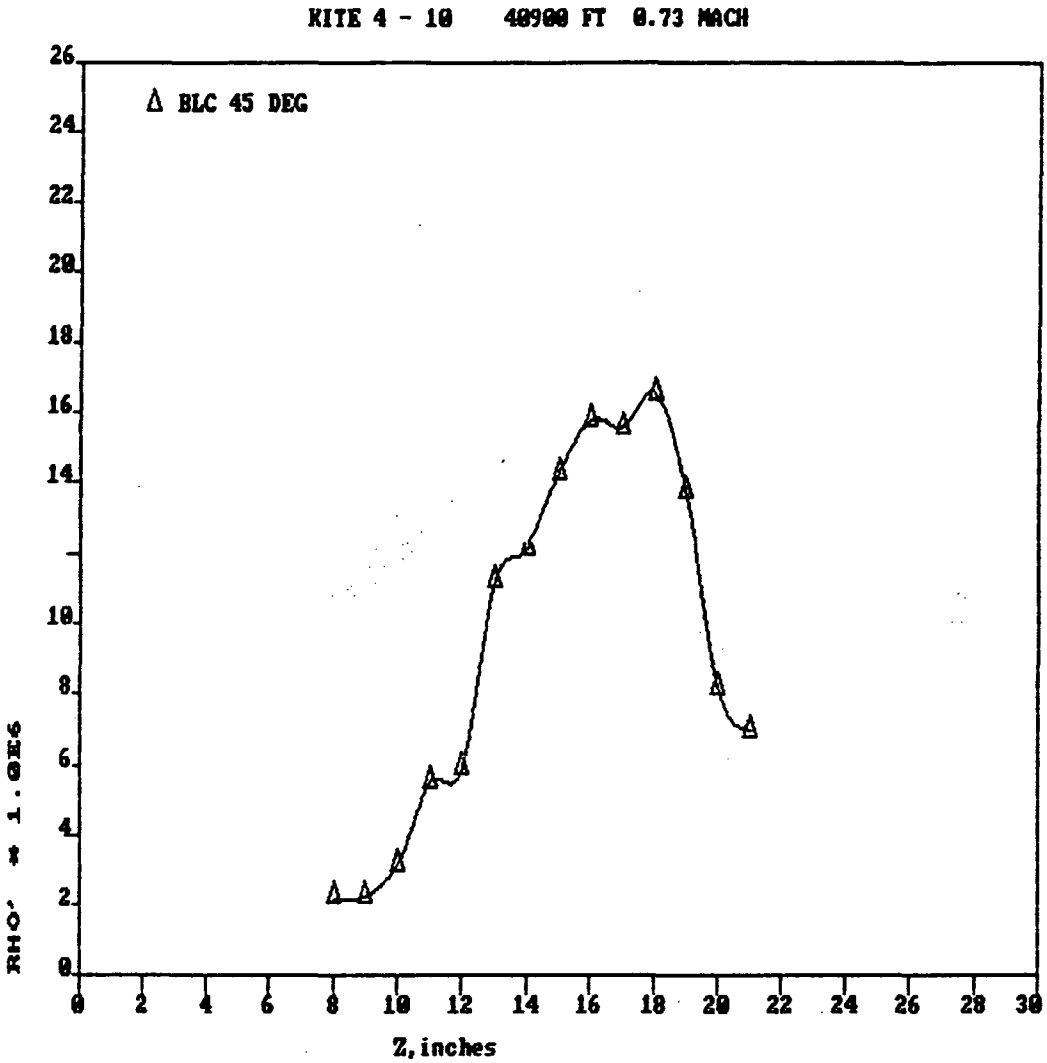
KITE 4 - 10 40000 FT 0.73 MACH
Δ BLC 45 DEG
RHO' * 1.0E6
Z, inches
0
2
4
6
8
10
12
14
16
18
20
22
24
26
28
30

ANEMOMETER DATA SET

ALTITUDE: 41000 FT
MACH NO: 0.73
BLC POS: 60 DEG
SEQ NOS: 9A, 9B, 9C

FLIGHT NO: KITE 4
DATE: 25 JANUARY 1986

AIR TEMP: -39.6

SEN NO	DIST	DC VOL	RMS VOL	MACH NO	FLU DEN	RHO'*1.0E6	Lz
19	8	3.4344	0.3273	0.120	0.0005215	1.423140	2.19
21	9	3.5208	0.3198	0.130	0.0005242	1.598545	1.77
23	10	3.5512	0.3489	0.138	0.0005242	1.946773	1.40
24	11	3.4255	0.2976	0.140	0.0005269	1.780458	1.95
25	12	3.9713	0.3506	0.169	0.0005293	2.639071	1.99
26	13	3.8576	0.4028	0.205	0.0005302	4.576252	2.47
27	14	4.0548	0.3438	0.248	0.0005320	5.415348	2.36
28	15	4.1090	0.3626	0.291	0.0005347	7.729491	2.92
29	16	5.5124	0.4608	0.346	0.0005387	10.289321	2.60
30	17	4.5700	0.3120	0.420	0.0005438	12.234752	2.73
31	18	5.0542	0.3113	0.478	0.0005503	14.191575	2.87
32	19	4.6860	0.1991	0.566	0.0005570	13.440738	2.77
33	20	5.2122	0.1872	0.612	0.0005652	13.224852	3.11
34	21	4.4631	0.1512	0.668	0.0005718	14.669540	2.50
35	22	6.0366	0.0670	0.703	0.0005770	5.285143	2.18
36	23	6.0246	0.0428	0.724	0.0005805	3.574027	0.57
37	24	6.2562	0.0472	0.724	0.0005805	3.795541	

AERODYNAMIC WAVEFRONT ERROR

DIST	RHO'SQ*Lz	SIGMA SQ
8	2.994E-08	
9	3.053E-08	8.1250E-17
10	3.581E-08	1.7040E-16
11	4.173E-08	2.7458E-16
12	9.355E-08	4.5635E-16
13	3.492E-07	1.0512E-15
14	4.672E-07	2.1481E-15
15	1.178E-06	4.3580E-15
16	1.858E-06	8.4368E-15
17	2.758E-06	1.4640E-14
18	3.902E-06	2.3589E-14
19	3.378E-06	3.3370E-14
20	3.672E-06	4.2841E-14
21	3.631E-06	5.2654E-14
22	4.110E-07	5.8086E-14
23	4.915E-08	5.8704E-14

SIGMA = 2.4229E-07 , meters

SIGMA = 0.242 , microns

SIGMA/LAMDA = 0.457 , wave

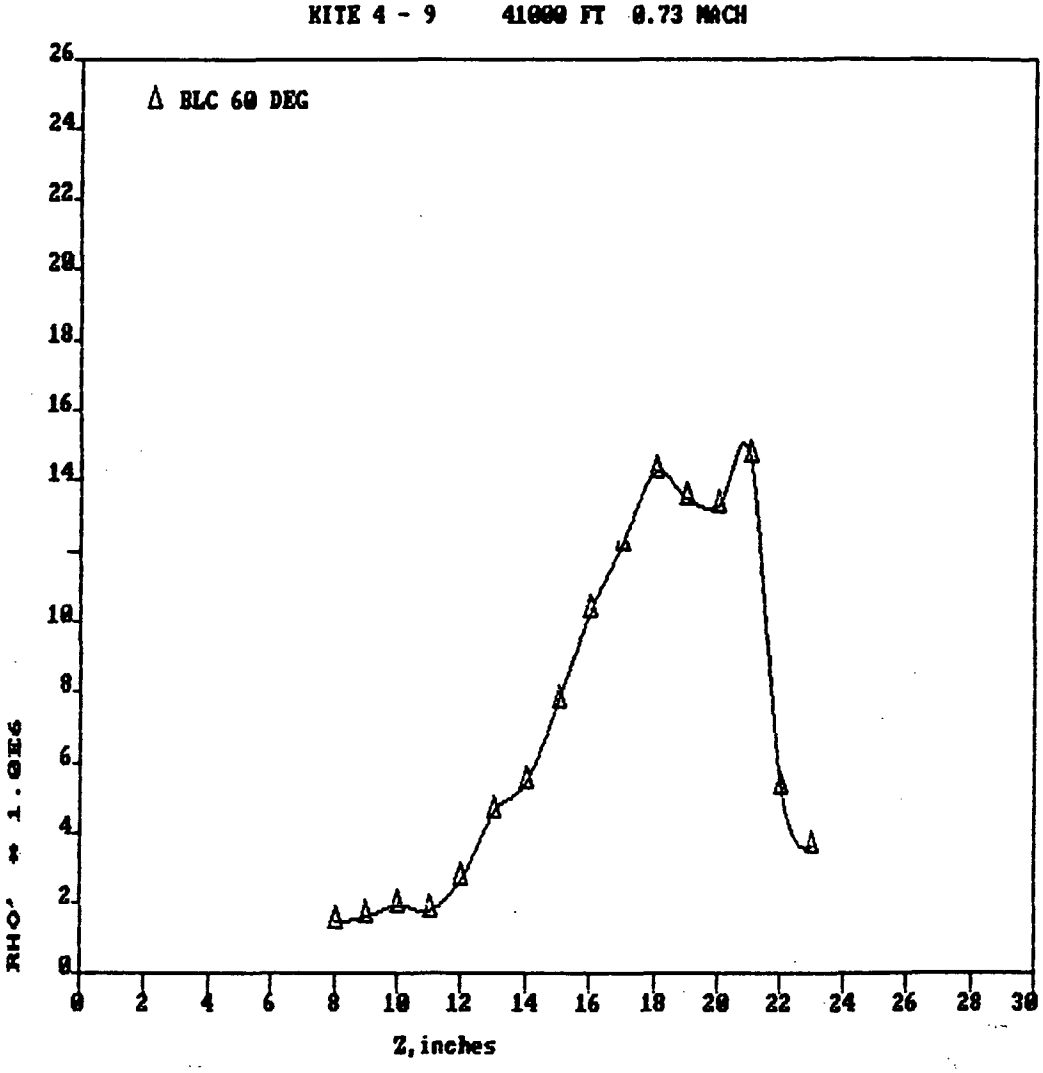
KITE 4 - 9 41000 FT 0.73 MACH
Δ BLC 60 DEG
RHO' * 1.0E6
Z, inches
0
2
4
6
8
10
12
14
16
18
20
22
24
26
28
30

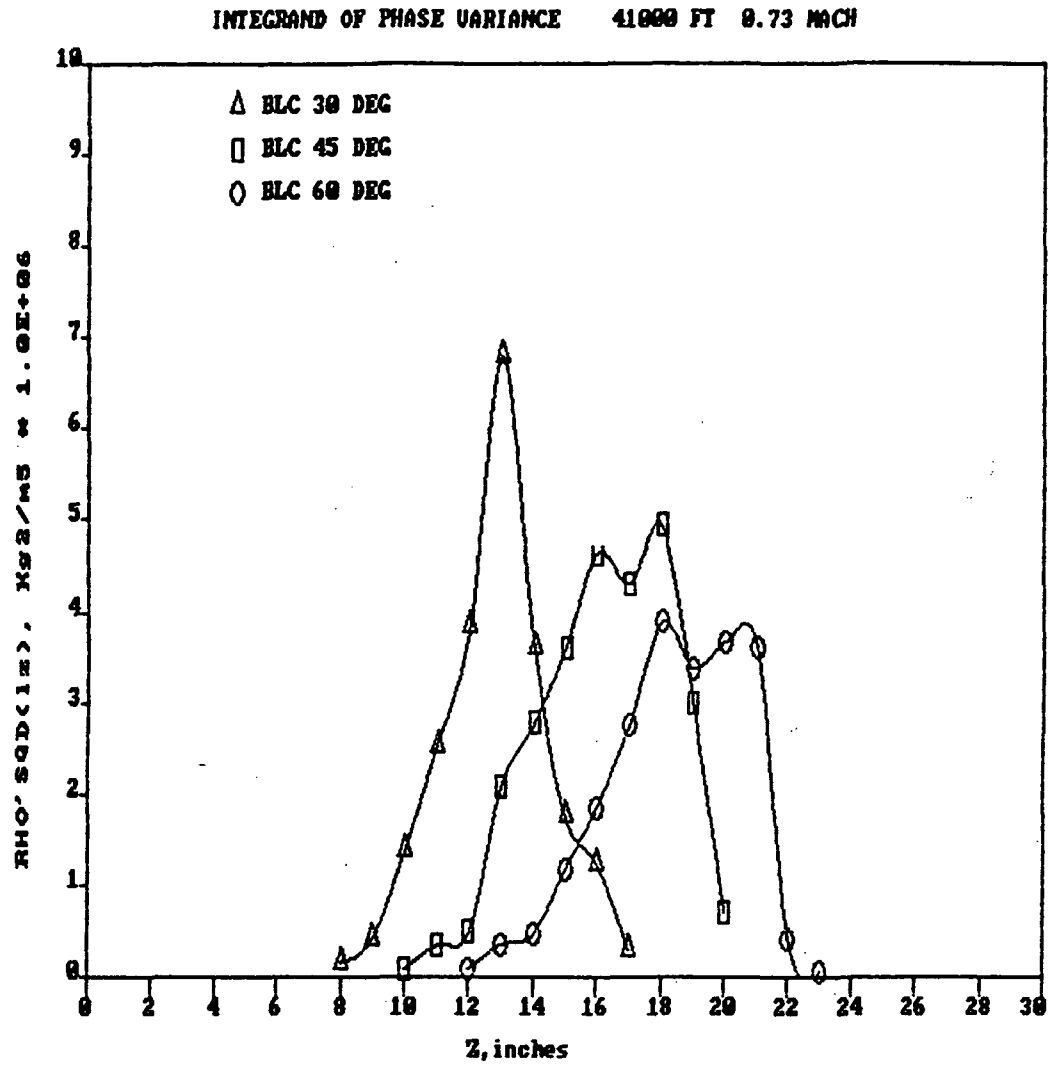
INTEGRAND OF PHASE VARIANCE 41000 FT 0.73 MACH
Δ BLC 30 DEG
□ BLC 45 DEG
○ BLC 60 DEG
RHO*SQD(1st), Kg2/m5 * 1.0E+06
Z, inches
0
1
2
3
4
5
6
7
8
9
10
0
2
4
6
8
10
12
14
16
18
20
22
24
26
28
30

APPENDIX C

DATA OBTAINED AT M = 0.80

APPENDIX C.1

FLIGHT ALTITUDE 37,000 ft

BLC ANGLES 30°, 60°, 90°

ANEMOMETER DATA SET

ALTITUDE: 36300 FT
MACH NO: 0.80
BLC POS: 30 DEG
SEQ NO: 7

FLIGHT NO: KITE 5
DATE: 28 JANUARY 1986

AIR TEMP: -32.3

SEN NO	DIST	DC VOL	RMS VOL	MACH NO	FLU DEN	RHO'*1.0E6	Lz
21	9	4.3094	0.4111	0.190	0.0006330	4.29779	2.47
24	11	4.6412	0.3100	0.362	0.0006456	10.73876	2.31
26	13	5.5201	0.2854	0.560	0.0006696	19.29328	2.41
28	15	5.5767	0.1209	0.712	0.0006935	12.67360	1.66
30	17	5.5696	0.0212	0.773	0.0007052	2.58903	
32	19	5.1479	0.0168	0.775	0.0007060	2.23156	
34	21	4.6790		0.775	0.0007060		
36	23	6.3523		0.775	0.0007060		

AERODYNAMIC WAVEFRONT ERROR

DIST	RHO'SQ*Lz	SIGMA SQ
9	3.080E-07	
11	1.798E-06	5.6598E-15
13	6.055E-06	2.6764E-14
15	1.800E-06	4.7873E-14
15.5	0	4.9082E-14

SIGMA = 2.2155E-07 ,meters

SIGMA = 0.222 ,microns

SIGMA/LAMDA = 0.418 ,wave

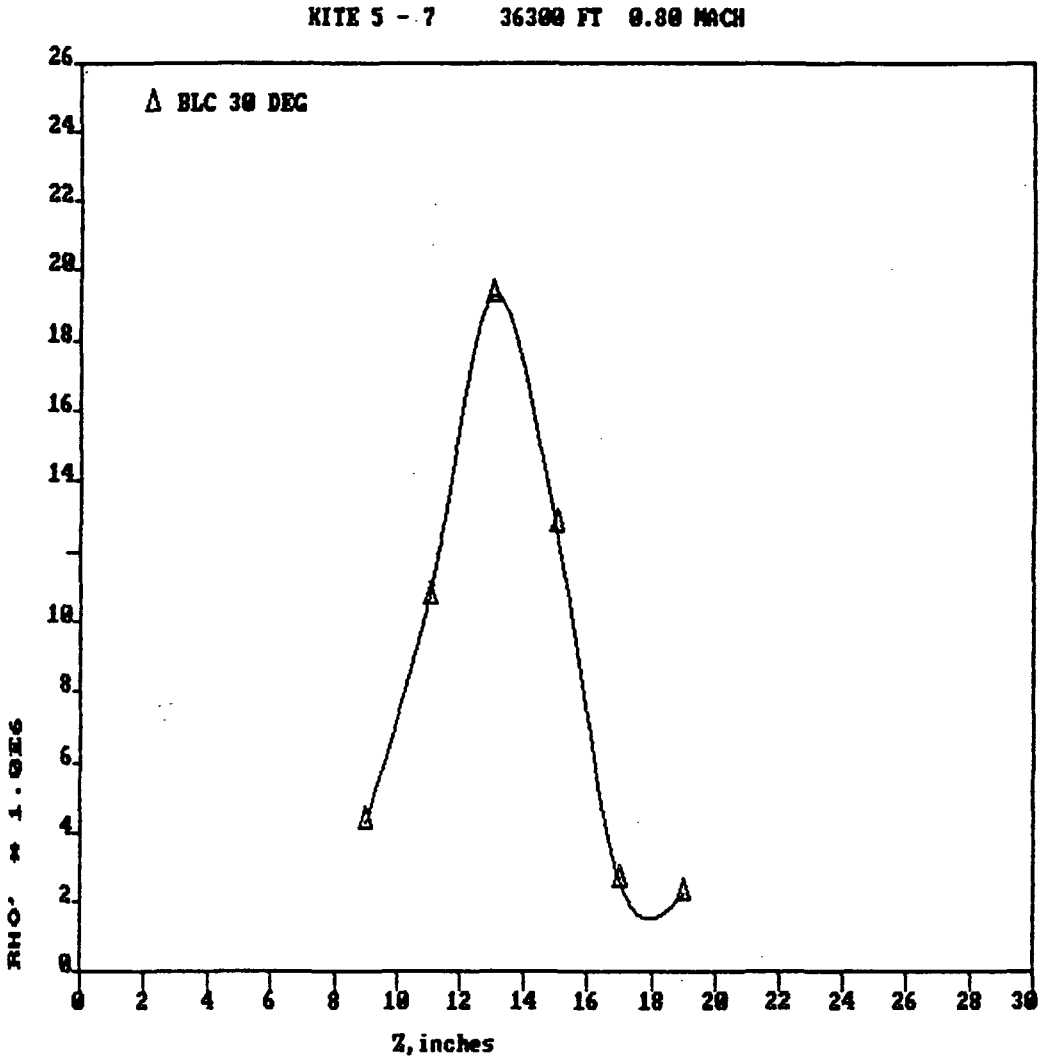
KITE 5 - 7 36300 FT 0.80 MACH
Δ BLC 30 DEG
RHO' * 1.0E6
Z, inches
0
2
4
6
8
10
12
14
16
18
20
22
24
26
28
30

ANEMOMETER DATA SET

ALTITUDE: 36700 FT
MACH NO: 0.80
BLC POS: 60 DEG
SEQ NO: 6

FLIGHT NO: KITE 5
DATE: 28 JANUARY 1986

AIR TEMP: -33.0

SEN NO	DIST	DC VOL	RMS VOL	MACH NO	FLU DEN	RHO'*1.0E6	Lz
21	9	3.3394	0.2903	0.025	0.0006053	0.06576	1.89
24	11	3.5844	0.3511	0.050	0.0006136	0.30022	2.03
26	13	4.4365	0.4632	0.168	0.0006220	3.62486	2.12
28	15	4.8825	0.3082	0.320	0.0006303	7.82769	2.08
30	17	5.1987	0.2055	0.500	0.0006491	11.66289	2.57
32	19	4.9330	0.1667	0.652	0.0006716	16.49146	2.19
34	21	4.6315	0.0694	0.755	0.0006897	9.59445	1.24
36	23	6.3433		0.785	0.0006954		

AERODYNAMIC WAVEFRONT ERROR

DIST	RHO'SQ*Lz	SIGMA SQ
9	5.517E-11	
11	1.235E-09	3.4671E-18
13	1.880E-07	5.1208E-16
15	8.603E-07	3.3292E-15
17	2.360E-06	1.1982E-14
19	4.020E-06	2.9127E-14
21	7.705E-07	4.2002E-14
21.5	0	4.2520E-14

SIGMA = 2.0620E-07 , meters

SIGMA = 0.206 , microns

SIGMA/LAMDA = 0.389 , wave

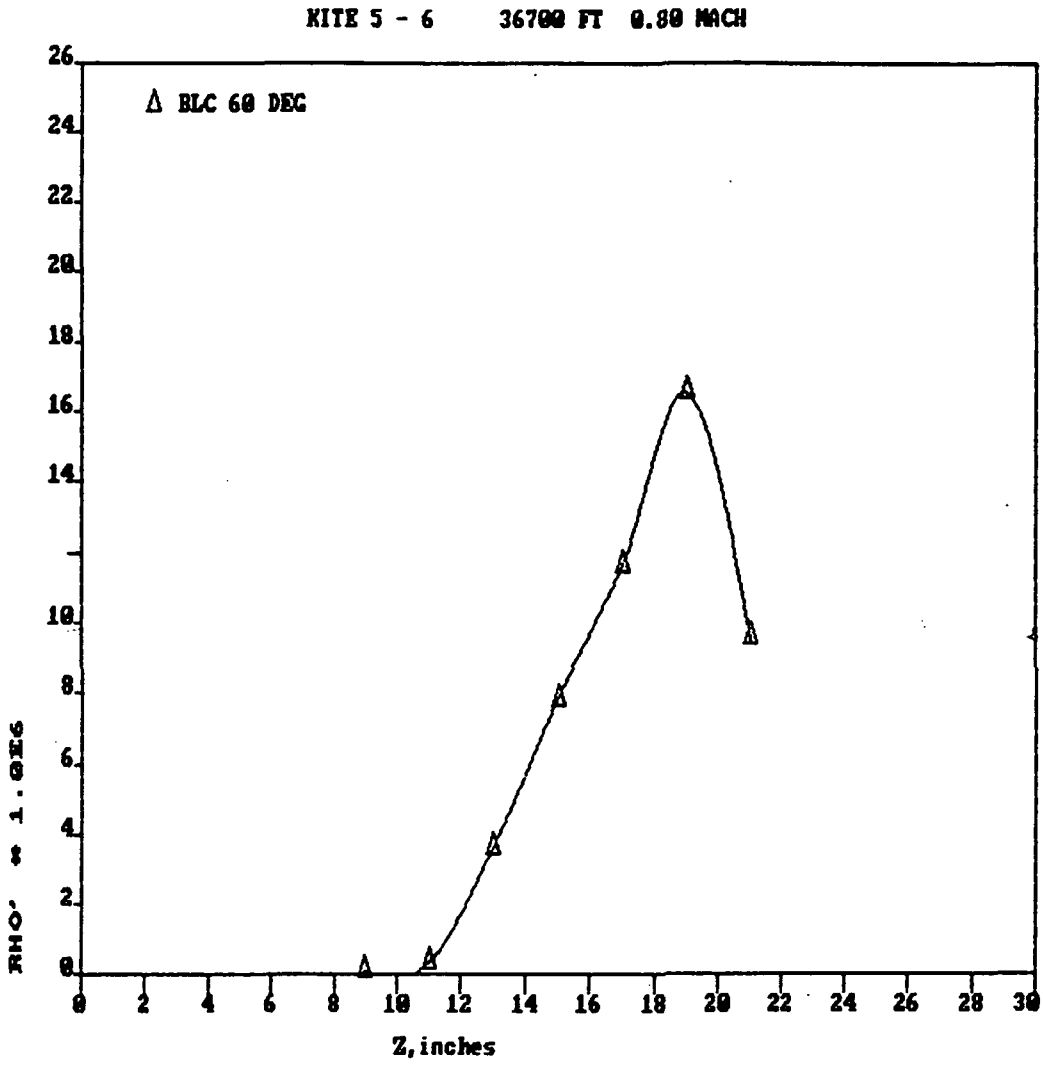
KITE 5 - 6 36700 FT 0.80 MACH
Δ BLC 60 DEG
RHO' * 1.0E6
Z, inches
0
2
4
6
8
10
12
14
16
18
20
22
24
26
28
30

ANEMOMETER DATA SET

ALTITUDE: 36900 FT
MACH NO: 0.80
BLC POS: 90 DEG
SEQ NO: 5

FLIGHT NO: KITE 5
DATE: 28 JANUARY 1986

AIR TEMP: -32.5

SEN NO	DIST	DC VOL	RMS VOL	MACH NO	FLU DEN	RHO'*1.0E6	Lz
21	9	3.5566	0.2968	0.070	0.0006038	0.49283	3.25
24	11	3.6392	0.2664	0.138	0.0006129	1.69594	2.70
26	13	4.3267	0.3328	0.218	0.0006190	4.44101	2.24
28	15	4.6040	0.2693	0.308	0.0006251	6.68355	2.17
30	17	4.9709	0.2005	0.430	0.0006366	8.84148	2.18
32	19	4.7888	0.1632	0.570	0.0006544	12.82488	2.20
34	21	4.5237	0.1210	0.692	0.0006750	14.51199	2.01
36	23	6.3247	0.0264	0.768	0.0006893	2.74619	

AERODYNAMIC WAVEFRONT ERROR

DIST	RHO'SQ*Lz	SIGMA SQ
9	5.328E-09	
11	5.242E-08	1.5519E-16
13	2.982E-07	1.0974E-15
15	6.543E-07	3.6571E-15
17	1.150E-06	8.5067E-15
19	2.442E-06	1.8162E-14
21	2.857E-06	3.2404E-14
25	0	4.7761E-14

SIGMA = 2.1854E-07 ,meters

SIGMA = 0.219 ,microns

SIGMA/LAMDA = 0.412 ,wave

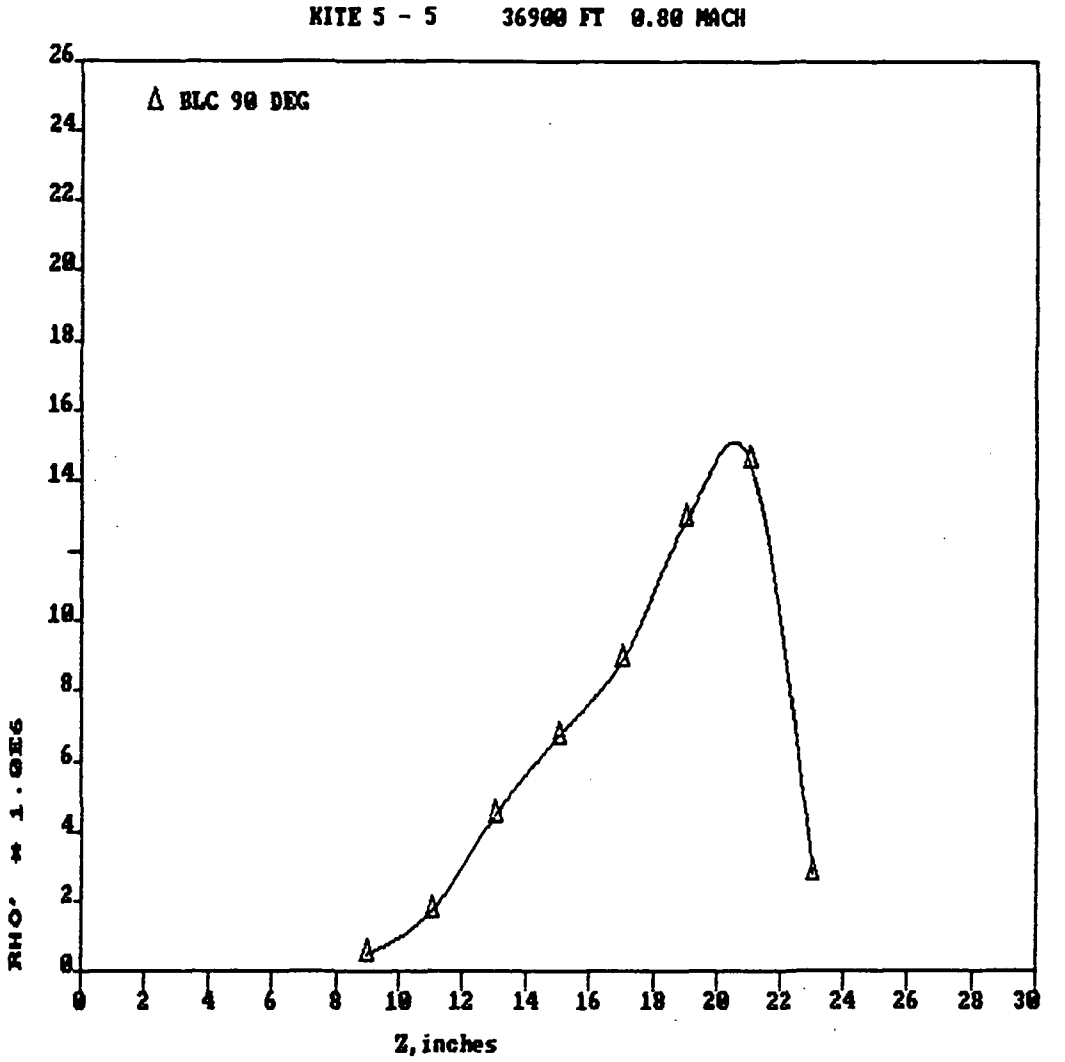
KITE 5 - 5 36900 FT 0.80 MACH
Δ BLC 90 DEG
RHO' * 1.0E6
Z, inches
0
2
4
6
8
10
12
14
16
18
20
22
24
26
28
30

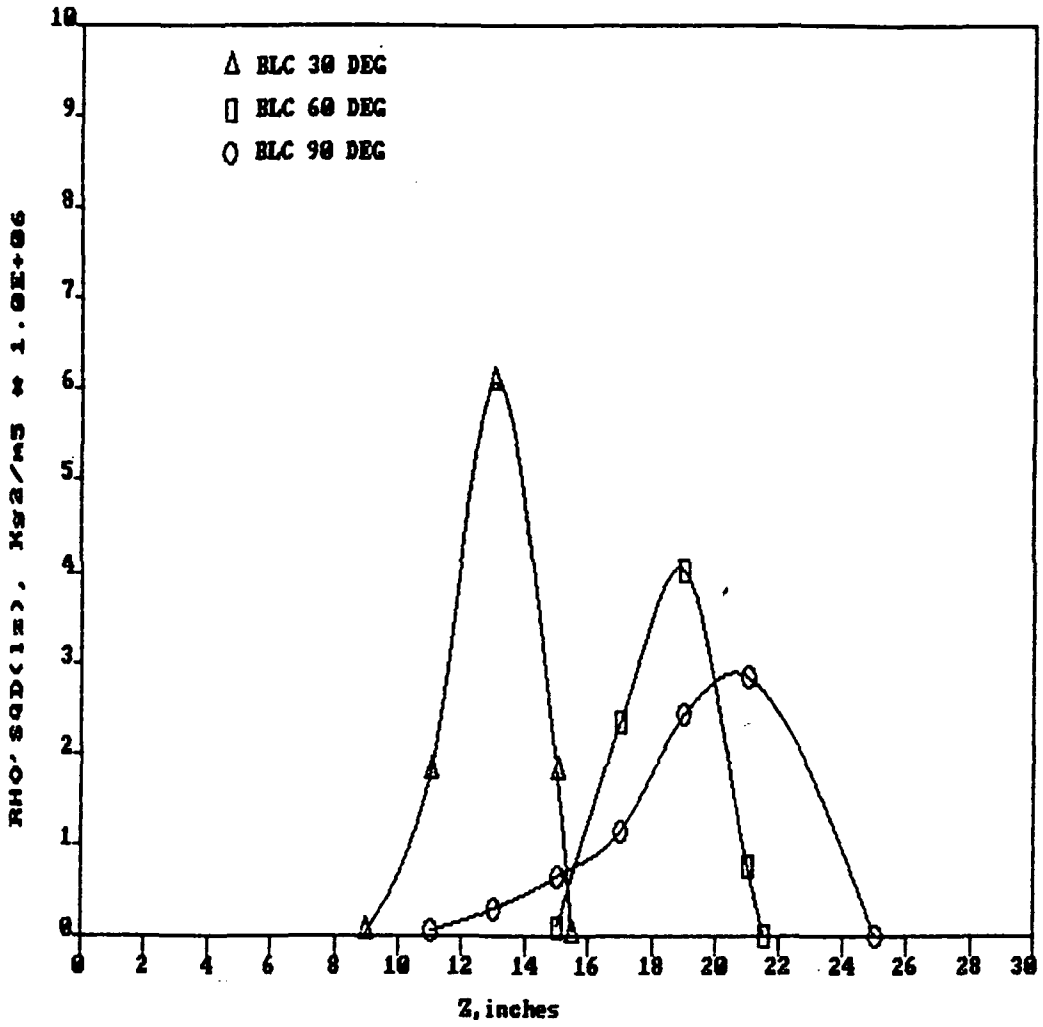
INTEGRAND OF PHASE VARIANCE 37000 FT 0.80 MACH
Δ ELC 30 DEG
▯ ELC 60 DEG
○ ELC 90 DEG
RHO*SQDC(1,2), Kg2/m5 * 1.0E+06
Z, inches
0
1
2
3
4
5
6
7
8
9
10
0
2
4
6
8
10
12
14
16
18
20
22
24
26
28
30

APPENDIX C.2

FLIGHT ALTITUDE 39,000 ft

BLC ANGLES 30°, 45°, 60°

ANEMOMETER DATA SET

ALTITUDE: 38500 FT
MACH NO: 0.80
BLC POS: 30 DEG
SEQ NOS: 4A, 4B

FLIGHT NO: KITE 4
DATE: 25 JANUARY 1986

AIR TEMP: -38.4

SEN NO	DIST	DC VOL	RMS VOL	MACH NO	FLU DEN	RHO'*1.0E6	Lz
19	8	3.7987	0.4034	0.120	0.0005888	1.790469	1.68
21	9	3.3465	0.3141	0.206	0.0005906	4.626206	1.87
23	10	3.9992	0.3483	0.293	0.0005953	8.606336	1.98
24	11	4.2836	0.3303	0.369	0.0006015	11.978049	2.26
25	12	4.4938	0.2684	0.448	0.0006098	13.533348	2.30
26	13	4.4327	0.2613	0.544	0.0006205	19.357686	2.30
27	14	4.5954	0.1944	0.646	0.0006317	19.113287	2.09
28	15	5.3839	0.1115	0.718	0.0006432	11.386232	1.74
29	16	6.2296	0.0811	0.755	0.0006526	7.887325	1.30
30	17	5.6475	0.0254	0.777	0.0006571	2.874334	
31	18	5.1767	0.0312	0.783	0.0006585	3.908043	
32	19	5.1834	0.0103	0.781	0.0006589	1.283983	
33	20	4.9213		0.780	0.0006603		

AERODYNAMIC WAVEFRONT ERROR

DIST	RHO'SQ*Lz	SIGMA SQ
8	3.635E-08	
9	2.701E-07	4.1183E-16
10	9.899E-07	2.1049E-15
11	2.189E-06	6.3759E-15
12	2.843E-06	1.3137E-14
13	5.818E-06	2.4775E-14
14	5.154E-06	3.9516E-14
15	1.523E-06	4.8487E-14
16	5.459E-07	5.1267E-14

SIGMA = 2.2642E-07 , meters

SIGMA = 0.226 , microns

SIGMA/LAMDA = 0.427 , wave

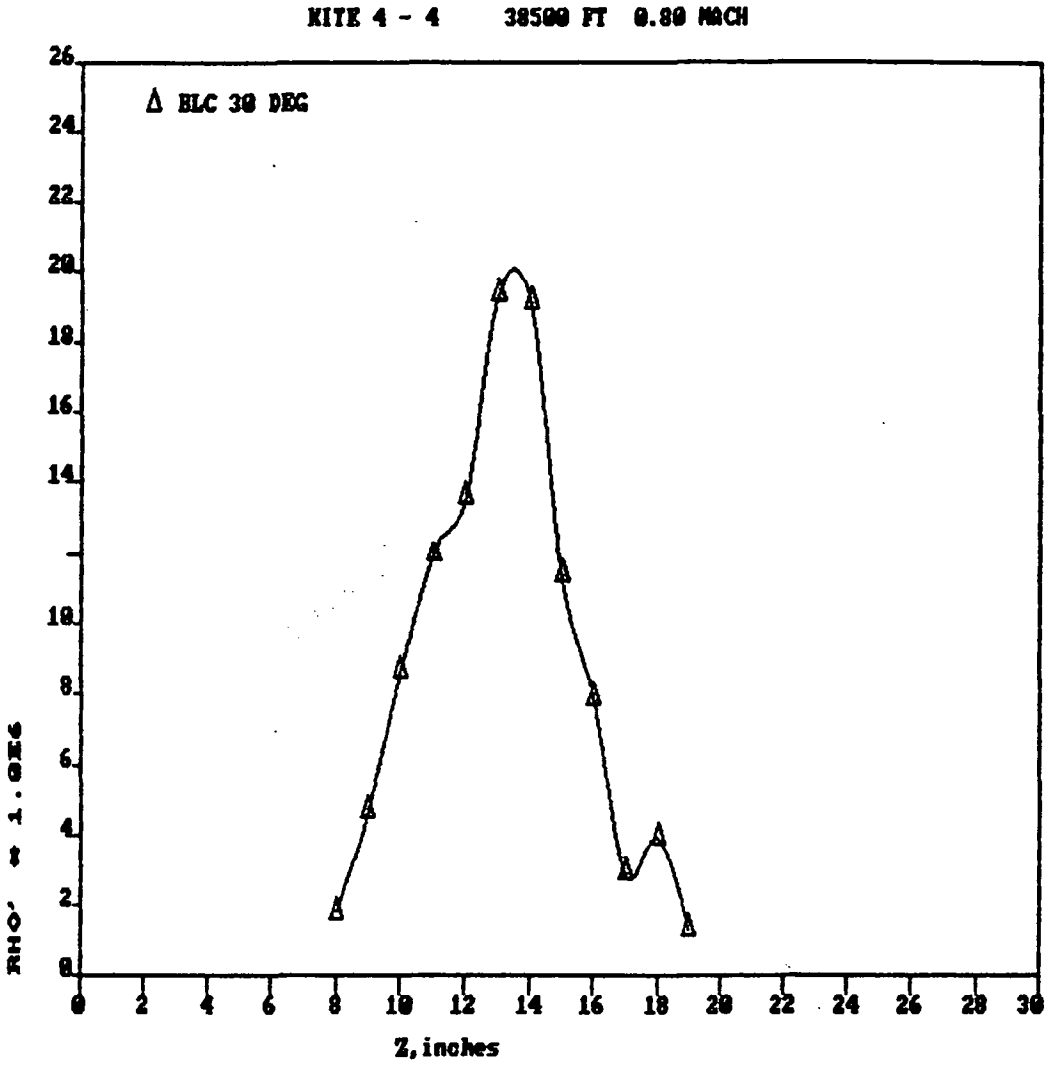
KITE 4 - 4 38500 FT 0.80 MACH
Δ HLC 30 DEG
RHO' * 1.0E6
Z, inches
0
2
4
6
8
10
12
14
16
18
20
22
24
26
28
30

ANEMOMETER DATA SET

ALTITUDE: 38700 FT
MACH NO: 0.80
BLC POS: 45 DEG
SEQ NOS: 5A, 5B, 5C

FLIGHT NO: KITE 4
DATE: 25 JANUARY 1986

AIR TEMP: -40.5

SEN NO	DIST	DC VOL	RMS VOL	MACH NO	FLU DEN	RHO'*1.0E6	Lz
19	8	3.2449	0.2807	0.094	0.0005947	0.905925	1.79
21	9	3.1311	0.2674	0.094	0.0005947	0.894367	1.08
23	10	3.4504	0.3412	0.109	0.0005948	1.391024	1.32
24	11	3.7113	0.3498	0.137	0.0005954	2.090862	1.68
25	12	3.8827	0.3976	0.195	0.0005973	4.581929	2.10
26	13	4.5878	0.4652	0.285	0.0006016	9.597915	2.36
27	14	4.2503	0.3486	0.378	0.0006086	13.493209	2.36
28	15	5.0797	0.2574	0.464	0.0006168	12.390922	2.17
29	16	5.9230	0.2314	0.548	0.0006264	13.121978	2.24
30	17	5.4564	0.1581	0.631	0.0006376	12.690543	2.06
31	18	5.1094	0.1482	0.701	0.0006480	15.437775	1.82
32	19	5.1798	0.0750	0.749	0.0006558	8.701414	1.57
33	20	4.9452	0.0317	0.771	0.0006598	4.062415	0.88
34	21	4.7120	0.0236	0.777	0.0006612	3.220830	
35	22	5.7170	0.0200	0.777	0.0006612	2.249691	
36	23	5.5525		0.777	0.0006615		
37	24	5.8306		0.777	0.0006615		

AERODYNAMIC WAVEFRONT ERROR

DIST	RHO'SQ*Lz	SIGMA SQ
8	9.916E-09	
9	5.831E-09	2.1159E-17
10	1.724E-08	5.2159E-17
11	4.958E-08	1.4194E-16
12	2.976E-07	6.0841E-16
13	1.467E-06	2.9801E-15
14	2.900E-06	8.8489E-15
15	2.249E-06	1.5768E-14
16	2.603E-06	2.2288E-14
17	2.239E-06	2.8795E-14
18	2.928E-06	3.5738E-14
19	8.024E-07	4.0750E-14
20	9.803E-08	4.1960E-14

SIGMA = 2.0484E-07 , meters

SIGMA = 0.205 , microns

SIGMA/LAMDA = 0.386 , wave

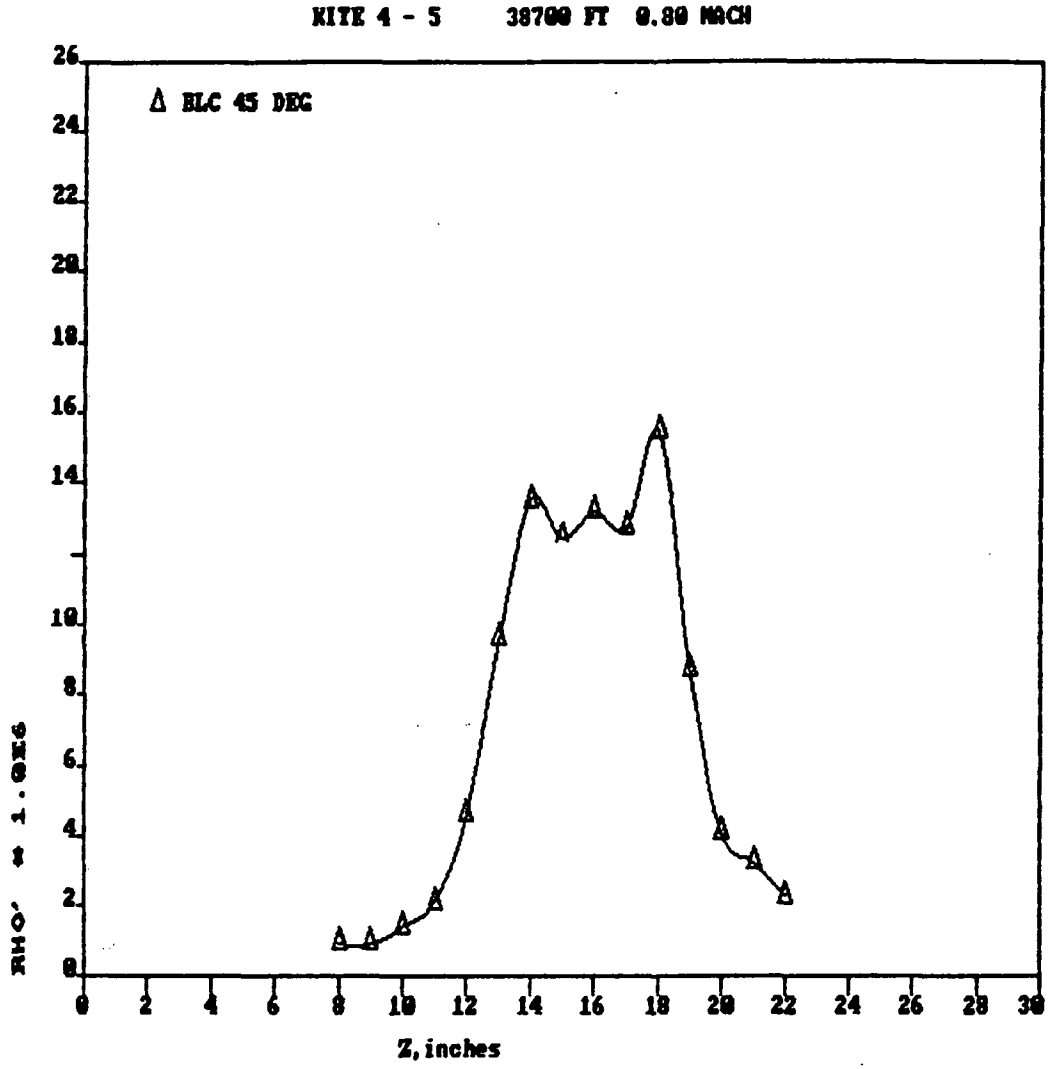
KITE 4 - 5 38700 FT 0.80 MACH
Δ ELC 45 DEG
RHO' * 1.0E6
Z, inches
0
2
4
6
8
10
12
14
16
18
20
22
24
26
28
30

ANEMOMETER DATA SET

ALTITUDE: 38800 FT
MACH NO: 0.80
BLC POS: 60 DEG
SEQ NOS: 6A, 6B, 6C

FLIGHT NO: KITE 4
DATE: 25 JANUARY 1986

AIR TEMP: -43.4

SEN NO	DIST	DC VOL	RMS VOL	MACH NO	FLU DEN	RHO'*1.0E6	Lz
19	8	2.9994	0.2615	0.057	0.0005721	0.32369	1.74
21	9	2.9903	0.2451	0.057	0.0005757	0.30622	1.53
23	10	3.2282	0.3093	0.066	0.0005822	0.48512	1.54
24	11	3.5283	0.3312	0.090	0.0005859	0.88809	1.99
25	12	3.5871	0.3477	0.107	0.0005921	1.30819	2.00
26	13	4.1415	0.4535	0.134	0.0005984	2.33638	2.10
27	14	3.9251	0.3697	0.201	0.0006029	4.51548	2.35
28	15	4.6902	0.3217	0.267	0.0006062	5.76391	2.39
29	16	5.5656	0.3440	0.341	0.0006106	8.38683	2.44
30	17	5.0291	0.2454	0.420	0.0006173	9.92655	2.16
31	18	4.8504	0.2123	0.506	0.0006267	12.74143	2.41
32	19	4.9376	0.1664	0.584	0.0006362	12.86906	2.61
33	20	4.8792	0.1660	0.661	0.0006469	16.37108	2.23
34	21	4.7066	0.1406	0.722	0.0006566	16.92122	1.97
35	22	5.7704	0.0793	0.757	0.0006628	8.49263	1.76
36	23	5.6039	0.0238	0.777	0.0006664	2.75264	1.15
37	24	5.8421	0.0218	0.777	0.0006678	2.42361	

AERODYNAMIC WAVEFRONT ERROR

DIST	RHO'SQ*Lz	SIGMA SQ
8	1.231E-09	
9	9.684E-10	2.9547E-18
10	2.446E-09	7.5431E-18
11	1.059E-08	2.5065E-17
12	2.310E-08	7.0344E-17
13	7.738E-08	2.0535E-16
14	3.234E-07	7.4390E-16
15	5.360E-07	1.8986E-15
16	1.158E-06	4.1754E-15
17	1.437E-06	7.6624E-15
18	2.641E-06	1.3141E-14
19	2.918E-06	2.0610E-14
20	4.034E-06	2.9951E-14
21	3.807E-06	4.0488E-14
22	8.568E-07	4.6755E-14
23	5.882E-08	4.7985E-14

SIGMA = 2.1906E-07 , meters

SIGMA = 0.219 , microns

SIGMA/LAMDA = 0.413 , wave

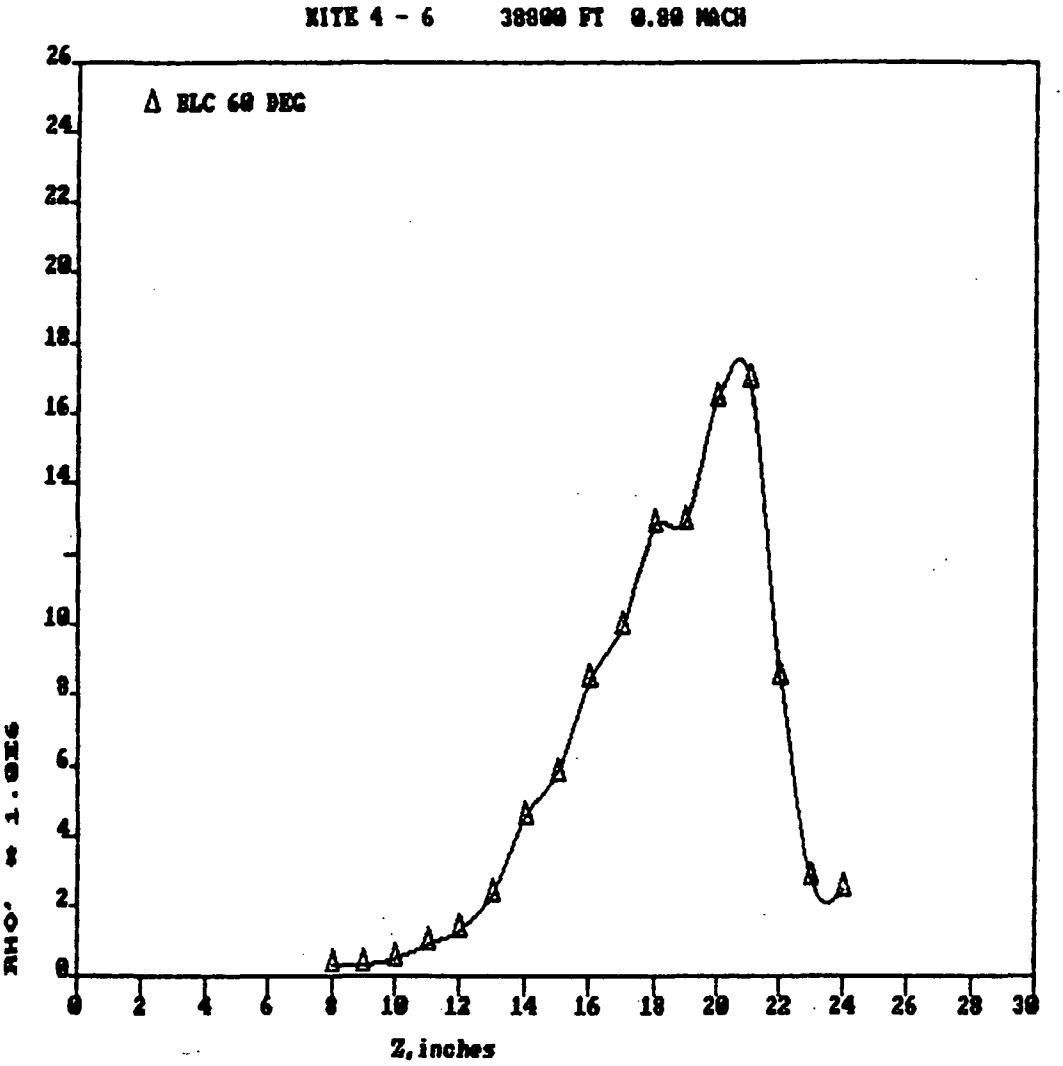
XITE 4 - 6 38000 FT 0.80 MACH
Δ ELC 60 DEG
RHO' ± 1.0E6
Z, inches
0
2
4
6
8
10
12
14
16
18
20
22
24
26
28
30

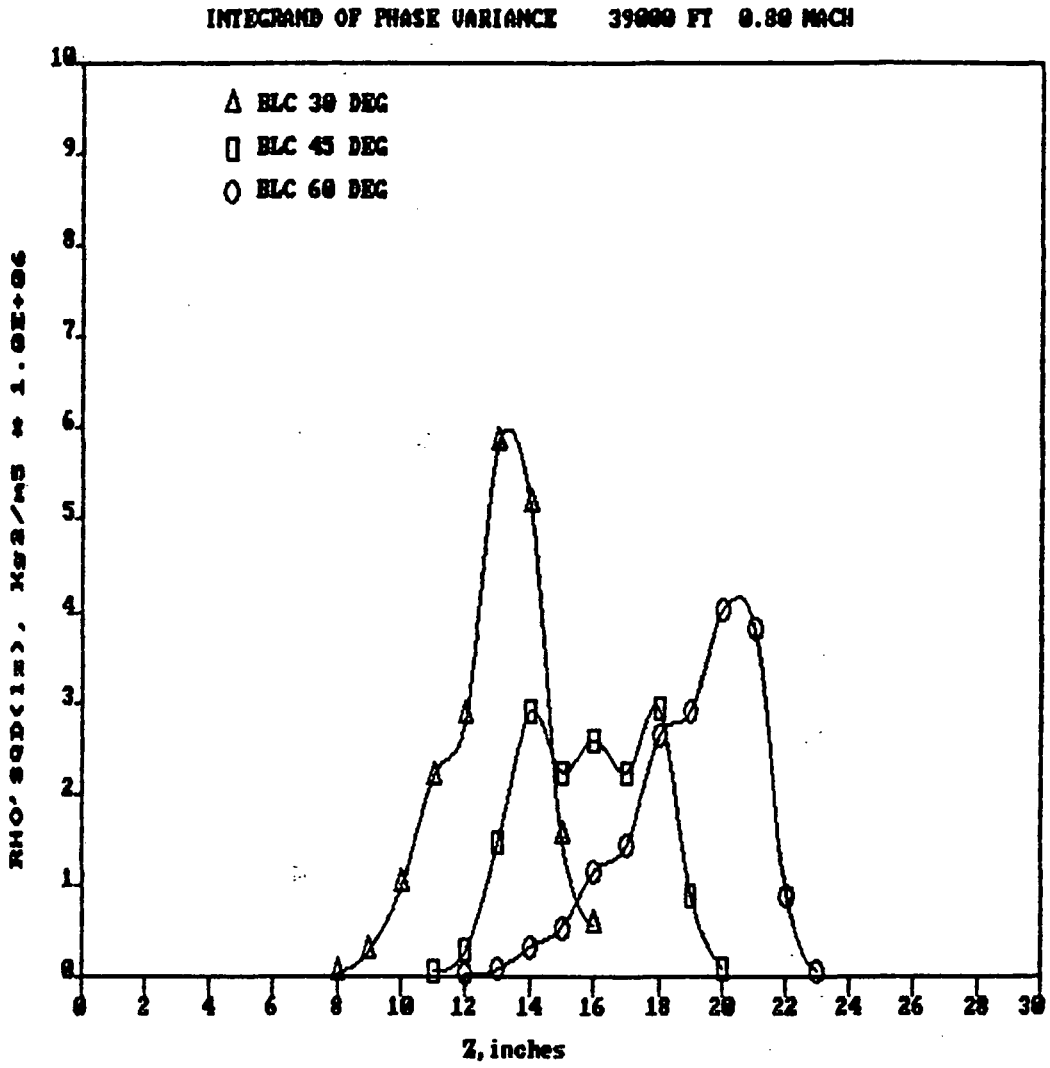
INTEGRAND OF PHASE VARIANCE 39000 FT 0.80 MACH
Δ ELC 30 DEG
□ ELC 45 DEG
○ ELC 60 DEG
RHO*SQDC(1,1), KG2/M5 * 1.0E+06
Z, inches
0
1
2
3
4
5
6
7
8
9
10
0
2
4
6
8
10
12
14
16
18
20
22
24
26
28
30

APPENDIX C.3

FLIGHT ALTITUDE 41,000 ft

BLC ANGLES 30°, 45°, 60°, 90°

ANEMOMETER DATA SET

ALTITUDE: 40800 FT
MACH NO: 0.80
BLC POS: 30 DEG
SEQ NOS: 7A,7B

FLIGHT NO: KITE 4
DATE: 25 JANUARY 1986

AIR TEMP: -35.7

SEN NO	DIST	DC VOL	RMS VOL	MACH NO	FLU DEN	RHO'*1.0E6	Lz
19	8	3.7539	0.3798	0.187	0.0005234	3.652469	1.75
21	9	3.3254	0.3123	0.265	0.0005253	6.739476	2.18
23	10	4.3897	0.4125	0.340	0.0005296	10.997491	2.18
24	11	4.1578	0.3256	0.408	0.0005358	13.097190	2.45
25	12	4.9428	0.3110	0.483	0.0005440	14.607132	2.47
26	13	5.0642	0.3017	0.575	0.0005535	19.257745	2.35
27	14	5.1751	0.1744	0.663	0.0005635	14.198258	2.46
28	15	5.2194	0.1114	0.731	0.0005742	10.791090	1.78
29	16	5.9254	0.0944	0.774	0.0005824	8.967996	1.32
30	17	6.0125	0.0306	0.787	0.0005855	2.958325	
31	18	5.6416	0.0301	0.790	0.0005862	3.123987	
32	19	5.0169	0.0091	0.785	0.0005862	1.051314	
33	20	5.5045	0.0070	0.785	0.0005862	0.737066	

AERODYNAMIC WAVEFRONT ERROR

DIST	RHO'SQ*Lz	SIGMA SQ
8	1.576E-07	
9	6.684E-07	1.1098E-15
10	1.780E-06	4.3992E-15
11	2.837E-06	1.0602E-14
12	3.557E-06	1.9194E-14
13	5.883E-06	3.1878E-14
14	3.347E-06	4.4280E-14
15	1.399E-06	5.0658E-14
16	7.166E-07	5.3501E-14

SIGMA = 2.3130E-07 , meters

SIGMA = 0.231 , microns

SIGMA/LAMDA = 0.436 , wave

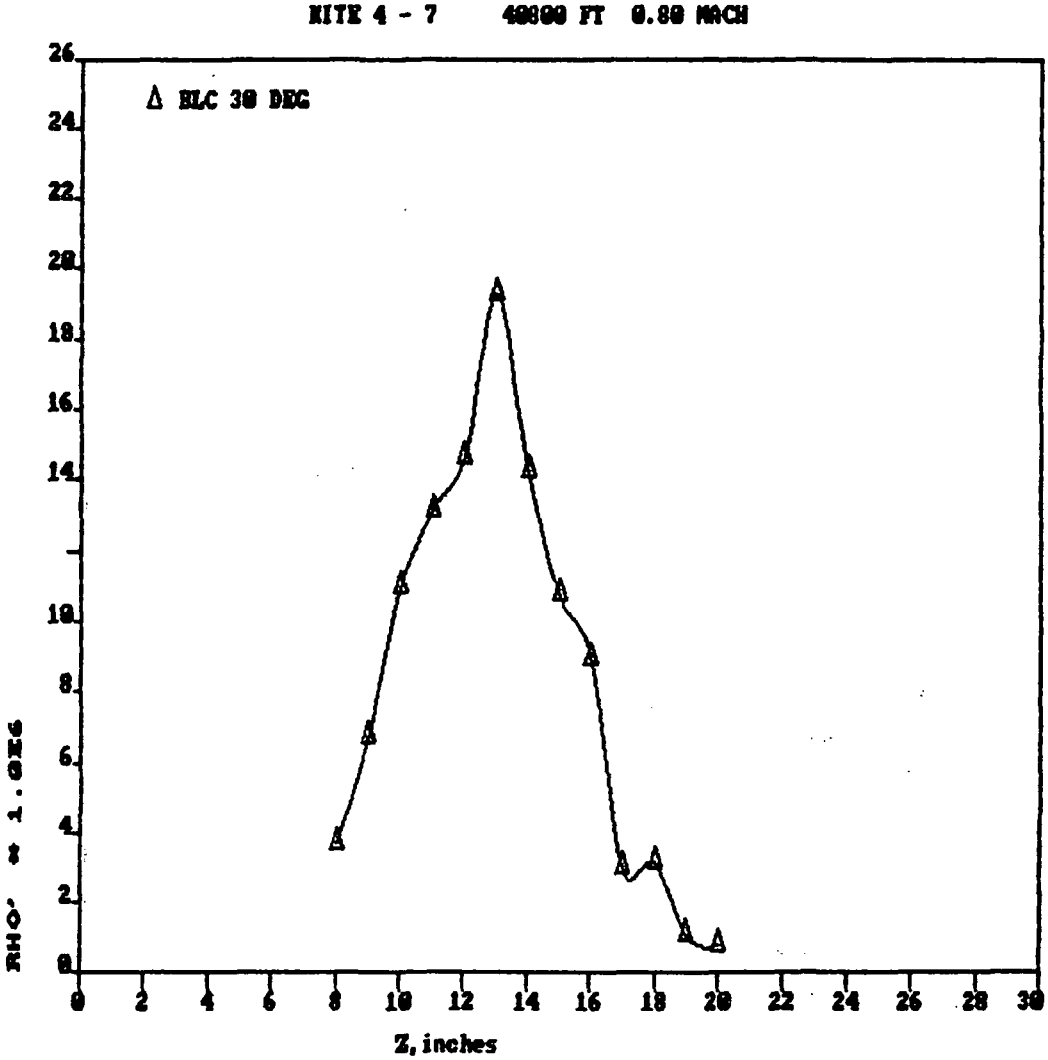
KITE 4 - 7 40000 FT 0.80 MACH
Δ ELC 30 DEG
RHO' * 1.0E6
Z, inches
0
2
4
6
8
10
12
14
16
18
20
22
24
26
28
30

ANEMOMETER DATA SET

ALTITUDE: 40800 FT
MACH NO: 0.80
BLC POS: 45 DEG
SEQ NOS: 8A, 8B, 8C

FLIGHT NO: KITE 4
DATE: 25 JANUARY 1986

AIR TEMP: -34.7

SEN NO	DIST	DC VOL	RMS VOL	MACH NO	FLU DEN	RHO'*1.0E6	Lz
19	8	3.6532	0.3035	0.148	0.0005304	1.913611	1.92
21	9	3.4724	0.2831	0.148	0.0005304	1.877926	1.58
23	10	3.8030	0.3450	0.159	0.0005306	2.409431	1.38
24	11	3.5427	0.3074	0.190	0.0005317	3.283575	1.57
25	12	4.0901	0.3912	0.251	0.0005346	6.284382	1.71
26	13	4.2315	0.4580	0.339	0.0005396	12.833760	2.29
27	14	4.5297	0.3767	0.428	0.0005464	15.511149	2.33
28	15	5.4134	0.3346	0.515	0.0005546	16.439540	2.32
29	16	5.8742	0.1616	0.599	0.0005639	9.734966	2.53
30	17	5.9383	0.1281	0.669	0.0005732	9.387558	2.27
31	18	5.5865	0.1024	0.725	0.0005807	9.245766	1.97
32	19	4.9761	0.0677	0.761	0.0005856	7.492266	1.62
33	20	5.4815	0.0204	0.777	0.0005882	2.129041	0.76
34	21	4.5304	0.0275	0.780	0.0005891	3.499512	
35	22	6.1641		0.780	0.0005891		
36	23	5.4049		0.780	0.0005981		
37	24	6.2853		0.780	0.0005891		

AERODYNAMIC WAVEFRONT ERROR

DIST	RHO'SQ*Lz	SIGMA SQ
8	4.746E-08	
9	3.761E-08	1.1430E-16
10	5.408E-08	2.3750E-16
11	1.143E-07	4.6369E-16
12	4.559E-07	1.2297E-15
13	2.546E-06	5.2631E-15
14	3.784E-06	1.3768E-14
15	4.232E-06	2.4539E-14
16	1.618E-06	3.2401E-14
17	1.350E-06	3.6390E-14
18	1.137E-06	3.9731E-14
19	6.138E-07	4.2084E-14
20	2.325E-08	4.2940E-14

SIGMA = 2.0722E-07 , meters

SIGMA = 0.207 , microns

SIGMA/LAMDA = 0.391 , wave

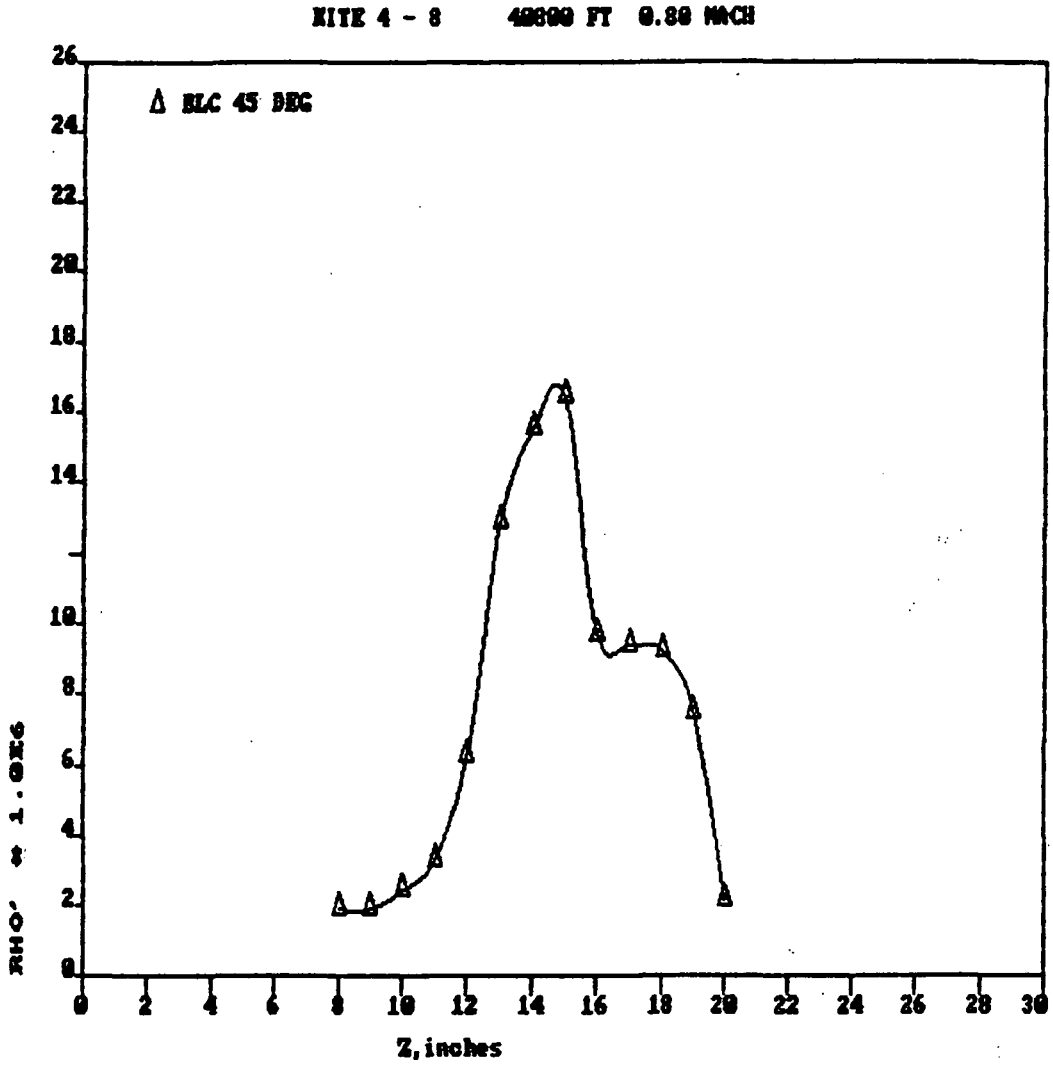
KITE 4 - 8 40000 FT 0.80 MACH
Δ SLC 45 DEG
RHO' * 1.0E6
Z, inches
0
2
4
6
8
10
12
14
16
18
20
22
24
26
28
30

ANEMOMETER DATA SET

ALTITUDE: 41000 FT
MACH NO: 0.80
BLC POS: 60 DEG
SEQ NOS: 8A1,8B1,8C1

FLIGHT NO: KITE 4
DATE: 25 JANUARY 1986

AIR TEMP: -36.2

SEN NO	DIST	DC VOL	RMS VOL	MACH NO	FLU DEN	RHO'*1.0E6	Lz
19	8	3.3762	0.2724	0.085	0.0004999	0.581134	1.90
21	9	3.2968	0.2553	0.090	0.0005074	0.634481	1.75
23	10	3.5783	0.3113	0.108	0.0005149	1.040115	1.50
24	11	3.2657	0.2769	0.130	0.0005166	1.470591	1.74
25	12	3.8715	0.3550	0.165	0.0005224	2.580158	1.81
26	13	3.7780	0.4184	0.190	0.0005282	4.163312	2.30
27	14	4.0619	0.3732	0.235	0.0005299	5.261177	2.33
28	15	4.8910	0.3959	0.285	0.0005326	6.783016	2.40
29	16	5.2872	0.3977	0.362	0.0005374	10.066687	2.52
30	17	4.7256	0.2837	0.430	0.0005427	11.218660	2.54
31	18	5.1813	0.2766	0.512	0.0005507	13.950575	2.47
32	19	4.6922	0.1852	0.590	0.0005593	13.490501	2.64
33	20	5.2796	0.1783	0.670	0.0005686	14.615603	2.64
34	21	4.4587	0.1476	0.720	0.0005759	16.371308	1.74
35	22	6.1463	0.0300	0.760	0.0005820	2.665726	
36	23	6.0470	0.0125	0.780	0.0005852	1.183850	
37	24	6.2933	0.0214	0.790	0.0005853	1.987985	

AERODYNAMIC WAVEFRONT ERROR

DIST	RHO'SQ*Lz	SIGMA SQ
8	4.331E-09	
9	4.755E-09	1.2209E-17
10	1.095E-08	3.3317E-17
11	2.540E-08	8.2164E-17
12	8.133E-08	2.2558E-16
13	2.691E-07	6.9644E-16
14	4.353E-07	1.6430E-15
15	7.454E-07	3.2294E-15
16	1.724E-06	6.5471E-15
17	2.158E-06	1.1763E-14
18	3.245E-06	1.9022E-14
19	3.243E-06	2.7739E-14
20	3.807E-06	3.7212E-14
21	3.148E-06	4.6556E-14
23	0	5.5016E-14

SIGMA = 2.3455E-07 , meters

SIGMA = 0.235 , microns

SIGMA/LAMDA = 0.443 , wave

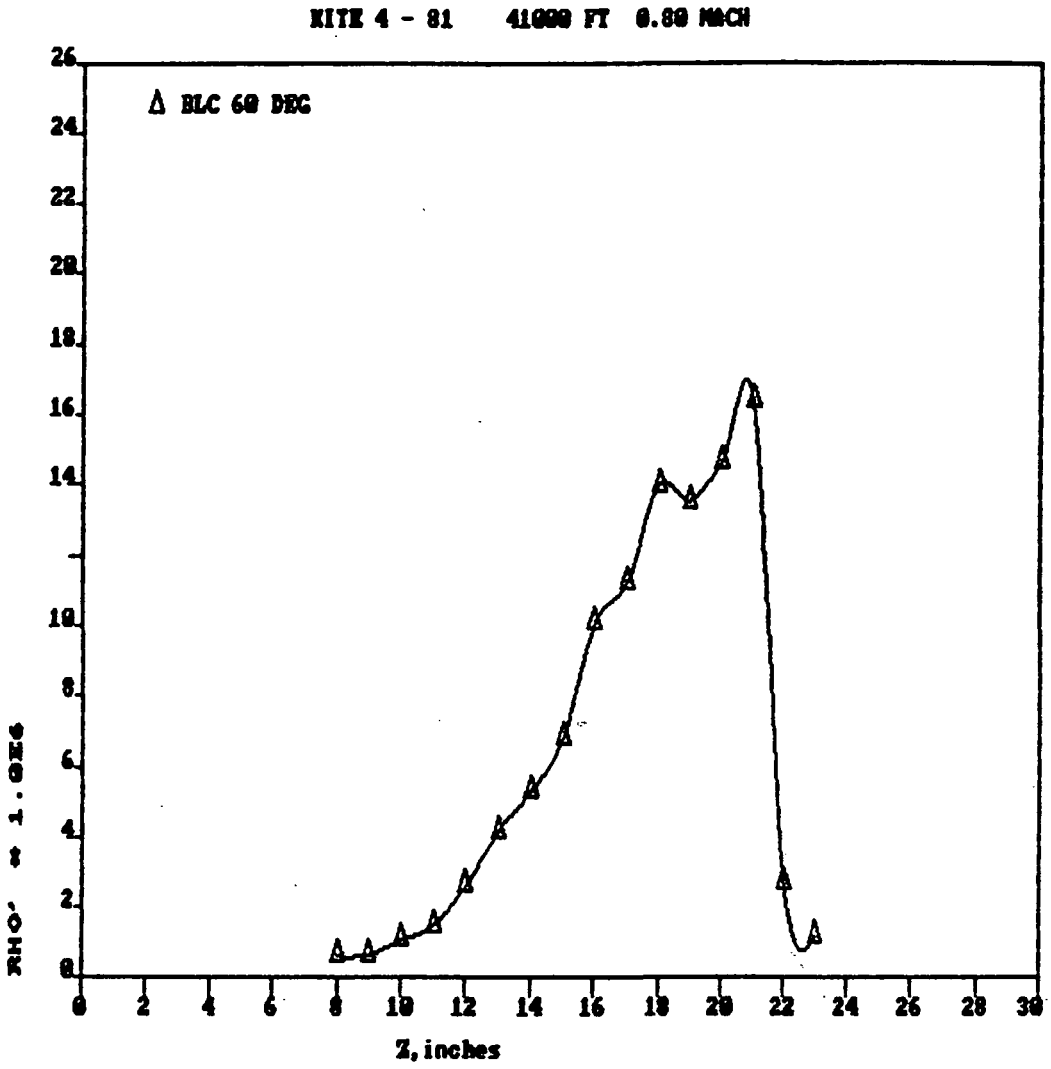
KITE 4 - 81 41000 FT 0.80 MACH
Δ BLC 60 DEG
RHO' * 1.0E6
Z, inches
0
2
4
6
8
10
12
14
16
18
20
22
24
26
28
30

ANEMOMETER DATA SET

ALTITUDE: 41400 FT
MACH NO: 0.80
BLC POS: 90 DEG
SEQ NO: 13

FLIGHT NO: KITE 5
DATE: 28 JANUARY 1986

AIR TEMP: -34.7

SEN NO	DIST	DC VOL	RMS VOL	MACH NO	FLU DEN	RHO'*1.0E6	Lz
21	9	3.4425	0.2767	0.100	0.0005140	0.82299	3.44
24	11	3.5718	0.2538	0.142	0.0005190	1.47533	2.81
26	13	4.0464	0.3194	0.198	0.0005240	3.19301	2.50
28	15	4.3867	0.2588	0.300	0.0005290	5.42244	2.24
30	17	4.6656	0.2068	0.426	0.0005381	8.07089	2.13
32	19	4.5979	0.1582	0.570	0.0005520	10.92201	2.24
34	21	4.3473	0.1129	0.698	0.0005682	12.03349	2.18
36	23	6.0352	0.0257	0.778	0.0005796	2.40546	

AERODYNAMIC WAVEFRONT ERROR

DIST	RHO'SQ*Lz	SIGMA SQ
9	1.573E-08	
11	4.128E-08	1.5321E-16
13	1.720E-07	7.2650E-16
15	4.446E-07	2.3835E-15
17	9.365E-07	6.0950E-15
19	1.804E-06	1.3459E-14
21	2.131E-06	2.4032E-14
25	0	3.5484E-14

SIGMA = 1.8837E-07 ,meters

SIGMA = 0.188 ,microns

SIGMA/LAMDA = 0.355 ,wave

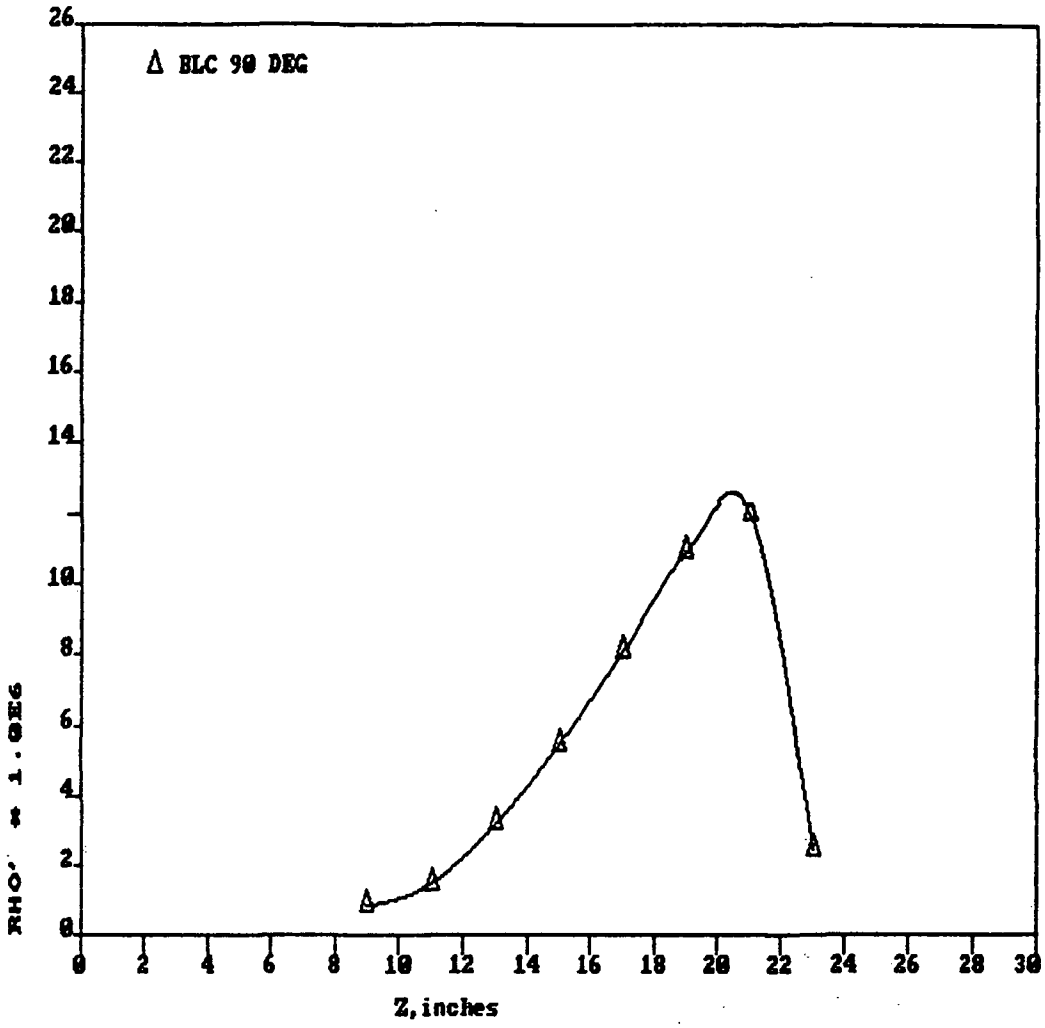
KITE 5 - 13 41400 FT 0.80 MACH
Δ BLC 90 DEG
RHO' * 1.0E6
Z, inches
0
2
4
6
8
10
12
14
16
18
20
22
24
26
28
30